Transcriptional regulation of macrophage migration in the *Drosophila melanogaster* embryo

by

Vera Belyaeva

July, 2018

A thesis presented to the

Graduate School

of the

Institute of Science and Technology Austria, Klosterneuburg, Austria

in partial fulfillment of the requirements

for the degree of

Doctor of Philosophy

I|S|T AUSTRIA

Institute of Science and Technology

The dissertation of Vera Belyaeva, titled "Transcriptional regulation of the macrophage migration in *Drosophila* embryo", is approved by:

Supervisor: Prof. Daria Siekhaus, IST Austria, Klosterneuburg, Austria

Signature: _____

Committee Member: Prof. Carl-Philipp Heisenberg, IST Austria, Klosterneuburg, Austria

Signature: _____

Committee Member: Prof. Paul Martin, University of Bristol, Bristol, UK

Signature: _____

Committee Member: Prof. Michael Sixt, IST Austria, Klosterneuburg, Austria

Signature: _____

Exam Chair: Prof. Martin Loose, IST Austria, Klosterneuburg, Austria

Signature: _____

I hereby declare that this dissertation is my own work and that it does not contain other people's work without this being so stated; this thesis does not contain my previous work without this being stated, and the bibliography contains all the literature that I used in writing the dissertation.

I declare that this is a true copy of my thesis, including any final revisions, as approved by my thesis committee, and that this thesis has not been submitted for a higher degree to any other university or institution.

I certify that any republication of materials presented in this thesis has been approved by the relevant publishers and co-authors.

Signature: _____

[Student Name]

Abstract

Immune cells migrating to the sites of infection navigate through diverse tissue architectures and switch their migratory mechanisms upon demand. However, little is known about systemic regulators that could allow the acquisition of these mechanisms.

We performed a genetic screen in *Drosophila melanogaster* to identify regulators of germband invasion by embryonic macrophages into the confined space between the ectoderm and mesoderm. We have found that bZIP circadian transcription factors (TFs) Kayak (dFos) and Vrille (dNFIL3) have opposite effects on macrophage germband infiltration: Kayak facilitated and Vrille inhibited it. These TFs are enriched in the macrophages during migration and genetically interact to control it. Kayak sets a less coordinated mode of migration of the macrophage group and increases the probability and length of Levy walks. Intriguingly, the motility of *kayak* mutant macrophages was also strongly affected during initial germband invasion but not along another less confined route. Inhibiting Rho1 signaling within the tail ectoderm partially rescued the Kayak mutant phenotype, strongly suggesting that migrating macrophages have to overcome a barrier imposed by the stiffness of the ectoderm. Also, Kayak appeared to be important for the maintenance of the round cell shape and the rear edge translocation of the macrophages invading the germband. Complementary to this, the cortical actin cytoskeleton of Kayak-deficient macrophages was strongly affected. RNA sequencing revealed the filamin Cheerio and tetraspanin TM4SF to be downstream of Kayak. Chromatin immunoprecipitation and immunostaining revealed that the formin Diaphanous is another downstream target of Kayak. Immunostaining revealed that the formin Diaphanous is another downstream target of Kayak. Indeed, Cheerio, TM4SF and Diaphanous are required within macrophages for germband invasion, and expression of constitutively active Diaphanous in macrophages was able to rescue the *kayak* mutant phenotype. Moreover, Cher and Diaphanous are also reduced in the macrophages overexpressing Vrille.

We hypothesize that Kayak, through its targets, increases actin polymerization and cortical tension in macrophages and thus allows extra force generation necessary for macrophage dissemination and migration through confined stiff tissues, while Vrille counterbalances it.

Acknowledgments

I would like to acknowledge the Siekhaus group and Daria for the opportunity to do the Thesis work.

 I would like to thank my PhD committee – Carl-Philipp Heisenberg, Paul Martin and Michael Sixt - for discussions, advice, support and guidance through the project. I would like to thank IST facilities and grad school for the organization of work and education, opportunity to attend exciting courses and talks and to meet interesting people.

I dedicate this Thesis to my family, in particular, to my parents and my sisters, who have always supported me. Last but not least I dedicate this Thesis to my husband, Igor, for his eternal support, patience and love.

Table of Contents

1 Introduction

Cell migration: how do cells migrate?

The ability to migrate is one of the fundamental properties of the animal eukaryotic cells. It is absolutely crucial during the development of the embryo as multiple dynamic cell and, hence, tissue rearrangements occur at this stage that underlie the formation of the adult organism. Examples of such active cell movements include germ layer rearrangements during gastrulation (Smutny et al., 2017; Supatto, McMahon, Fraser, & Stathopoulos, 2009), development of the branched organs such as trachea (Ghabrial & Krasnow, 2006) or blood vessels (Gerhardt et al., 2003), and the developmental migration of the microglia (Casano, Albert, & Peri, 2016) etc. Later, in an adult organism, immune cells are the primary cells that actively migrate towards the sites of infection and perform their tasks there such as engulfment of pathogens and an inflammatory response (Lämmermann et al., 2013). Upon tissue wounding, the cells of the surrounding epithelium receive the wound signals, reactivate and start their path towards the site of injury to enclose it (Shaw & Martin, 2016). In pathology, cancer cells modify the normal cellular program to propagate themselves, spread and populate other organs through metastasis formation during invasive migration (Friedl, Locker, Sahai, & Segall, 2012).

Clearly, cell migration is a widespread process that is essential for the functioning of an animal organism. But how do cells perform this task of purposefully moving themselves? As it appears now, there could be diverse mechanisms depending on the cell type and the conditions of the surroundings. However, there are some basic features that serve as a foundation for the formulation of the classical model of cell migration. They were discovered and formulated in 1980's by Abercrombie (Danuser, Allard, & Mogilner, 2013). At this time, the question of cell polarization was not addressed. However, once the cell has designated a front and a rear, the next four steps are described as crucial for migration (Fig.1). Step 1 is a growing lamellipodia at the front edge, this growth being driven by the polymerization of actin at the leading edge. Step 2 is the formation of adhesion contacts (usually, Integrin-mediated focal adhesions) at the leading edge which are necessary to anchor the propulsive forces at the front as well as the forces of retraction that appear at

the cell rear at step 4. These adhesions are disassembled in step 3, and in step 4 the rear of the cell contracts.

Abercrombie has proposed that the front to rear gradient of adhesion determines the direction of cell migration towards the front, and that the contraction of the rear occurs similarly to actomyosin contraction in the muscles. Importantly, Abercrombie has suggested the presence of rearward movement of the cell cytoplasm, the prominence of this movement being dependent on the interplay of the front adhesion and the rear contraction forces. Later it was found out that this rearward movement is a retrograde actin flow. Now it is well established that all four steps are mechanochemically, spatially, and temporally coordinated to ensure directed cell migration (Labrousse et al., 2003).

As the mechanism of the rear contraction in migrating cell is the main mechanism discussed in this Thesis, we will go in a bit more details into current understanding of this process.

In most of the cell-migratory systems contraction is generated by Myosin motors attached to the actin filaments and pulling on them using the energy of ATP hydrolysis (C. A. Wilson et al., 2010). There are several conceptual models that explain why and how the system of the force-generating elements, such as actomyosin filaments, would produce overall network contraction rather than expansion. Some models assume that actomyosin fibers in migrating cell are organized into the sarcomeric structure that acts as a unit of contraction in the muscle cell (Naumanen, Lappalainen, & Hotulainen, 2008). One of the proposals of how actin and myosin filaments can self-organize into a sarcomeric structure is that myosins remain bound to the barbed end of an actin filaments. When several actin bundles with opposing polarity are connected to the same myosin cluster they slide into a mini-sarcomere configuration (Zumdieck, Kruse, Bringmann, Hyman, & Jülicher, 2007). Even without this property it is predicted that myosin would sort actin filaments based on their polarity, thus generating fibers with alternating polarity (Craig, Dey, & Mogilner, 2011).
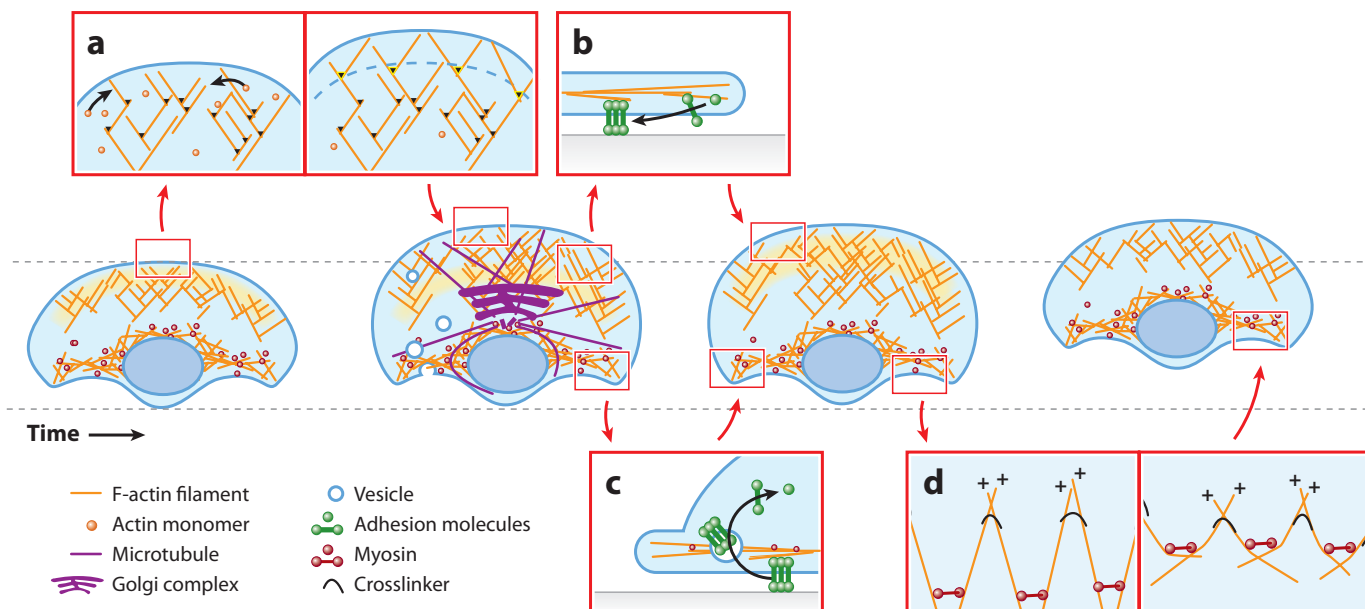
Figure 1. Abercrombie model of metazoan cell crawling. Cell migration is divided into discrete steps: (*a*) protrusion based on actin growth and polymerization force; (*b*) formation of new adhesions at the front; (*c*) release and recycling of adhesions at the rear; and finally, (*d*) actin-myosin-powered contraction of the cytoplasm, resulting in forward translocation of the cell body. We are showing schematically the centrosome and microtubules originating from it, as well as the Golgi complex and Golgi-derived microtubules that play important roles in guiding migration (Danuser et al., 2013).

The more complete model includes cross-linkers that are permanently attached to the barbed ends of actin filaments but still allow polymerization of actin to occur. This sort of arrangement should allow a proper mini-sarcomere contraction (Friedrich, Fischer-Friedrich, Gov, & Safran, 2012). Interestingly, it was also proposed that contraction of the actin filaments can occur independent of the myosin motors, given that actin fibers are bound by cross-linkers and at the same time actin depolymerization occurs: cross-linkers would compensate for reduced actin mesh density by crosslinking the remaining filaments and, thus, contracting the whole network (Sun & Hemler, 2001).

Cell migration in confinement: a special circumstance

As the research of cell migration has expanded, it became clear that Abecrombie's classical model of cell migration holds for 2D type of migration: the cell has to be attached to the substrate through the specific adhesions at the front edge to generate sufficient traction forces to counteract Brownian motion and to propel itself forward. However, when a cell is confined in a 3D environment, there is enough surface contact that secures forward motion

(Paluch, Aspalter, & Sixt, 2016). Indeed, there are several studies showing that 3D migration can occur without Integrin-mediated adhesion (Lämmermann et al., 2008; Ruprecht et al., 2015). In general, there is a continuum of different cell-migratory modes, spanning from adhesion-dependent (mesenchymal) to a more adhesion-independent mode (amoeboid). In turn, there are cell intrinsic and cell extrinsic factors that define the position of the migrating cell within this continuum and, hence, its preferred migratory mode.

One of the instrinsic factors predisposing a cell to move in an adhesion-independent, amoeboid fashion is the absence of Integrins. High actomyosin contractility is another factor favoring the amoeboid type of locomotion. Cortical contractility at the cell rear is important not only for generation of the cytoplasmic flow forward, but also to counteract and weaken adhesion and to promote a rounded cell morphology. (This is a bit logically odd as you first are focusing on absence of adhesion and now on how this works in the context of the presence of adhesion). Accordingly, myosin II knock-out in T-cells induced cell spreading and impaired migration (Jacobelli et al., 2010), while activation of Rho/Rock pathway in isolated zebrafish progenitors in confinement induced adhesion-independent migration (Ruprecht et al., 2015).

Among extrinsic factors favoring amoeboid migration, the most obvious one is using non-adhesive substrates for cells to migrate on. Interestingly, decreasing substrate adhesiveness increased the speed of migration of several mesenchymal cell types, when they were placed in 2D confinement between two glass plates (Liu et al., 2015). Despite the fact that decreases in adhesion can improve the efficiency of migration, some degree of adhesiveness to the substrate due to friction is necessary to generate traction and forward motion: that has been confirmed by the inability of Walker cells to move on an inert polyethylene glycol surface even when confined (Bergert et al., 2015). Finally, confinement *per se* promotes cell-substrate interaction in the absence of specific (focal) adhesions and favors rapid cell locomotion (Toyjanova, Flores-Cortez, Reichner, & Franck, 2015). However, when confinement is too strong due to the stiffness of the substrate, cell migration is impeded, presumably because too strong confinement imposes a barrier on nuclear translocation (Davidson, Sliz, Isermann, Denais, & Lammerding, 2015).

There are several models describing mechanisms that cells can utilize to migrate in confinement without the use of focal adhesions (Paluch et al., 2016). One of the models assumes a cell inserting lateral protrusions, such as blebs or pseudopods, into the gaps of

discontinuous surrounding tissues, thus generating traction forces (Fig. 2a). Indeed, this sort of locomotion was observed in migrating neutrophils that were pasting their pseudopods into surrounding 3D matrix, deforming it and moving themsleves forward (Mandeville, Lawson, & Maxfield, 1997; Tozluoğlu et al., 2013). Another proposed model is called chimneying and does not require a discontinuous environment around the migrating cell. Instead, the actin polymerizes against the walls of the channel in which the cell moves, and exerts a pushing force on the walls (Fig. 2b); the dense elastic actin meshwork at the cell rear prevents counterproductive retrograde flow and rear bleb formation (Hawkins et al., 2011; Malawista, De Chevance, & Boxer, 2000). Indeed, such a network of actin filaments growing perpendicular to the walls of confinement has been observed (K. Wilson et al., 2013). Finally, non-specific friction between the migrating cell and the confining walls could generate traction forces to promote cell migration (Hawkins et al., 2011). Intracellular forces generated by the retrograde actin flow can provide sufficient friction on the substrate, if the extracellular domains of the transmembrane proteins carried by the flow are in the proximity to the substrate (Fig. 2c). Cadherins and extracellular glycocalyx matrix proteins are candidate molecules that could generate transient interaction with the substrate favored by confinement (P. Friedl & Bröcker, 2000).

It could be beneficial for certain types of cells to possess the ability to acquire certain migratory strategy (such as mesenchymal or amoeboid) on demand. This could be particularly crucial for highly motile cells that are exposed to multiple environments, such as immune cells navigating in the developing embryo, in which tissues are constantly reorganising and presenting diverse environments to migrating cells.

The role of the AP1 transcription factor in invasive migration

The invasive migration of cells can be a transcriptionally acquired behavior (Bradford W. Ozanne, Spence, McGarry, & Hennigan, 2006). During the development of an embryo and in tumor spreading, cell invasion is linked to epithelial-to-mesenchymal transitions (EMTs), the process through which epithelial cells downregulate cell–cell adhesions and lose polarity, thus becoming mesenchymal-like cells with invasive capabilities (B. W. Ozanne et al., 2000). Transcription factors Snail, Slug, Twist, and Zeb1/2 are involved in EMT (Ordway, Fenster, Ruan, & Curran, 2005). Tumor cell invasion has common features with the development of

the embryo, during which epithelial cells initiate migration in response to extracellular signals such as TGFβ (transforming growth factor beta) (Derynck, Akhurst, & Balmain, 2001; Zavadil & Böttinger, 2005), HGF (hepatocyte growth factor) (Thiery, Acloque, Huang, & Nieto, 2009) or EGF (epidermal growth factor) (Lu, Ghosh, Wang, & Hunter, 2003). All of these ligands are known to activate AP1 (activating protein 1), another transcription factor linked to invasion and EMT. AP1 is also implicated in the transformation of cells by various oncogenes that participate in the growth factor Ras pathway and increasing tumor invasiveness.

AP1 is composed primarily of heterodimers of Fos and Jun family proteins. The Fos family includes Fos, Fra1 and Fra2, and the Jun family is made up of c-Jun, JunB and JunD, respectively. Originally, Fos and Jun were first identified as retroviral oncogenes that were able to induce tumors *in vivo* and transform fibroblasts into tumorogenic cells in culture (Curran, Peters, Van Beveren, Teich, & Verma, 1982). v-fos-transformed rat fibroblast cells, 208F, adopted a bipolar spindle shape that didn't have actin stress fibers and had only weak adhesion structures. In one study the target genes of v-fos in transformed 208F cells were identified (Bradford W. Ozanne et al., 2006) and they were consistent with the previously identified AP1 target genes associated with invasion such as members of the matrix metalloproteinase (MMP) family of extracellular proteases (Bradford W. Ozanne et al., 2006). Transformed 208 fibroblast cells perform invasive migration in an *in vitro* invasion assay where cells migrate in 3D through a thick layer of matrigel. These cells migrate by extending a long pseudopod that forms membrane ruffles at its tip and this invasive migration and pseudopod formation was dependent on AP1 activity (Lamb et al., 1997). Among genes upregulated in v-fos-transformed 208 fibroblasts were CD44, a cell surface hyaluronan-receptor that links to the actin cytoskeleton, and ezrin, a member of the ERM (ezrin–radixin–moesin) family of protein that connects CD44 to the actin cytoskeleton. Both of these genes were shown to be important for pseudopod formation and the invasive migration of transformed fibroblasts. Another Fos ortholog, FOSL1, was shown to regulate the adhesion and migration of endothelial cells of the forming vessel by directly regulating the transcription of integrins (Galvagni, Orlandini, & Oliviero, 2013).

In an elegant study of the invasion of anchor cells moving through the basement membrane of developing *Caenorhabditis elegans*, the FOS-1A transcription factor has been shown to upregulate the transcription of a set of genes that in combination were important

for anchor cell invasion. These genes were protocadherin, MMP and hemicentin, a component of the ECM. Altogether they were sufficient to allow anchor cells to anchor on the basement membrane, dissolve it, adhere again and migrate through (Hagedorn & Sherwood, 2011).

AP1 in *Drosophila* is important for the formation of metastasis by *Rasv12, scrib*-mediated tumors (Atkins et al., 2016; Igaki, Pagliarini, & Xu, 2006; Kulshammer & Uhlirova, 2013; Uhlirova & Bohmann, 2006). There are several cytoskeleton regulators found to be transcriptionally regulated by AP1 in this model system, among them were MMPs, the formin Diaphanous and the filamin Cheerio. It was shown that filamin Cheerio is involved in proliferation, formation of metastasis and invasiveness of this tumor (Kulshammer & Uhlirova, 2013).

Thus, AP1 transcription factor (and Fos in particular) is the key transcription factors linked to the regulation of cell migration and invasion in different model systems. AP1 usually regulates actin cytoskeleton components and MMPs. However, the exact underlying molecular mechanisms could be different and strongly depend on the context.

Both Fos and Jun protein families are parts of of basic leucine zipper (bZIP) superfamily of transcription factors (Miller, 2009). Members of the bZIP superfamily form homo- and heterodimers and activate transcription upon binding to specific sites on the DNA. CCAAT/enhancer binding protein α (C/EBPα) was the first cloned and characterized bZIP transcription factor. The researchers identified that the bZIP DNA binding domain contains a positively charged segment, the basic region, that is connected to the repeats of leucine comprising the leucine zipper. Following studies of the crystal structure of bZIP transcription factors have demonstrated that these factors bind to DNA as dimers that form a chopstick-like structure and that dimerization occurs because the leucine zippers of monomers havie coiled-coil alpha-helical structures which wrap around other (Ellenberger, Brandl, Struhl, & Harrison, 1992; Miller, 2009). The basic region of each of the protein helices binds to the DNA major groove at one-half of a palindromic site.

bZIP proteins are classified into several protein families each having their own DNA specificities (Garvie & Wolberger, 2001). Each bZIP transcription factor recognizes its specific DNA region thanks to five basic residues located in the conserved positions in the basic region. The ability to form heterodimers by certain members of bZIP proteins further broadens the range of possible DNA binding sites (Vinson & Boyd, 1993).
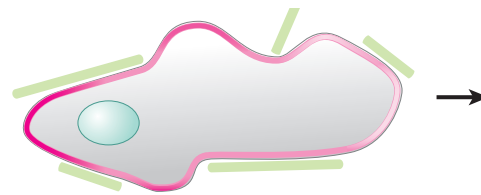
- c-Jun bZIP transcription factors, in addition to heterodimerization with c-Fos and AP1 formation, can also form homodimers but with a lower affinity (John, Leppik, Busch, Granger-schnarr, & Schnarr, 1996; Krieger, 2015a; Nakabeppu, Ryder, & Nathans, 1988). Some studies have found that c-Fos, unlike c-Jun, lacks the ability to homodimerize and can bind to DNA only in complex with c-Jun (Chinenov & Kerppola, 2001; Curran, Peters, Van Beveren, Teich, & Verma, 1982). It is thought that leucine zippers of c-Fos repulse each other thus preventing stable homodimerization. However, a study detected stable c-Fos dimers bound to DNA by determining its dissociation constants from FRET transitions and using imaging fluorescence cross-correlation spectroscopy (SPIM-FCCS) and molecular dynamics modeling (Krieger, 2015b). In another study it was shown that a single amino acid substitution within the leucine zipper region confers DNA binding and homodimerization capacity to mammalian Fos (Porte, Oertel-buchheit, John, Granger-schnarr, & Schnarr, 1997). Interestingly, it was shown that in *Drosophila* both Fos (dFos) and Jun (dJun) can form both stable hetero- and homodimers (Alerting, 1990). dFos homodimerizes, possibly because there are more hydrophobic residues in zipper region responsible for dimerization as opposed to mammalian Fos and, therefore, more stable homodimer can form. However, the most stable dimer *in vitro* was AP1 followed by the dJun homodimer and only then the dFos homodimer. Both dFos and dJun homodimers formed complexes with AP1 DNA binding sites in band shift assays and were able to activate transcription *in vitro* (Alerting, 1990).

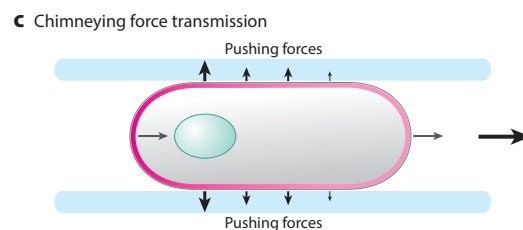### Tissue boundaries in the embryo: confinement for the cells to migrate in?

The developing embryo is an excellent example of a "collection" of tissues each of which possesses a unique combination of physical properties such as, for example, adhesiveness or rigidity. These properties define the way the tissue develops and changes, as well as the way it interacts with the neighboring tissues and with the cells that migrate through it. All these processes are parts of the morphogenesis that causes an organism to develop its shape.

One of the key features of morphogenesis is tissue separation, the process when boundaries form between different cell populations. Interestingly, tissue separation can occur even before the cells acquire their fates, indicating that its function is not to simply draw borders between organs, but to also pattern and organize the tissue within the single organ (Fagotto, 2014).
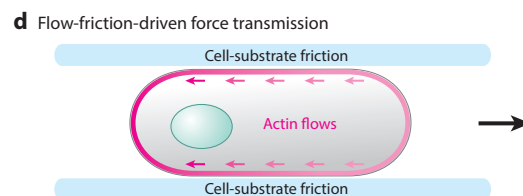
a.

b.

c Chimneying force transmission

Pushing forces

Pushing forces

c.

d Flow-friction-driven force transmission

Cell-substrate friction

Actin flows

Cell-substrate friction

Figure 2. Different physical mechanisms of force generation and transmission during focal adhesion–independent migration. The pink line represents the actomyosin cortex, with dark pink showing strong cortex contractility and light pink a weak cortex. (*a*) Swimming migration of blebbing cells. Asymmetric shape deformations during bleb expansion and bleb retraction combined with hydrodynamic interactions with the surrounding fluid may lead to cell locomotion. (*b*) Intercalation of lateral protrusions into substrate gaps may serve as footholds to drive cell migration. This type of migration may be particularly effective in 3D matrices and in crowded, inhomogeneous environments in vivo. (*c*) Chimneying migration of cells in confinement. Lateral pushing forces against the surrounding substrate keep the cell body in place, allowing for high cortical contractility at the rear and protrusion expansion at the front to drive locomotion. (*d*) During flow-friction-driven migration, forces generated by contractile flows of the actomyosin cortex are transmitted to the substrate via nonspecific friction. The molecular origin of friction is not known (Paluch et al., 2016).

The study that laid a foundation for our understanding of tissue separation was an experiment in which dissociated embryonic tissues sorted themselves out from the mixed aggregates (Steinberg & Gilbert, 2004). This process was later confirmed by the observation of cell sorting during normal tissue formation (Wacker, Grimm, Joos, & Winklbauer, 2000). A smooth interface between tissues is considered to be a good criterion for the existence of a tissue boundary as this reflects an abrupt discontinuity in cell adhesion/tension (Dahmann, Oates, & Brand, 2011).

There are two key molecular players in tissue separation: the actin cytoskeleton and the cell-cell adhesion molecules (Fagotto, 2014). The level of actomyosin contractility defines the stability and rigidity of the tissue. Homophilic cell-cell adhesion molecules, such as cadherins, through their extracellular domains define the way cells connect to each other and through their cytoplasmic region couple cell-cell adhesion to the actin machinery. Epithelial E-cadherin and mesodermal N-cadherin are the classical cadherins that are thought to define differential tissue adhesion. Both of these cadherins connect to the actin cytoskeleton through catenins that are also required for adhesion formation. Cadherins form clusters that associate with the actin cytoskeleton regulators, such as actin filament nucleating factors and Rho GTPases (Ratheesh et al., 2012).

One model describing the biophysical properties of the tissue is based on an analogy to the physics of a fluid (Fagotto, 2014). In this model there are two forces opposing each other: the contractility of the actin cytoskeleton that minimizes the surface of the cell and the cell-cell adhesion that favors cell spreading (Lecuit & Lenne, 2007). At the equilibrium of these two forces certain interfacial cell tension arise that could cause tissue separation.

There are several models describing the tissue separation process. One of them is the differential adhesion hypothesis (DAH) that states that tissues sort based on the differential affinity of adhesion molecules on the surface of different cell types: cells with the highest adhesion will tend to sort together thus minimizing their surface. However, this model didn't withstand attempts at experimental validation *in vivo* (Ninomiya et al., 2012).
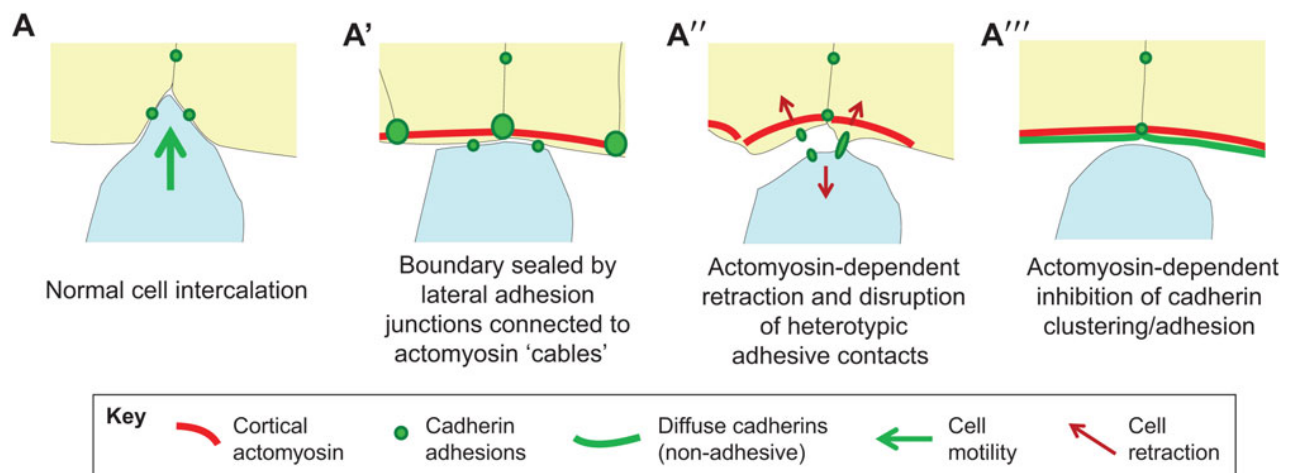
Figure 3. Cortical contractility and mechanisms of separation. (A) Mechanisms of inhibition of cell mixing. Cell intercalation may be inhibited by different mechanisms, all of which are dependent on actomyosin contractility. (A′) Actomyosin structures connect and reinforce cadherin junctions, building supracellular 'cables' that seal the boundary. (A″) Actomyosin contractility leads to cell retraction and disruption of cell contacts. (A‴) Contractility prevents cadherin clustering and the establishment of heterotypic adhesive contacts (Fagotto, 2014).

Another model is called differential interfacial tension hypothesis (DITH) and is based on the differential contractility of the tissues that would lead to the different levels of interfacial tension. This model has been confirmed experimentally in zebrafish germ layers *in vitro* (Krieg et al., 2008; Maitre & Heisenberg, 2011). However, this model assumes actomyosin tension and cell-cell adhesion to be two independent variables, which is hardly the case given the strong crosstalk between the actin machinery and cadherin complexes. A local contractility model is yet another model that is considered to be an adaptation of the DITH. The difference is that this model assumes that tissue separation depends on the local differences in the tissue contractility at the boundary and not on the global tissue properties.

Interestingly, the concept of tissue separation based on differential tension was complemented by the recent *in vivo* study by (Krens et al., 2017). Researchers have demonstrated that in zebrafish embryo cortical tension was the same in the separating germ layers, and this was caused by the higher osmolarity of the interstitial fluid of the embryo as compared to the culture medium where previous *in vitro* experiments have been done.

Still in other *in vivo* cases actomyosin tension appears to be highest at the tissue boundary, as confirmed by laser ablation assays in *Drosophila* imaginal disc and myosin accumulation at the imaginal disc boundaries (Aliee et al., 2012). At the molecular level it can be explained in the two following ways. In the first one, the boundary is thought of as a supracellular seal formed because increased actomyosin contractility consolidates lateral homophilic junctions, generates the "seal" and prevents intercalation of another tissue (Fig. 3a'). Another way to view it, is that actomyosin tension at the boundary prevents (Fig. 3a'') or disrupts (Fig. 3a''') formation of the heterophilic adhesion between two tissues by counteracting adhesive force.

A certain degree of interfacial tension at the boundary of the tissues will result in a certain degree of stiffness of these tissues. This stiffness along with the low level of adhesion between these tissues provide an opportunity and confinement for the motile cells to migrate in, which may or may not be used to the advantage of the migratory cells. The outcome will depend in part on the balance between the tissue stiffness and the physical properties of the migratory cells: when the stiffness of the migrating cell and the surrounding tissues are at optimal ratio, confinement would be beneficial for the migrating cell to generate a traction force. When that ratio is suboptimal, the cell may not be able to move within the overly stiff tissues. Alternatively, too soft tissues would not sustain traction generation and would yield under the force applied by the migrating cell.

We would like to find out which properties and corresponding molecular regulators allow cells to successfully move through the confined tissue environment, and how this movement occurs.

There are several *in vivo* systems that allow this question to be addressed. One of them are border cells migrating in the ovary of *Drosophila*. These are a collective of 4-6 cells that delaminate from the epithelium of the egg and migrate between nurse cells to reach another side of the egg and form a special structure for the sperm entry. The front border cell forms a leading edge protrusion, and all border cells form adherent junctions between each other to move coherently. Multiple regulators and players of this process have been described (Montell, Yoon, & Starz-Gaiano, 2012). Another *in vivo* system to study invasive migration is the anchor cell of *Caenorhabditis elegans*. The anchor cell is a specialized uterine cell that undergoes stereotypic developmental migration through the epidermal basement membrane and further moves between central vulval precursor cells to form to

form uterine-vulval connection. It was demonstrated that there is a transcriptional FOS-1A-dependent program that consists of several molecular players crucial to regulate invasion of the anchor cell (Hagedorn & Sherwood, 2011).
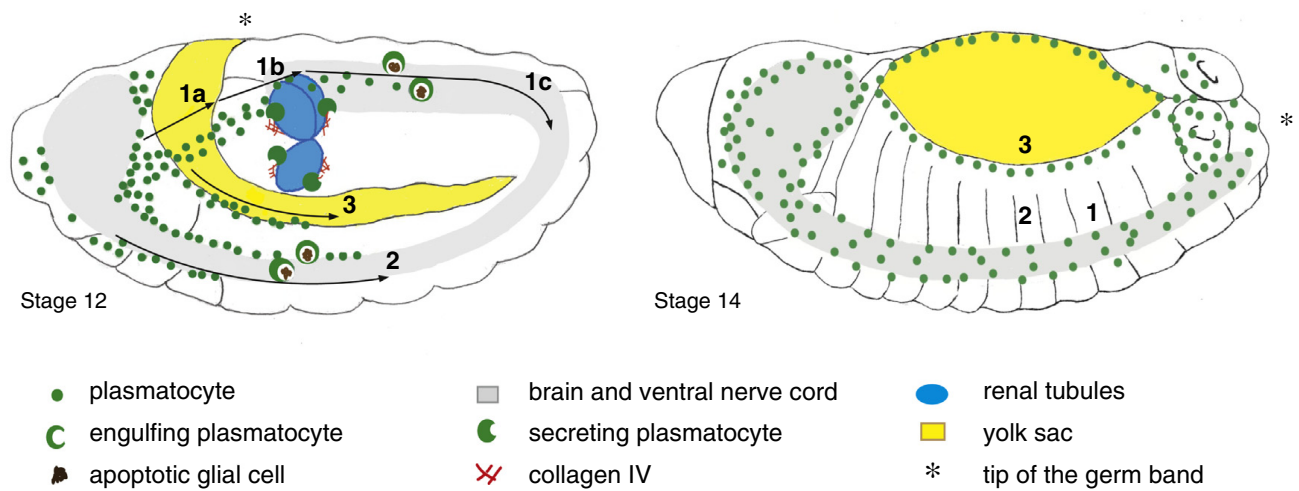
We are investigating invasive migration of *Drosophila* embryonic macrophages as this system provides a huge array of genetic tools to manipulate different genes and tissues as well as provides good imaging opportunities (for details see *"Drosophila* genetics and imaging tools allow dissecting the mechanisms underlying macrophage migration *in vivo"* below). Unlike border cells that migrate as highly cohesive group of cells, *Drosophila* embryonic macrophages disseminate during their migration and move as single cells that physically contact each other and surrounding tissues from time to time. This mode of migration is similar to the migration of the vertebrate macrophages that constantly probe environment to carry out their tasks. Conservation of the macrophage functions (i.e. engulfing pathogens, clearing dead cells and secretion of the extracellular matrix) and corresponding molecular players (e.g. scavenger receptors) across vertebrate and insect groups makes *Drosophila* macrophages a very suitable, simple and genetically tractable *in vivo* system to investigate migration of immune cells and to find molecular mechanisms underlying this process that could be relevant for the vertebrate counterparts.

Drosophila embryonic macrophages is a model system to study cell migration *in vivo*

Immune cells fight external infections, help the organism to heal itself and are, therefore, essential for its normal functioning (Luster, Alon, & von Andrian, 2005; Munoz, Biro, & Weninger, 2014). Unlike vertebrates that rely on a highly complex immune system containing both innate and adaptive parts, *Drosophila melanogaster* has only an innate immune system consisting of macrophages (Lemaitre & Hoffmann, 2007). *Drosophila* macrophages are important to both prevent infections and cancer and to sculpt the development of an embryo (Parisi, Stefanatos, Strathdee, Yu, & Vidal, 2014; Pastor-Pareja, Wu, & Xu, 2008). Macrophages migrate during embryonic development along the paths where their functions are required and eventually populate the embryo (Cho et al., 2002).

Macrophages originate in the head mesoderm (Holz, 2003; Lebestky, Chang, Hartenstein, & Banerjee, 2000) from where they delaminate over time and spread along three main routes (Fig. 4). In route 1, macrophages move over the yolk sac and beneath the amnioserosa to the tip of the germband (route 1a). They then invade the extended germband (Bruckner et al., 2004; Cho et al., 2002; Siekhaus, Haesemeyer, Moffitt, & Lehmann, 2010) and head towards kidney-like organs called the renal tubules (route 1b); macrophages secrete collagen IV which facilitates BMP signaling required for the proper development of these organs (Bunt et al., 2010). In route 2, that goes along the vnc, macrophages engulf apoptotic glial cells and facilitate vnc condensation (Sears, 2003; Zhou, Hashimi, Schwartz, & Nambu, 1995). Macrophages also spread along the dorsal vessel in route 3, however, their function there has not been demonstrated yet.

Macrophages are thought to be guided by PDGF/VEGF-related ligands (Pvfs), however, there are certain clarifications that need to be introduced. First, it was shown that the loss of function of PDGF/VEGF-related receptor, PVR, expressed in the macrophages causes defects in their migration along their routes (Bruckner et al., 2004; Cho et al., 2002; Parsons & Foley, 2013; Wood & Jacinto, 2007). However, later it was proven that PVR plays an essential role in the macrophage survival (Bruckner et al., 2004). Complementary to this it was shown that PVR-deficient macrophages with restored survival are deficient in the germ band entry thus demonstrating the importance of PVR in this type of migration (Bruckner et al., 2004; Parsons & Foley, 2013). The role of Pvf signaling for the macrophage migration in route 2 is to guide macrophage migration as was demonstrated when the macrophage survival defect was rescued (Brückner et al., 2004). In route 3 removal of the Pvf is sufficient to cause migratory defects without affecting survival (Wood, Faria, & Jacinto, 2006). It is also not established solidly whether Pvfs act as chemoattractants: on one hand, Pvf2 over-expression causes macrophage accumulation (Cho et al., 2002), on the other hand, Pvfs were not tested for their ability to redirect macrophage direction of migration. In addition, expression of Pvf2 or dominant active form of PVR in the macrophages did not stop macrophage migration, arguing against the role of Pvfs in chemoattraction (McDonald, Pinheiro, & Montell, 2003; Parsons & Foley, 2013). In summary, the presumable functions for Pvfs in the embryo are to increase invasion in route 1 as well as mediate adhesion or guidance on several macrophage routes.

Stage 12

Stage 14

|		
● plasmatocyte	▢ brain and ventral nerve cord	⬤ renal tubules
C engulfing plasmatocyte	C secreting plasmatocyte	▢ yolk sac
🝁 apoptotic glial cell	✕ collagen IV	* tip of the germ band

Figure 4. Plasmatocyte migration routes and their functional roles during embryonic development. Schematic of two embryos (early Stage 12 on the left and Stage 14 on the right) showing that plasmatocytes specified in the head mesoderm migrate along three main routes during embryonic development. One sub population migrates in Stage 10-11 over the yolk sac to the edge of the extended germband indicated by an asterisk (route 1a). They then penetrate the germband and cluster around the renal tubules where they secrete collagen IV which ensheathes the tubules (route 1b). These and other plasmatocytes that have entered the germband continue along the posterior ventral nerve cord (vnc, route 1c in left embryo, route 1 in right embryo). Another subpopulation migrates out from the head (route 2 in both embryos) along the anterior ventral nerve cord. In both of these routes plasmatocytes engulf apoptotic midline glia. The third group of plasmatocytes migrates along the developing heart also towards the posterior of the embryo (route 3 in both embryos). Arrows indicate the migration routes (Ratheesh, Belyaeva, & Siekhaus, 2015).

As the focus of the current thesis is the investigation of the macrophage invasion into the germ band (route 1), this process is described in more details here.

(Siekhaus et al., 2010) have shown that macrophage invasion into the germ band requires Rap1, RhoL and α-Integrin. The mammalian orthologs of these proteins are known to be involved in the process of vessel extravasation by immune cells, thus hinting at the conservation of certain parts of this process with germband invasion. (Ratheesh et al., 2018) have further explored this process and found that the *Drosophila* orthologs of TNF and its receptor are involved in control of the germband properties that define the efficiency of macrophage invasion. At stage 12 of embryonic development macrophages start to invade the germ band between the ectoderm and mesoderm that were closely juxtaposed at previous stages, and these two tissues separate (Fig.5a, b). The TNFα family receptor ortholog, Grindelwald, expressed in the ectoderm of the germband and its ligand

Eiger, expressed in the amnioserosa, affect the localization of the components of the Crumbs apical complex in the ectoderm. The result is decreased levels of the ectodermal apical phosphorylated Myosin II and, as a consequence, a lowered apparent stiffness of the ectoderm that favors macrophage germband invasion. When the stiffness of the ectoderm was increased by the overexpression of dominant active Rho1, macrophages were stalled at the germband entry point.
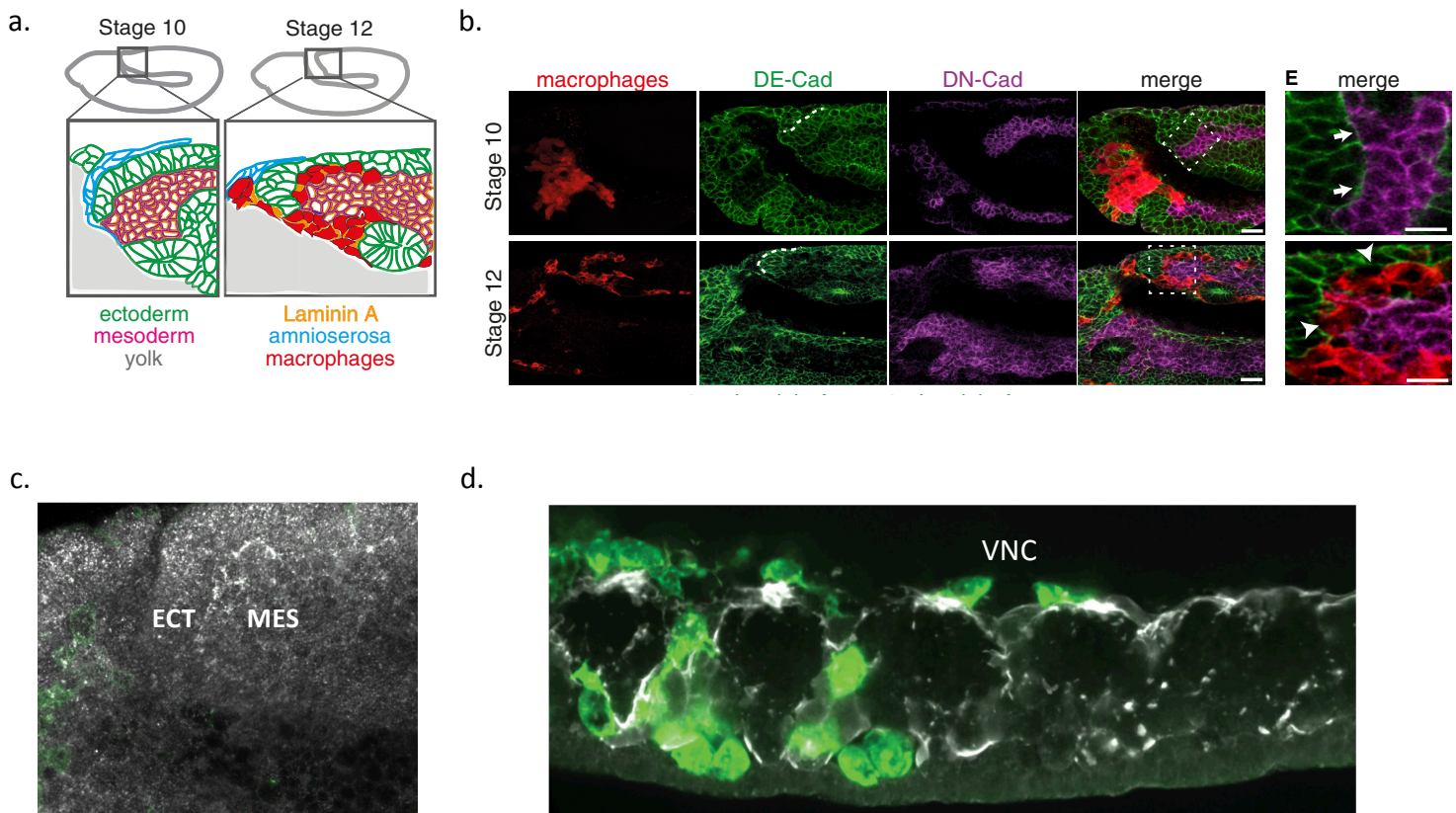
Figure 5. a. Schematics of stage 10 and stage 12 embryos (gray) with box indicating the region magnified below to illustrate the morphology of the germband before (stage 10) and after (stage 12) macrophage invasion. Macrophages (red) enter between the caudal ectoderm (green), and the visceral mesoderm (magenta) along a track of Laminin A (orange). The AS adjacent to the ectoderm is in blue and the yolk in gray.
 b. Confocal images of fixed lateral stage 10 and 12 wild-type embryos with macrophages visualized by

srpHemo-3XmCherry expression (red), ectoderm by antibody staining against DE-Cadherin (green) and mesoderm by antibody staining against DN-Cadherin (magenta), along with a merge of all channels. The dotted white line in the green channel indicates the apical side of the ectoderm cells (Ratheesh et al., 2018). c. LanA staining in the germband. d. LanA staining along VNC. ECT – ectoderm, MES – mesoderm, macrophages are labeled in green

This finding implies that the stiffness of the ectoderm has to reach a certain value to allow macrophage passage into the germband. This situtaion is reminiscent of a cell migrating in a confinement channel where the degree of confinement has to be at a certain, optimal, level that does not obstruct forward cell movement and allows generation of the traction force on the walls. It is also striking that at the stage of macrophage germband invasion the components of the extracellular matrix are just starting to be deposited (Matsubayashi et al., 2017). This is evident, for example, through the staining of Laminin A (LanA): LanA is visible at early stage 12 in the germ band (Fig. 5c), while later at stage 13 macrophages migrate along much thicker LanA tracks in the VNC route (Fig. 5d). This further parallels germband invasion with the adhesion-independent migration under confinement.

Drosophila genetics and imaging tools allow dissecting the mechanisms underlying macrophage migration *in vivo*

Drosophila melanogaster has proven itself to be an excellent model system for genetic studies and dissecting regulatory pathways. This began in the time of Thomas Morgan when he adopted fruit flies in the lab because they were cheap and easy to maintain. Later it appeared that many developmental processes are conserved between flies and vertebrates, and out of 15,000 *Drosophila* genes about half have clear human homologues. Moreover, flies possess multiple morphological features that could be easily measured and quantified. The most powerful advantage of *Drosophila* as a model system is therefore the ability to carry out forward genetic screens to find the key components regulating a process of interest (St Johnston, 2002).

The Nobel-Prize-winning genetic screen was carried out by Christiane Nüsslein-Volhard and

Eric Wieschaus in which they chemically mutagenized flies and attempted to find all or almost all genes involved in the patterning of the embryo (Nüsslein-volhard & Wieschaus, 1980). One class of genes missed in this screen were the genes involved in the development of the fly brain, that were discovered in a separate screen through which several conserved axon pathfinding regulators were identified (Seeger, Tear, Ferres-Marco, & Goodman, 1993). As the tools advanced, Gal4 system and GFP came into play allowing labeling of individual neurons and to carry out successful screens to find genes controlling dendritic morphology (Gao, Brenman, Jan, & Jan, 1999). Modern libraries of mutants keep multiple fly lines with P-elements incorporated into different locations in the genes. P-elements can carry special cassettes that allow activation or inhibition of nearby genes. Finally, several repositories maintain libraries of flies with interfering RNAs designed to knock-down nearly every gene in the *Drosophila* genome placed under control of the UAS regulatory sequence. Thus they can be driven in any desired time and place in the fruit fly if the corresponding Gal4 driver is available (Dietzl et al., 2007). And since the *Drosophila* genome is less redundant than, for example, the genome of the mouse, it is easier to interfere with a certain function or a process because there are less genes that regulate it.

These diverse approaches that allow genetic manipulations of one or several genes in the tissue of interest can be combined with the modern imaging techniques to visualize and quantify the process of interest. The *Drosophila* embryo is particularly amenable to imaging due to its relative thinness and translucency. Various types of mutants, fluorescent reporters and Gal4 drivers were combined to perturb the function of genes and to observe the corresponding morphogenetic changes and phenotypes (Collinet, Rauzi, Lenne, & Lecuit, 2015; Razzell, Wood, & Martin, 2014; Weng & Wieschaus, 2017).

 In our group we use the advantages of the *Drosophila* embryo as an excellent model system for genetic studies and imaging to unravel mechanisms underlying migration of the immune cells, macrophages (introduced above). Our goal is to find regulators of the macrophage germ band invasion and our central approach is to carry out genetic screens for genes affecting this process. As a primary read-out we use the number of the macrophages in the germ band (macrophages are labelled with specific Gal4 enhancer trap driving fluorescent protein (Brückner et al., 2004)) and compare these numbers between wild type and the mutant different genetic situations (Fig. 6a). As a control to be able to

detect general migration defects we analyse macrophage numbers along a second route, the VNC: normal numbers and speed along this route in the mutant embryo indicate the absence of a defect in general migration (Fig. 6b).

Figure 6. Schematics of *Drosophila* embryo showing macrophages spreading along the routes. a. Lateral view of the middle stage 12 embryo with the germband outlined with the dashed line (route 1). b. Lateral view of the middle stage 12 embryo with the VNC outlined with the dashed line (route 2).

Aims of the Thesis

I. Identification and description of molecular players and mechanisms key for the macrophage invasive migration

Aim 1: to identify systemic regulators of the macrophage germ band invasion

By means of a genetic screen and consequent detailed genetic characterization we aimed to find transcription factors and their partners that could act as master regulators of macrophage germ band invasion. This is important as through transcription expression of a number of proteins could be tuned that together set the properties of macrophages that are beneficial for migration in confinement. It is an interesting biological question if such master regulators exist. It is also an important task to describe our system further by identifying the genes controlling germ band invasion.

Aim 2: to identify the molecular mechanisms acting downstream of these systemic regulators

We would like to unravel mechanisms and players acting downstream of transcription factors that are key to tuning germ band invasion. We would like to identify several principle downstream targets that could, together or separately, explain the strategy utilized by the macrophage when they are trying to migrate in confinement. We hope that this will shed more light on this process *per se* and will aid our understanding of the parameters crucial for this mode for migration.

II. Identification of novel molecular players with the previously unknown role in migration

Aim 3: to identify novel regulators of migration in confinement

As macrophage germ band invasion parallels cell migration in confinement we would use the main advantage of *Drosophila* as a model system, i.e. relative ease of genetic screens, to find novel regulators of this process with previously unknown role in migration. We would test their possible interaction with the other components identified in the screen. This possible novel piece of information could have important practical implications and would have to be tested in vertebrate model organisms.

Methods

Fly strains and genetics

Flies were raised on standard food bought from IMBA (Vienna, Austria) which contained agar, cornmeal, and molasses with the addition of 1.5% Nipagin. Adults were placed in cages in a Percival DR36VL incubator maintained at 25ºC and 65% humidity; embryos were collected on standard plates prepared in house from apple juice, sugar, agar and Nipagin supplemented with yeast from Lesaffre (Marcq, France) on the plate surface. Fly crosses and embryo collections for RNA interference experiments (7 hour collection) as well as live imaging (6 hour collection) were conducted at 29ºC.

Fly stocks and extended genotypes

srpHemo-GAL4 was provided by K. Brückner (UCSF, USA) (Brückner et al., 2004). *kay^1* was provided by O. Schuldiner (Weizmann Institute of Science, Israel) . *kay^2, vri^{k05901}, tkv^4, cwoB9, gb^{kg07905}*, P{EP}CG10413^{EP2164}, PBac{PB}CG5850^{c03122}, P{EPgy2}MFS15^{EY06280}, P{lacW}Bsg^{k13638}. *(UAS-Fra)2, UAS-Rho.N19, UAS-fbz, UAS-kay* RNAi (TRIP HMS00254, TRIP JF02804) lines, *UAS-vri* RNAi (TRIP HMS02029) line, *UAS-tkv* RNAi (TRIP GL00035, TRIP GLV21018), *UAS-cher* RNAi (TRIP HMS01501), *UAS-dia RNAi* (TRIP HMS05027, TRIP HMS00308) lines, *e22c-GAL4* line were obtained from the Bloomington Stock Center (USA). *UAS-vrille* line was provided by J. Blau (NYU, USA). *UAS-dia.deltaDad.EGFP* line was provided by B. Stramer (KCL, UK). *UAS-cher.FLAG* line was provided by M. Uhlirova (CECAD, Germany). Dad::GFP.nls line was provided by T. Kornberg (UCSF, USA). The *UAS-cher* RNAi line (KK107518), *UAS-bsg* RNAi (KK108920), and *UAS-tm4sf* RNAi (KK111096) lines were obtained from the Vienna Drosophila Resource Center (VDRC), Vienna, Austria.

The lines used in each figure:

Figures 1C, 1D: *Oregon R.* Figures 1G, 1H, 1K, 1L: *srpHemo-GAL4, UAS-GFP.* Figure 1J: *srpHemo-GAL4, UAS-GFP; ; kay^1/kay^1.* Figure 1M: *, vri^{k05901}/, vri^{k05901}; srpHemo-GAL4, UAS-GFP.* Supplementary figure 1A, 1B: *srpHemo-Gal4, UAS-mCD8::GFP*

Figures 2A, 2F, 2M, 2N, 2P and supplementary figures 2D, 2G, 2H: *srpHemo-GAL4, UAS-GFP.nls.* Figures 2B, 2F : *srpHemo-GAL4, UAS-GFP.nls; kay^2/kay^2.* Figures 2C, 2F : *srpHemo-*

GAL4, UAS-GFP.nls/(UAS-Fra)2; kay^2/kay^2. Figures 2D, 2F: *srpHemo-GAL4, UAS-GFP.nls; kay^1/kay^1.* Figures 2G, 2I and supplementary figures 2A, 2C, 2F, 2I, 2K: *srpHemo-Gal4, srpHemo-H2A::3xmCherry.* Figures 2H, 2I and supplementary figures 2A, 2C, 2F, 2I, 2K: *srpHemo-Gal4, srpHemo-H2A::3xmCherry/UAS-fbz.* Figures 2K, 2M*: , vri^{k05901}/, vri^{k05901}; srpHemo-GAL4, UAS-GFP.nls.* Figures 2L, 2N, 2P and supplementary figures 2D, 2G, 2H:: *srpHemo-GAL4, UAS-GFP.nls, UAS-vrille.* Figures 2J, 2O: *srpHemo-GAL4, UAS-GFP, UAS-H2A::RFP.* Figure 2J: *srpHemo-GAL4, UAS-GFP, UAS-H2A::RFP* /UAS-*kayak* RNAi (TRIP HMS00254, TRIP JF02804). Figure 2O: *srpHemo-GAL4, UAS-GFP, UAS-H2A::RFP/* UAS-*vrille* RNAi (TRIP HMS02029). Figures 2P: *srpHemo-GAL4, UAS-GFP.nls; +/kay^1*.

Figures 3A, 3C, 3D, 3E, 3J, 3K, 3H, 3I and supplementary figure 3C : *Resille::GFP/ srpGal4, srpHemo-H2A::3xmCherry.* Figures 3A, 3C, 3D, 3E, 3J, 3K, 3H, 3I and supplementary figure 3C: *Resille::GFP/ srpHemo-H2A::3xmCherry; srpHemo-Gal4/UAS-fbz.* Supplementary figures 2A, 2B, 2D: *srpHemo-GAL4, UAS-GFP.nls.* Supplementary figures 2A, 2B, 2D: *srpHemo-GAL4, UAS-GFP.nls; kay^2/kay^2.* Supplementary figure 3E: *srpGal4, srpHemo-H2A::3xmCherry.* Supplementary figure 3E: *srpHemo-H2A::3xmCherry, srpHemo-Gal4/UAS-fbz.*

Figures 4B, 4D, 4F, 4H, 4I and supplementary figure 4E, 4F, 4G, 4H, 4I, 4J, 4K, 4L, 4M, 4N, 4R, 4S: *srpHemo-Gal4, srpHemo-3xmCherry.* Figures 4B, 4D, 4F and supplementary figures 4E, 4F, 4G, 4H, 4I, 4J, 4K, 4L, 4M, 4N: *srpHemo-Gal4, srpHemo-3xmCherry/UAS-fbz..* Figures 4H, 4I and supplementary figure 4O: *UASDicer2; srpHemo-Gal4, srpHemo-3xmCherry.* Figures 4H, 4I and supplementary figure 4O: *UASDicer2; srpHemo-Gal4, srpHemo-3xmCherry/UAS-cheerio RNAi* (TRIP HMS01501). Figures 4H, 4I and supplementary figure 4O: *UASDicer2; srpHemo-Gal4, srpHemo-3xmCherry/UAS-tm4sf RNAi* (VDRC KK111096). Figures 4J, 4K, 4N: *UASDicer2; srpHemo-Gal4, srpHemo-H2A::3xmCherry.* Figure 4J, 4K: *UASDicer2; srpHemo-Gal4, srpHemo-H2A::3xmCherry/UAS-diaphanous RNAi* (TRIP HMS05027, TRIP HMS00308). Figure 4N: *srpHemo-Gal4, srpHemo-H2A::3xmCherry/UAS-cheerio RNAi* (TRIP HMS01501, VDRC KK107518). Figure 4N: *srpHemo-Gal4, srpHemo-H2A::3xmCherry/UAS-tm4sf RNAi* (VDRC KK111096). Figures 4L: *srpHemo-GAL4, UAS-mCherry.nls.* Figures 4L: *srpHemo-GAL4, UAS-mCherry.nls/UAS-fbz.* Figures 4L, 4M: *srpHemo-GAL4, UAS-mCherry.nls; UAS-diaCA/UAS-fbz.* Figures 4L, 4M: *srpHemo-GAL4, UAS-mCherry.nls; UAS-cheerio/UAS-fbz.* Supplementary figures 4B, 4C, 4D: *srpHemo-Gal4, UAS-mCD8::GFP.* Supplementary figure 4B: *srpHemo-Gal4, UAS-mCD8::GFP/UAS-fbz.*

Supplementary figures 4B, 4C, 4D: *srpHemo-Gal4, UAS-mCD8::GFP/UAS-vrille.*

Supplementary figures 4R, 4S: *srpHemo-Gal4, srpHemo-3xmCherry/UAS-vrille.*

Figures 5A, 5B and supplementary figure 5A, 5B, 5G, 5H : *srpHemo-Gal4, UAS-mCD8::GFP.*
Figures 5A, 5B and supplementary figure 5A, 5B, 5G, 5H: *srpHemo-Gal4, UAS-mCD8::GFP/UAS-fbz.* Figures 5C, 5D, 5E: *srpHemo-Gal4, UAS-LifeAct::GFP, UAS-RedStinger.*
Figures 5C, 5D, 5E: *srpHemo-Gal4, UAS-LifeAct::GFP, UAS-RedStinger/UAS-fbz.* Figures 5F, 5G, 5H and supplementary figure 5C, 5D, 5E, 5F: *srpHemo-Gal4, UAS-CLIP::GFP.* Figures 5F, 5G, 5H and supplementary figure 5C, 5D, 5E, 5F: *srpHemo-Gal4, UAS-CLIP::GFP/UAS-fbz.*
Figures 5I: *srpHemo-H2A*::3x*mCherry.* Figures 5I: *srpQF/ e22CGal4, srpHemo-H2A*::3x*mCherry; QUAS-fbz/UAS-Rho.N12.*

Figure 6A: *srpHemo-GAL4, UAS-GFP, UAS-H2A::RFP.* Figure 6A: *srpHemo-GAL4, UAS-GFP, UAS-H2A::RFP/UAS-thickveins* RNAi (TRIP GL00035, TRIP GLV21018). Figure 6C: *srpHemo-3xmCherry.* Figure 6D: *srpHemo-H2A*::3x*mCherry; UAS-dad.GFP.nls.* Figure 6E: *srpHemo-GAL4, UAS-GFP.nls.* Figures 6E: *srpHemo-GAL4, UAS-GFP.nls; kay^2/+.* Figures 6E: *srpHemo-GAL4, UAS-GFP.nls; +/tkv^4.* Figures 6E: *srpHemo-GAL4, UAS-GFP.nls; kay^2/ tkv^4.*

Figure 7B: *srpHemo-GAL4; UAS-srcEGFP.* Figure 7B: *srpGFP; cwoB9/cwoB9.* Figure 7C: *srpHemo-GAL4, UAS-mCherry.nls.* Figure 7C: *srpHemo-GAL4, UAS-mCherry.nls; cwoB9/cwoB9.* Figure 7E: *srpHemo-GAL4, UAS-GFP.nls.* Figure 7E: *srpHemo-GAL4, UAS-GFP.nls; gb^{kg07905}/ gb^{kg07905}.* Figure 7E: *srpHemo-GAL4, UAS-GFP, UAS-H2A::RFP.* Figure 7E: P{EP}CG10413^{EP2164}/ P{EP}CG10413^{EP2164}; *srpHemo-GAL4, UAS-GFP, UAS-H2A::RFP.* Figure 7E: PBac{PB}CG5850^{c03122}/ PBac{PB}CG5850^{c03122}; *srpHemo-GAL4, UAS-GFP, UAS-H2A::RFP.* Figure 7E: P{EPgy2}MFS15^{EY06280}/ P{EPgy2}MFS15^{EY06280}; *srpHemo-GAL4, UAS-GFP, UAS-H2A::RFP.* Figure 7E: P{lacW}Bsg^{k13638}/ P{lacW}Bsg^{k13638}; *srpHemo-GAL4, UAS-GFP, UAS-H2A::RFP.* Figure 7F: *srpHemo-GAL4, UAS-GFP, UAS-H2A::RFP.* Figure 7F: P{lacW}Bsg^{k13638}/ P{lacW}Bsg^{k13638}; *srpHemo-GAL4, UAS-GFP, UAS-H2A::RFP.* Figure 7F: P{EP}CG10413^{EP2164}/ P{EP}CG10413^{EP2164}; *srpHemo-GAL4, UAS-GFP, UAS-H2A::RFP.*

Cloning and generation of *QUAS-kayDN* line

The fragment of dominant negative Kayak (Kay DN) was amplified from the genomic DNA of *UAS-fbz (UAS-kayDN)* fly line generated by (Eresh, Riese, Jackson, Bohmann, & Bienz, 1997) using primers that encompass a 5' consensus translation initiation sequence followed by bZIP fragment (dominat negative fragment capable of dimerization but not of transactivation) and contain restriction sites for further cloning: 5'-GAAGATCTATTGGGAATTCAACATGACCCCG-3' and 5'-CCCTCGAGTCAGGTGACCACGCTCAGCAT-3'. The resulting fragment was cut using BglII and XhoI resctriction enzymes and ligated into the pQUASt vector to place the gene under the control of 5xQUAS using standard procedures. The final construct was sequenced and injected into the attP2 landing site by the BestGene (https://www.thebestgene.com/).

Embryo staging

Embryos which had completed germband extension were staged for imaging based on the invagination of the stomodeum as well as germband retraction away from the anterior in embryos oriented laterally. Embryos which showed stomodeum invagination but no germ band retraction were classified as Stage 11, embryos which showed stomodeum invagination and germ band retraction with the tip of the germband at 70% embryonic length were classified as early Stage 12, embryos with germband retraction with the tip of the germ band at 60% embryonic length were classified as Stage 12, embryos with the germband fully retracted with the tip of the germ band at 30% embryonic length were classified as Stage 13.

In situ hybridization and immunofluorescence

Embryos were fixed with 3.7% formaldehyde/heptane for 20 min followed by methanol devitellinization for *in situ* hybridization. The *kayak* cDNA clone SD04477 and the *vrille* cDNA clone RE29005 were obtained from the *Drosophila* Genomics Resource Centre (DGRC). T7 or T3 polymerase-synthesized digoxigenin-labelled anti-sense probe preparation and *in situ* hybridization was performed using standard methods (Lehmann and Tautz, 1994). Images were taken with a Nikon-Eclipse Wide field microscope with a 20X 0.5 NA DIC water Immersion Objective. For most antibody stainings, embryos were fixed with 4.0% methanol-free formaldehyde and heptane for 40 min at RT followed by hand devitellinesitaion. Vrille staining was conducted on embryos devitellinized with ethanol. Embryos were mounted

after immunolabeling in Vectashield Mounting Medium (Vector Labs, Burlingame, USA) and imaged with a Zeiss Inverted LSM700 Confocal Microscope using a Plain-Apochromat 20X/0.8 Air Objective or a Plain-Apochromat 63X/1.4 Oil Objective as required. All antibodies and dilutions used are listed in Supplemental Table 2.

Time-Lapse Imaging

Embryos were dechorionated in 50% bleach for 4 min, washed with water, and mounted in halocarbon oil 27 (Sigma) between a coverslip and an oxygen permeable membrane (YSI). The anterior dorsolateral region of the embryo was imaged on an upright multiphoton microscope (TrimScope, LaVision) equipped with a W Plan-Apochromat 40X/1.4 oil immersion objective (Olympus). GFP and mCherry were imaged at 860 nm and 1100 nm excitation wavelengths, respectively, using a Ti-Sapphire femtosecond laser system (Coherent Chameleon Ultra) combined with optical parametric oscillator technology (Coherent Chameleon Compact OPO). Excitation intensity profiles were adjusted to tissue penetration depth and Z-sectioning for imaging was set at 1 µm for tracking. For long-term imaging, movies were acquired for 60 - 150 minutes with a frame rate of 25-40 seconds. Embryos were imaged with a temperature control unit set to either 25 or 29°C depending on the genotype.

Image Analysis

Macrophage cell counts: Autofluorescence of the embryo was used to measure the position of the germ band to determine the stages for analysis of fixed samples. Embryos in which the tip of the germ band retracted up to 60% of embryonic length (Stage 12) were analysed for the number of macrophages that had entered the germband, for the number along the ventral nerve cord (vnc) and in the whole embryo. Macrophages were visualized using confocal microscopy with a Z-resolution of 2µm and the number of macrophages within the germband or the segments of vnc was calculated in individual slices (and then aggregated) using the Cell Counter plugin in FIJI. Total macrophage numbers were obtained using Imaris (Bitplane) by detecting all the macrophage nuclei as spots.

Macrophage Tracking, Speed, Persistence. Mode of Migration and Macrophage GB Entry Delay Analysis

Embryos in which either the macrophage nuclei were labeled with *srpHemo-H2A::3XmCherry* and the surrounding tissues with *Resille::GFP,* or only the macrophages were labeled with *srpHemo>GFP.nls* were imaged and 250x250x40μm^3 3D-stacks were typically acquired with about 0.2x0.2x1μm^3 voxel size at every 39-41 seconds for approximately 2 hours. For imaging macrophages migrating along the VNC movies were acquired for 30 minutes from the time point when macrophages have started spreading into the 6th "segment" (see Fig. S2). Images acquired from multiphoton microscopy were initially processed with ImSpector software (LaVision Bio Tec) to compile channels from the imaging data, and the exported files were further processed using Imaris software (Bitplane) to visualize the recorded channels in 3D. Briefly,

i. The movie from each imaged embryo was rotated and aligned along the AP axis for tracking analysis.

ii. *Detailed description of the macrophage live migration analysis in germ band:*

Embryos expressing *srpHemo-H2A::3XmCherry* and *Resille::GFP* (for outlining germ band) were used for calculating macrophage migration parameters in germ band.

Germ band entry zone is defined as the continuous area starting between ectoderm of germ band and yolk sac, entering further an interface between ectoderm, mesoderm and yolk sac and continuing for the next 10 μm between ectoderm and mesoderm interface. Analysis of macrophage migration in germ band in each movie started at the time point of the first macrophage appearing between germ band ectoderm and yolk sac and ended when the germ band started retraction (typically 60 minutes from the movie was used for analysis).

Post germ band entry is the zone between ectoderm and mesoderm of germ band that starts immediately after germ band entry zone (after initial 10 μm of the interface between ectoderm and mesoderm of germ band) and continues indefinitely. Macrophage migration in post germ band entry zone was analyzed starting from the time when the first macrophage has entered post germ band entry zone and either for 30 minutes, or for less than 30 minutes (in this case until germ band has started its retraction). Only two out of four embryos with macrophages expressing *mac> kayDN* were analyzed for migration in post germ band entry zone as in another two embryos macrophages were not appearing in

post germ band entry zone before germ band retraction onset (due to migration defect in germ band entry zone).

Delay time is defined as the time macrophage nucleus spends at the interface between ectoderm, mesoderm and yolk sac in germ band entry (Delay 2) from the time when it appears there until the time when it starts to move forward along ectoderm mesoderm interface persistently, i.e. starts doing sequential steps in one direction between ectoderm and mesoderm (and consequently leaves the germband entry zone).

iii. Macrophage nuclei were extracted using the spot detection function and tracks generated in 3D over time. The edge of the germband was detected using either Resille::GFP fluorescence or autofluorescence from the yolk and germband. The mean position of the tracks in X- and Y-axis was used to restrict analysis to either of the migratory zones (pre germband, germband entry, post germband entry).

iv. Nuclei positions in XYZ-dimensions were determined for each time point and used for further quantitative analysis.

Cell speeds, trajectory persistence and fits of displacement distributions were calculated using custom Python scripts from single cell positions in 3D for each time frame measured in Imaris (Bitplane). Speed at each moment in time was calculated as an absolute value of the displacement divided by the time between position sampling. Briefly, instantaneous velocities from single cell trajectories were averaged to obtain a mean instantaneous velocity value over the course of measurement. The persistence of cell trajectory was calculated as a mean value of the cosine of the angle between subsequent displacements across the whole trajectory of the cell:

$$Pers(p_1, p_2, \ldots, p_n) = \frac{1}{n} \sum_{i=1}^{n-2} \cos\left(< p_{i+2} - p_{i+1}, p_{i+1} - p_i >\right)$$

where n is a number of position samples for every cell and $p_1, p_2, \ldots, p_n$ are the measured positions of the cell in the (x, y) space, so that $p_{i+1} - p_i$ is a vector indicating a displacement of the cell at the time point i, and $< a, b >$ denotes an angle between two vectors a and b. These persistence values were then averaged over all cell tracks to obtain the mean value for the measurement period.

Average distance to the two nearest cells was calculated for every cell and every time point and then averaged of all cells and all time points:

$$Distance_{2NN} = \frac{1}{T}\sum_{t=1}^{T}\frac{1}{N_t}\sum_{c=1}^{N_t}\frac{1}{2}(d\left(p_c^t, p_{k_c^t}^t\right) + d\left(p_c^t, p_{\hat{k}_c^t}^t\right))$$

where T is duration of the session, N_t is the number of tracked cells at time t and $d(p_c^t, p_i^t)$ is the Euclidean distance between positions of cells c and i at the time t, and k_c^t and $\hat{k}_c^t$ are the indices closest and the next closest cells to the cell with index c at time t correspondingly. I have used two closest cells instead of one to reduce the noisiness of the measure of a distance to a single nearest neighbor.

To characterize the cell migration strategy, maximum likelihood estimation of normal distribution parameters and Levy distribution parameters in the following form:

$$f(x; \mu, c) = \sqrt{\frac{c}{2\pi}}\frac{e^{-\frac{c}{2(x-\mu)}}}{(x-\mu)^{3/2}}$$

were calculated. Because both models have the same number of parameters (2), only the likelihoods of the best fits were compared to choose the best model. As Levy-like movements are described by occasional long displacements with periods of local exploration in-between, I have used average length of "jumps" to compare the movement patterns of different cell populations. The jumps were defined as displacements, whose length exceeded 5 µm per 40 seconds sampling period, so the average value of the jump across a measurement period can be calculated as:

$$Mean\ jump = \frac{1}{T}\sum_{t=1}^{T-1}\frac{1}{N_t}\sum_{c,|p_c^{t+1}-p_c^t|>5}|p_c^{t+1} - p_c^t|$$

where |x| denotes a length of the displacement vector x and the rest of the notations as described above.

Measurement of junctional fluorescence intensities

The cortical intensity of Dia and F-actin (Phalloidin) were calculated (for all genotypes except for *mac>vrille*) using linescan analysis as previously described (Smutny et al., 2010) with the following changes. The line length was approximately 5µm and the line was always drawn in the middle slice of the Z stack (1µm resolution) at the macrophage-macrophage contact. For every line, a Gaussian fit was applied and maximum intensities across the cell

contact were then normalized against average intensities of Dia or F-actin (Phalloidin) staining in the stereotypic germ band area of about 50x50µm^2 in each embryo. The average intensity of the Phospho-Myosin Regulatory Light Chain (MyoP) was calculated by outlining the periphery of the middle Z stack (1µm resolution) of the macrophage and then the average intensities along this line were normalized against average intensities of MyoP staining in the stereotypic germ band area of about 50x50µm^2 in each embryo. The average intensity of Dia staining in *mac>vrille* macrophages was calculated in the same way as for MyoP. Both analyses were carried out using standard Fiji software. 4-5 embryos were used for the analysis of each genotype. Only macrophages located in the pre germ band or germ band entry zones were analyzed.

Cell aspect ratio analysis and imaging actin dynamics

Embryos expressing *srpHemoGal4>UAS-CLIP::GFP* were used for measuring th maximal length and width of the macrophage. Briefly, 250x250x30µm^3 (1µm Z resolution) 3D-stacks were typically acquired at every 35-42 seconds for approximately 1 hour. To measure maximal width and length of cells we used standard Fiji software. We started the measurement from the time when the cell body of the first macrophage fully appeared in the Delay 2 zone (and only the first entering macrophage was analyzed) and for the next 20 µm along the ectoderm mesoderm interface (which corresponds to the germband entry zone). At every timeframe, the lines were drawn along the longest dimension of the cell (from the cell base until the tip of the cell or the tip of the filopodia, typically in the middle of the Z stack), which was considered to be a maximal cell length, and along the orthogonal longest dimension, which was considered to be a maximal cell width. The border between the first and the second entering macrophages was drawn based on the line of uninterrupted CLIP::GFP intensity at the base of the first macrophage. The length to width ratios were quantified for each timeframe and probability density function was plotted: 5 embryos were recorded for each genotype. The length of the filopodia (when it was present) was measured concomitantly. Embryos expressing *srpHemoGal4>UAS-LifeAct::GFP, UAS-RedStinger* were used to image actin dynamics live. Briefly, 250x250x30µm^3 (1µm Z resolution) 3D-stacks were typically acquired at every 35-42 seconds for approximately 1 hour. The filopodia length was measured only for the first entering macrophage from the time when filopodia was first pasted into Delay 2 zone and

until the macrophage has started translocating its cell body into Delay 2 zone (filopodia widens and resolves during this period). 3-4 embryos were recorded for each genotype.

Actin dynamics were measured in the first few entering macrophages from the time point when the first macrophage started its movement from the Delay 2 zone further along the ectoderm mesoderm interface (tail entry zone). Imaging was done until the germband retraction onset. 3 embryos were recorded for each genotype.

FACS sorting of the macrophages

For embryo collection adult flies of either *w+;;srpHemo-Gal4,srpHemo-3xmCherry/+* or w+;; *srpHemoGal4,srpHemo::3xmCherry /UAS-kayDN* genotypes were placed into plastic cages closed with apple juice plates with yeasts for egg laying. Collections were performed at 29°C at 8h-20h light-dark cycle. Since our aim was to obtain macrophages from a narrow developmental time window (stage 11- early stage 12, when macrophages undergo invasive migration into the germ band) we left adult flies to lay eggs for 1 hour, then isolated plates with embryos and let them reach a desired stage by keeping them at 29°C for additional 5 hours 15 minutes. Embryos were harvested in this way for 2 days with about 6-7 collections per day and stored meanwhile at +4°C to slow down development. Collected embryos were dissociated and the macrophages were sorted according to the procedure described in (Gyoergy et.al). About 1-1.5x10^5 macrophages were sorted within 30 minutes.

Sequencing of the macrophage transcriptome

Total RNA was isolated from the FACS-sorted macrophages using Qiagen RNeasy Mini kit (Cat No. 74104). The quality and concentration of RNA was determined using Agilent 6000 Pico kit (Cat No. 5067-1513) on Agilent 2100 Bioanalyzer: about 100ng of total RNA was extracted from 1.5x10^5 macrophages. RNA sequencing was performed by the CSF facility of Vienna Biocenter according to the standard procedures (https://www.vbcf.ac.at/facilities/next-generation-sequencing/). Briefly, cDNA library was synthesized using QuantSeq 3' mRNA-seq Library Prep kit and 3 replicates of each of the genotypes *w+;;srpHemoGal4,srpHemo::3xmCherry/+* or w+;; *srpHemoGal4,srpHemo::3xmCherry /UAS-kayDN)* were sequenced on the Illumina HiSeq 2500 platform.

The reads were mapped to the *Drosophila melanogaster* Ensembl BDGP6 reference genome with STAR (version 2.5.1b) The read counts for each gene were detected using HTSeq (version 0.5.4p3). The Flybase annotation (r6.19) was used in both mapping and read counting. The counts were normalised using the TMM normalization from edgeR package in R. Prior to statistical testing the data was voom transformed and then the differential expression between the sample groups was calculated with limma package in R. The functional analyses were done using the topGO and gage packages in R (Anders, Pyl, & Huber, 2015; Dobin et al., 2013).

qPCR

RNA was isolated from approximately 50,000 *w+;;srpHemoGal4,srpHemo::3xmCherry/+* or w+;; *srpHemoGal4,srpHemo::3xmCherry/UAS-vrille* macrophages using the the procedure described above. Isolated RNA was used for cDNA synthesis using Sensiscript RT Kit (Qiagen, Hilden, Germany) and oligodT primers. A Takyon qPCR Kit (Eurogentec) was used to mix qPCR reactions based on the provided protocol. qPCR was run on a LightCycler 480 (Roche, Basel, Switzerland) and data were analyzed in the LightCycler 480 Software and Prism (GraphPad Software). Data are represented as relative expression to a housekeeping gene (=2-Δct). Below are the sequences of the used primers:

RpL32: Fw pr AGCATACAGGCCCAAGATCG, Rv pr TGTTGTCGATACCCTTGGGC (http://www.flyrnai.org/FlyPrimerBank)

Cher: Fw pr ACCGATGCGGGCAACAACAT, Rv pr GCGATCGCGCACCAGATAC

TM4SF: Fw pr GCAGTCGCAGTTGCAATGCT, Rv pr TGACTCGTAGGCGTGCTCC

Statistics and Repeatability

Statistical tests as well as the number of embryos/ cells assessed are listed in the Figure legends. All statistical analyses were performed using R Studio and significance was determined using a 95% confidence interval. Data points from individual experiments / embryos were pooled to estimate mean and s.e.m. No statistical method was used to predetermine sample size and the experiments were not randomized. An unpaired t-test was used to calculate the significance in differences between two groups and One-Way ANOVA followed by Tukey HSD post tests were used for multiple comparisons.

Representative images in Figure 1, Figure 2, Figure S1 were from experiments that were repeated at least 3 and up to 5 times. In all live imaging experiments each embryo was recorded in a separate day; number of embryos recorded for tracking experiments is 3-4 for each genotype and set up; number of embryos recorded for the macrophage aspect ratio measurements is 4-5 for each genotype; number of embryos recorded with the macrophages expressing LifeAct and RedStinger is 2 for each genotype.

Representative images in Figure 4 and Figure S3 were from experiment that was carried out 1 time. Representative *in situ* images shown in Figure 1 were from an experiment repeated 1 time.

Results

Chapter I. Kayak (dFOS) and Vrille (dNFIL3) circadian transcription factors are regulators of _Drosophila_ macrophage invasion
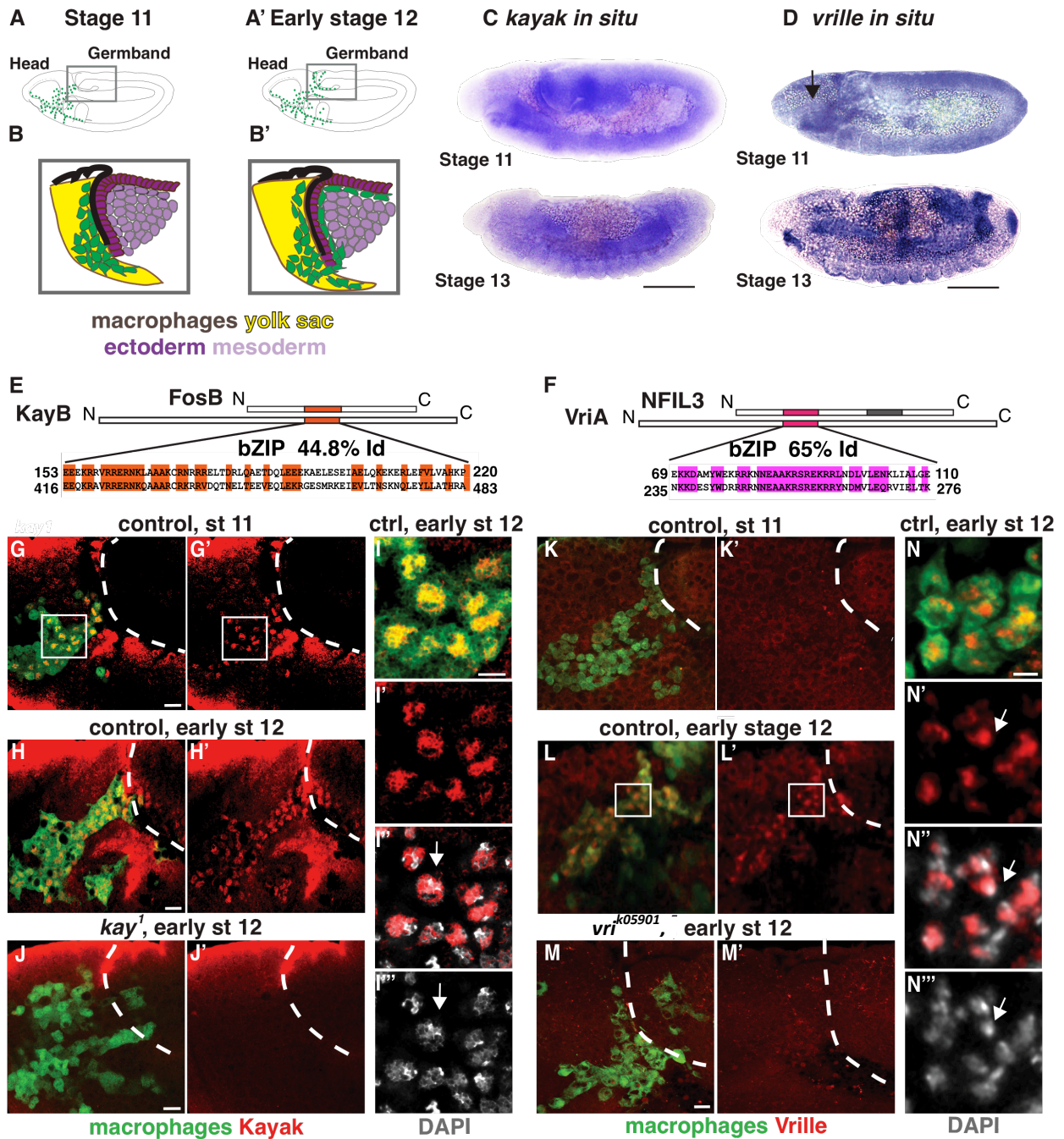
Kayak (dFOS) and Vrille (dNFIL3) circadian transcription factors have opposite effects on the macrophage germ band invasion

Drosophila macrophages originate in the head mesoderm of the embryo at stage 10 and start their movement towards other tissues at stage 11 (Fig .1A, A'). In one of their routes they move towards the germ band and penetrate it at early stage 12 in confined space between ectoderm and mesoderm, thus pushing these two tissues apart ((Ratheesh et al., 2018), Fig .1B and 1B'). The second route goes along the VNC where macrophages move in the less confined space between mesoderm and the yolk sac at late stage 12. Our aim was to identify regulators that could tune macrophage properties to allow efficient germ band invasion in confined conditions. We carried out a genetic screen on pre-selected genes with the enriched expression in the macrophages and focused on transcription factors (TFs) as they could tune cellular properties by switching on a system of downstream effectors. Two circadian TFs from the bZIP family – Kayak and Vrille, orthologs of the mouse FosB and NFIL3 (Fig.E, F) – are some of the few TFs that are transiently up-regulated in the macrophages (Table S1). Kayak (Kay) and Vrille (Vri) are co-expressed in the macrophages on the mRNA level at early stage 11 (Fig.C), and on the protein level at early stage 12 (Fig. G-M) where they persist in the nucleus until stage 13 (Sup.1).

We have used macrophage numbers in the germ band (GB) as a non-direct read out of macrophage GB invasion efficiency. Macrophage number in the GB was significantly reduced in kay^1, kay^2 and significantly increased in , vri^{k05901} homozygous null mutants (Fig.2 A-B, D-K, M). We have to notice that some fraction of kay^1, kay^2 and vri^{k05901} embryos had significant developmental defects (as judged from the gut morphology) and were excluded from the analysis. Macrophage-specific rescue of kay^2 mutant with the wild type counterpart (Fig.2C) as well as autonomous down-regulation of Kayak and Vrille with the _srpHemo::Gal4_ macrophage-specific driver (_mac>)_ and the corresponding RNAi lines and DN version of Kayak (_kayDN_) driven with macrophage specific Gal4 driver has a similar effect

on the macrophage numbers in the GB (Fig.H, L, I) thus implying that Kayak acts in the macrophages to facilitate GB invasion, and Vrille acts to inhibit this process. Moreover, overexpression of Vrille in the macrophages (*mac>vri*) leads to strongly reduced macrophage numbers in GB (Fig. 2N) further confirming the role of Vrille as an inhibitor of migration (overexpression of Kayak didn't have a significant effect, Sup.2A). As *mac>kayDN* and *mac>vri* perturbed function of the corresponding genes autonomously in the macrophages and resulted in the strongest alteration of macrophage numbers in the GB, we performed further experiments and analysis using first and foremost these two alleles. Macrophage numbers in the pre germband zone (between yolk sac and amnioserosa) were not altered in both *mac>kayDN* and *mac>vri* (Sup.2 B-D) suggesting that the earlier processes of macrophage differentiation and migration toward the GB were not regulated by Kayak and Vrille. Moreover, macrophages still spread normally along the second, less confined, VNC route in both *mac>kayDN* and *mac>vri* embryos (Sup. 2 E-G), preliminarily suggesting that Kayak and Vrille are required only for certain types of macrophage migration such as GB invasion. To rule out cell death or proliferation defects we have quantified the total macrophage number. *Mac>kayDN* embryos had decreased total macrophage numbers (Sup.2 I) that was likely a result of the missing last round of proliferation at stage 11 (staining for cleaved caspase CC3 (Sup.2 J-K) and inspecting nuclear integrity did not reveal any difference between control and *mac>kayDN* macrophage thus excluding cell death). Interestingly, reduced total cell number apparently did not prevent macrophages to populate the pre germband and VNC areas. In contrast, *mac>vri* embryos had similar to the wild type total number of the macrophages (Sup.2 H).

Finally, we have tested if Kayak and Vrille could interact genetically. As using classical epistasis test is not feasible (embryos having both kay^1 and, vri^{k05901} homozygous null alleles had severe developmental defects) we though of testing if one can enhance the phenotype of another. To this end we quantified macrophage number in the GB in the embryos of the following genotypes: heterozygous $kay^1/+$, $mac>vri^{weak}$ (attenuated Vrille overexpression in the macrophages) and $kay^1/mac>vri^{weak}$. Interestingly, we found that although $mac>vri^{weak}$ macrophages were present in lower numbers in the GB as compared to control, $kay^1/+$ has further non-additively enhanced this phenotype (Fig.2 P).

This data suggests that Kayak and Vrille have opposite effects on the macrophage germband invasion and could control them through the same pathway or by tuning the same cellular

A Stage 11

A' Early stage 12

C *kayak in situ*

D *vrille in situ*

macrophages yolk sac
ectoderm mesoderm

E
KayB
FosB
bZIP 44.8% Id

153 EEEKRRVRRERNKLAAAKCRNRRRELTDRLQAETDQLEEEKAELESEIAELQKEKERLEFVLVAHKE 220
416 EEQKRAVRRERNKQAAARCRKRRVDQTNELTEEVEQLEKRGESMRKEIEVLTNSKNQLEYLLATHRA 483

F
VriA
NFIL3
bZIP 65% Id

69 EKKDAMYWEKFRRKNNEAAKRSREKRRLNDILVLENKLIALGE 110
235 NKKDESYWDRRRFRNNEAAKRSREKRRYNDMVLEQRVIELTK 276

control, st 11 | ctrl, early st 12

G **G'**

H control, early st 12 **H'**

J *kay¹*, early st 12 **J'**

I **I'** **I''** **I'''**

macrophages Kayak | DAPI

control, st 11 | ctrl, early st 12

K **K'**

L control, early stage 12 **L'**

M *vri^{k05901}*, early st 12 **M'**

**N** **N'** **N''** **N'''**

macrophages Vrille | DAPI

process.

Figure 1. Kayak (Dm-Fos) and Vrille (Dm-NFIL3) transcription factors are co-expressed in migrating

macrophages at stage 12.

A. Schematics of a lateral view of stage 11 embryo showing macrophage (green) migratory routes and a blow-up of the dorsal route (A'): macrophages have left the head and moved onto yolk sac (yellow). Amnioserosa covering yolk sac is shown with the black line.
B. Schematics of a lateral view of an early stage 12 embryo and a blow-up of the macrophage dorsal route (B'): macrophages penetrate the germ band underneath the ectoderm (dark magenta) and appear at the ectoderm - mesoderm (light magenta) interface. They continue migration between ectderm and mesoderm of the germ band.
C. *In situ* hybridization of embryos with Kayak riboprobe detecting all isofroms: stage 11 lateral view; stage 13 lateral view. Kayak expression is enriched in the macrophages before migration.
D. In situ hybridization of embryos with Vrille riboprobe detecting all isofroms: stage 11 lateral view (e); stage 13 lateral view. Vrille expression is enriched in the macrophages before migration.
E-F. Alignment of Kayak (E) and Vrille (F) protein isoforms with the mouse orthologs. Orange and purple boxes indicate conserved bZIP regions of Kayak and Vrille correspondingly.
G. Expression of Kayak protein (red) detected with respective antibody at stage 11: Kayak is present in the subpopulation of macrophages (green).
H. Expression of Kayak protein at early stage 12: Kayak is present in all macrophages.
J. No Kayak staining is detected in the macrophages in kay^1 mutant.
I. Blow up of an area indivcated in (G) showing nuclear localization of Kayak (white arrow).
K. Expression of Vrille protein (red) detected with respective antibody at stage 11: Vrille is not present in the macrophages (green) yet.
L. Expression of Vrille protein at early stage 12: Vrille is present in all macrophages.
M. No Vrille staining is detected in the macrophages in vri^{k05901} mutant.
N. Blow up of an area indicated in (L) showing nuclear localization of Vrille (white arrow).
 In (f)-(h) and (j)-(l) scale bar corresponds to10 µm, in (i) and (m) to 5 µm. Macrophages are labeled using srp-Gal4 driving UAS-GFP. The edge of the germ band is indicated with the dashed line.

Kayak promotes macrophage motility and persistence at the GB entry

To further explore at what point on their way to and through the GB Kayak is important for

migration, we performed live imaging and tracking of macrophages. To outline the GB

borders we generated a line labeling the membranes of the whole embryo and combined it

with the macrophage reporter line in either the wild type or *mac>kayDN* background (Fig.

3A). We collected and recorded embryos at early stage 12, prior to the onset of GB

retraction. During analysis, we split the macrophage path to the GB into several zones in

each of which Kayak appeared to regulate a certain aspect of macrophage motility (Fig.3 B).

First of all, both 3D speed and directional persistence were not affected in the pre

germband zone (Fig.3 C, E) further suggesting that macrophage motility is not compromised

at earlier stages. However, *mac>kayDN* macrophages are delayed on average for 10-15

minutes in the initial entry into the GB (into the zone between ectoderm and the yolk sac -

Delay 1, Fig.3 A, B). This could be caused by either a deficient ability of *mac>kayDN*

macrophages to move into confinement, or by their autonomous inability to efficiently separate from each other. Indeed, wild type macrophages move as a dense group in the pre germband zone, and afterwards start to separate and disseminate along stereotypic routes such as GB and VNC (Sup.3 B).
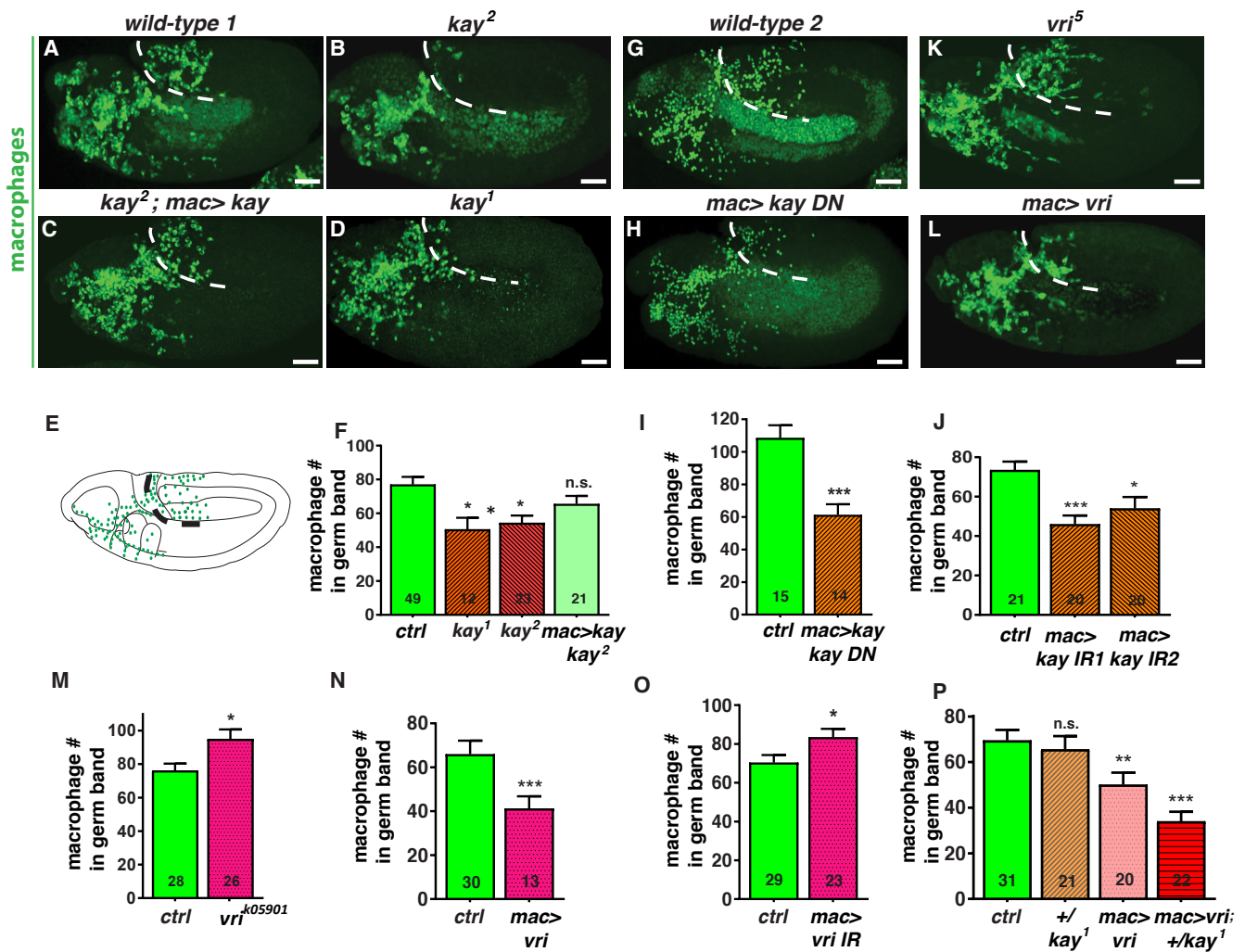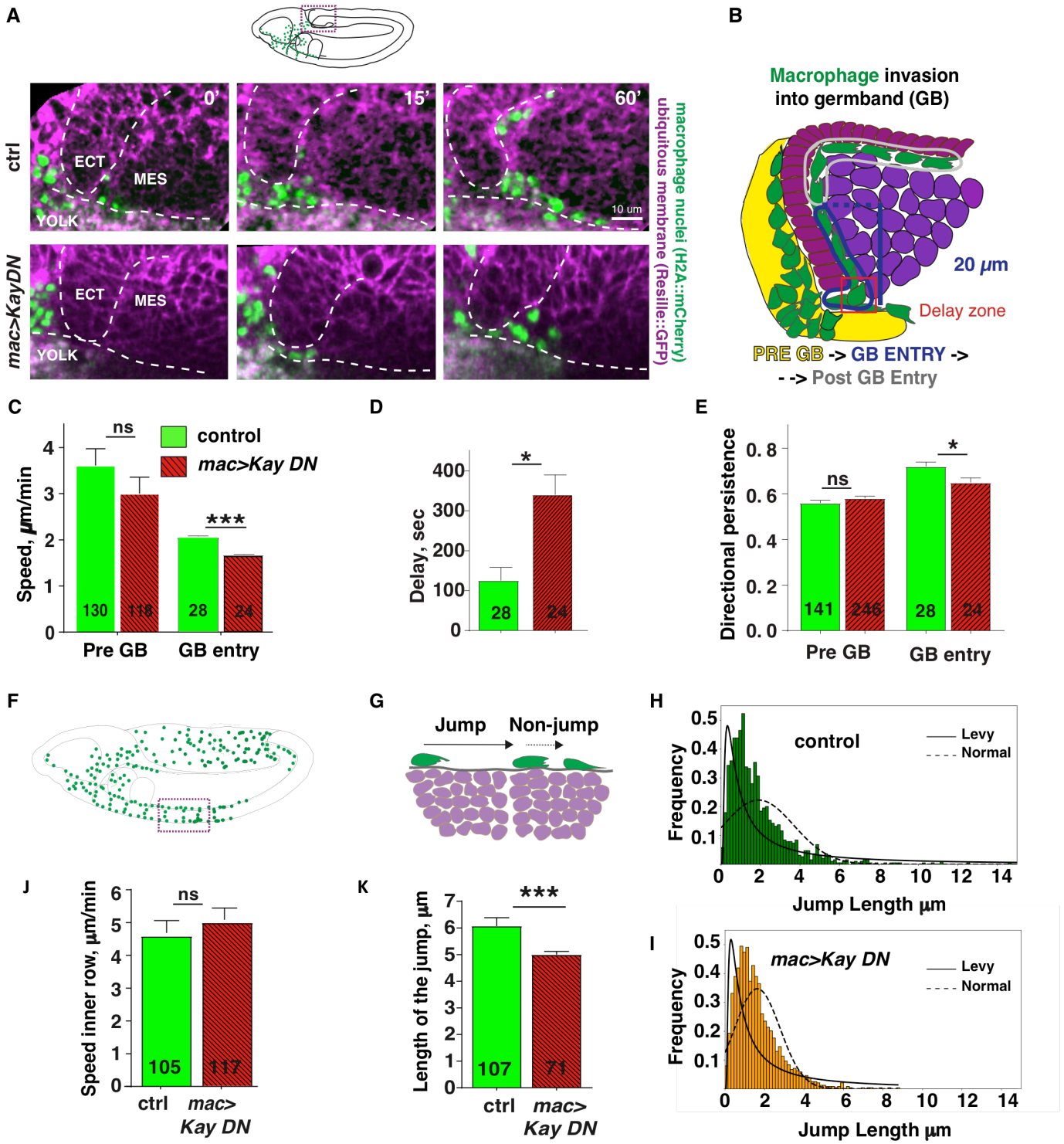
Figure 2. Kayak facilitates and Vrille inhibits macrophage migration into the germband.

A. Mid stage 12 wild type1 embryo.

B. Mid stage 12 *kay²* embryo: macrophage number in germband is reduced.

C. Mid stage 12 *kay²* embryo expressing wild type Kayak in the macrophages: macrophage number in germband is rescued.

D. Mid stage 12 *kay¹* embryo: macrophage number in germband is reduced.

E. Schematics of a lateral view of a mid stage 12 embryo with the macrophages (green) at germband border that is outlined with the black dashed line.

F. Quantification of the macrophage numbers in germband from experiments in (A) - (D).

G. Mid stage 12 wild type 2 embryo.

H. Mid stage 12 embryo expressing dominant negative version of Kayak in the macrophages: macrophage number in germband is reduced.

I. Quantification of the macrophage numbers in germband from experiment in (G-H).

J. Quantification of the macrophage numbers in germband from the embryos expressing Kayak RNAi in the macrophages: macrophage number in germband is reduced.

K. Mid stage 12 , *vri^{k05901}* embryo: macrophage number in germband is increased.

L. Mid stage 12 embryo overexpressing wild type version of Vrille in the macrophages: macrophage number in germband is reduced.

M. Quantification of the macrophage numbers in germband from experiments in (K).

N. Quantification of the macrophage numbers in germband from experiments in (L).

O. Quantification of the macrophage numbers in germband from the embryos expressing Vrille RNAi in the macrophages: macrophage number in germband is increased.

P. Quantification of the macrophage numbers in germband from the embryos having *kay¹*/+ genotype, embryos weakly overexpressing Vrille in the macrophages and embryos with a combination of both:
 macrophage number in germband is non-additively reduced when *kay¹*/+ is combined with the Vrille overexpression..

In (b) - (e), (g) - (h) and (k) - (l) germband border is outlined with the white dashed line. Scale bar corresponds to 10 µm.
 Macrophages are labeled using either srp-Gal4 driving UAS-GFP ((b) - (e), (g) - (h)) or srp::3xH2AmCherry ((k) - (l)).
Histograms show mean +/- s.e.m. ***P<0.005, **P<0.01, *P<0.05. Unpaired t-test was used for statistics of (I), (M), (N), (O) quantifications; one way ANOVA with Tukey post hoc were used for statistics of quantifications (F), (J), (P).
 Number in the box corresponds to the number of analyzed embryos.

However, *mac>kayDN* macrophages do move less efficiently as single cells inside the GB (Fig. 3C, E): the 3D speed and directional persistence were reduced in the germband entry zone (which includes the initial entry between yolk and ectoderm as well as the first 20 uM along ectoderm-mesoderm interface). Moreover, there is the second delay zone (Delay 2, Fig. 3B) at the triple interface within the GB, i.e. between ectoderm, yolk and mesoderm. There the macrophage nucleus "wobbles" for some time before it continues moving persistently further along ectoderm-mesoderm interface. This "wobbling" time is longer for *mac>kayDN* macrophages as compared to wild type ones (Fig. 3D). Interestingly, there was no significant difference in the speed of wild type and *mac>kayDN* macrophages after they passed the first 20 uM along the ectoderm-mesoderm interface, i.e. in the post -germband entry zone (Sup. 3C). The motility phenotype of macrophages in *mac>kayDN* embryos was largely mirrored by the macrophages in kay^2 embryos with the exception of reduced speed in the pre germband zone (Sup. 3A, D), which we think is likely to be a non-autonomous effect of kay^2 mutation as Kayak is also strongly expressed in the ectoderm. Interestingly, *mac>kayDN* macrophages moved along the VNC (the second route that we used as a control) with unaltered 3D speed (Fig. 3J) and spread out normally (Sup..3E). However, the macrophage step size distribution in 2D was shifted: wild type macrophages made more steps with a length of 4 uM or greater while *mac>kayDN* macrophages made more steps shorter than 4 uM (Fig.3 G-I). This is reflected in the fact that the control step size distribution fits better to a Levy than to a normal distribution, while for *mac>kayDN* the situation is the opposite. The average size of the jump made by *mac>kayDN* is significantly smaller as well (Fig.3K).

The live imaging phenotype described above suggests that Kayak is important for macrophage dissemination, long step size generation and motility within the GB.

A

ctrl

0'   15'   60'

ECT   MES   YOLK

mac>KayDN

ECT   MES   YOLK

10 um

macrophage nuclei (H2A::mCherry)
ubiquitous membrane (Resille::GFP)

B

Macrophage invasion into germband (GB)

20 μm

Delay zone

PRE GB -> GB ENTRY ->
- -> Post GB Entry

C

Speed, μm/min

control
mac>Kay DN

ns

***

130 118   28 24

Pre GB   GB entry

D

Delay, sec

*

28   24

E

Directional persistence

ns   *

141 246   28 24

Pre GB   GB entry

F

G

Jump   Non-jump

H

Frequency

control

Levy
Normal

Jump Length μm

J

Speed inner row, μm/min

ns

105   117

ctrl   *mac>
Kay DN*

K

Length of the jump, μm

***

107   71

ctrl   *mac>
Kay DN*

I

Freqency

mac>Kay DN

Levy
Normal

Jump Length μm

47

Figure 3. Kayak facilitates macrophage motility at the germband entry

A. Stills from the movies showing wild type macrophages and macrophages expressing dominant negative version of Kayak entering the germ band (area shown in dashed square in schematics).
The borders of the ectoderm and yolk are shown with the dashed line.

B. Detailed schematics of the germ band showing different zones where the parameters of the macrophage invasion were quantified.

C. Quantification of the speed of the macrophages in the pre GB and GB entry: the speed of the macrophages expressing dominant negative version of Kayak was significantly reduced at the GB entry zone.

D. Quantification of the GB entry delay time: the delay time of the macrophages expressing dominant negative version of Kayak is significantly increased.

E. Quantification of the directional persistence: the directional persistence of the macrophages expressing dominant negative version of Kayak is smaller at the GB entry.

F. Schematics of a lateral view of a stage 13 with the macrophages (green) migrating along the VNC fragment of which is outlined with the black dashed line.
Quantification of the speed of the macrophages moving along the VNC: the speed of the macrophages expressing dominant negative version of Kayak was is not altered.

G. Blow up of an area of the VNC inner row (outlined in (F)) showing macrophages moving on the top of the mesoderm. Macrophages perform two types of steps:
the short one (non-jump) and the long one (jump). The length of the jump of the macrophages expressing dominant negative version of Kayak was significantly reduced.

H-I. Distribution of the macrophage step sizes: distribution of the step sizes of the wild type macrophages fits to Levy distribution better than to normal.
(H: Levy Log-Likelihood: -2436.9129978; Normal Log-Likelihood: -2526.71421681); distribution of the step sizes of the macrophages expressing dominant negative
version of Kayak fits to normal distribution better than to Levy (I: Levy Log-Likelihood: -2918.17012744; Normal Log-Likelihood: -2474.99357689).

J. Quantification of the speed of the macrophages moving along VNC: the speed of the macrophages expressing dominant negative version of Kayak is not altered

K. Quantification of the jump length of the macrophages moving along VNC: the jump length of the macrophages expressing dominant negative version of Kayak is significantly reduced.

Macrophages are labeled using srp::3xH2AmCherry, the rest of the embryos is labeled using Resille::GFP-Histograms show mean +/- s.e.m. Unpaired t-test was used for statistics of all quantifications ***P<0.005, **P<0.01, *P<0.05.

Kayak and Vrille control cortical proteins to regulate GB invasion

To find the mechanisms acting downstream of Kayak and Vrille involved in the regulation of

GB invasion we performed FACS sorting of the macrophages from early stage 12 embryos of

wild type and *mac>kayDN* genotypes and RNA-sequencing of the corresponding

transcriptomes (Fig.4A). We have carried out three replicates and have found consistent

results in all of them. We found several differentially expressed genes with both down- and

up-regulated ones (Table S3.). As the up-regulated genes were mostly stress response

proteins we focused on the down-regulated ones (Fig. 4B-C). In an independent

immunostaining screen we found that the intensity of the formin Diaphanous (Dia) was

reduced at the junctions of the macrophages in germband entry and pre germband zones

in both *mac>kayDN* and *mac>vri* embryos (Fig.4D-E; Sup.4A-C), however, the average

intensity of myoP was normal in *mac>kayDN* (Sup.5 E-F). Given this finding, we decided to focus on two candidates from the list of down-regulated RNA seq targets that could be linked to the junctional localization of Dia: namely, the filamin Cheerio (Cher) and tetraspanin TM4SF. Interestingly, Cher but not TM4SF mRNA is significantly reduced in the *mac>vri* macrophages (Sup.4 Q-R). Indeed, RNAi knock-down of Cher, TM4SF and Dia resulted in significantly reduced macrophage numbers in the germband (Fig.H-I, L) but not in the pre-germband zone or VNC (Sup. 4O, P). Moreover, we were able to rescue the *mac>kayDN* phenotype by overexpressing a dominant active version of Dia (Fig. 4 J). In addition, we have identified a reduction of Dia intensity at the macrophage junctions in both Cher and TM4SF RNAis (Fig.4 F-G; Sup.4N). This suggests that Dia, Cher and TM4SF are targets of Kayak that act to regulate macrophage GB invasion. Cher and TM4SF are transcriptionally regulated by Kayak, while Cher could as well be a direct binding target of Kayak as indicated by Kayak ChIP seq results from the whole embryos (Fig.4 C). Cher and TM4SF in turn are important for localizing Dia at the macrophage junctions. Moreover, the results above suggest that Kayak and Vrille may interact via co-regulation of Cher and thus, non-directly, Dia.


Kayak promotes macrophage rear re-location under the load of the germband ectoderm
As Dia, Cher and TM4SF are known actin cytoskeleton regulators we stained embryos with phalloidin to see if F-actin is affected in the macrophages expressing the corresponding RNAis. Indeed, we saw a reduction in F-actin intensity at the macrophage junctions in the GB entry and pre germband zone in *mac>kayDN* macrophages (Fig.5 A,B).
To figure out what happens with the macrophage on the cellular level we performed live imaging of the macrophages labeled with different cytoskeletal markers – either LifeAct::GFP, RedStinger to label actin and the nucleus or CLIP::GFP to label microtubules. We found that macrophages entering the space between ectoderm, yolk and mesoderm – the place where Delay 2 occurs – first insert filopodia and then relocate there the whole body (Fig.5 C). Both wild type and *mac>kayDN* macrophages formed filopodia, however, as the cell body moved forward along the ectoderm mesoderm interface, intense actin structures were forming around the nucleus of the wild type cell. The first entering cell had the primary filopodia develop into a thicker protrusion, as well as intense F-actin structures

forming behind the nucleus (Fig.5 C). The second cell followed the first one in close proximity and had prominent actin structures forming in front of the nucleus that moved over a minute behind the nucleus (Fig.5 E). This coincided with the forward relocation of the
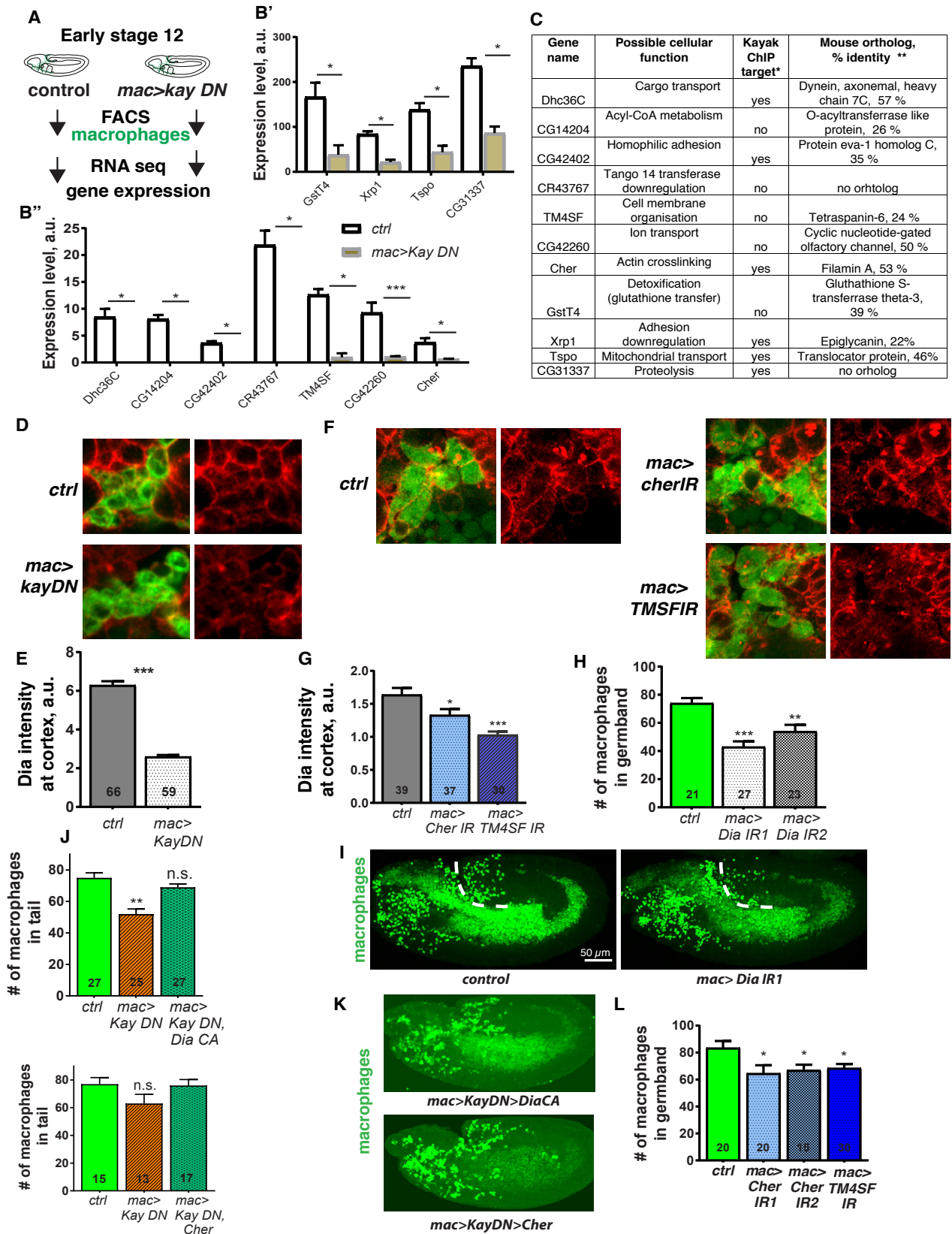
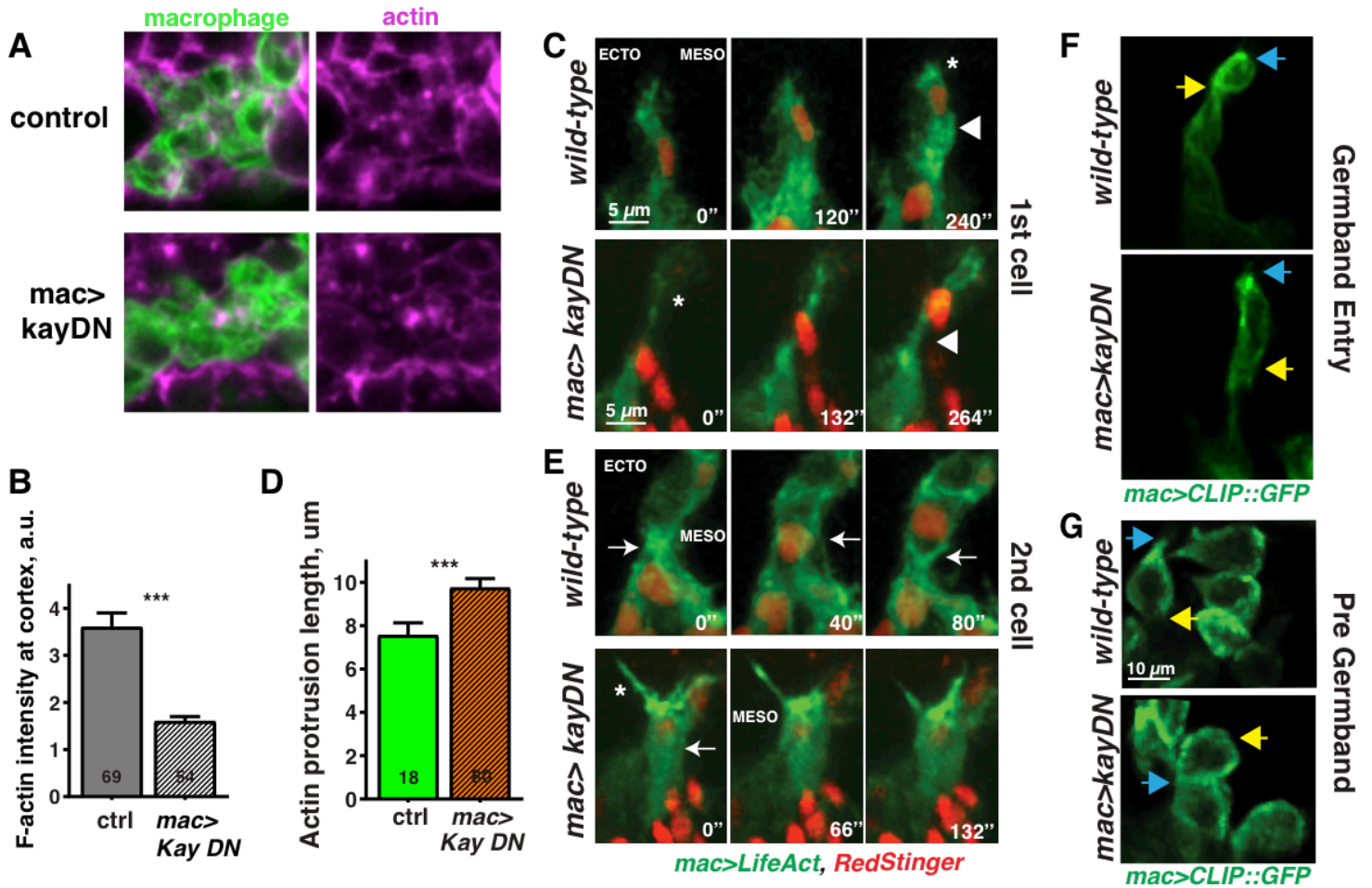**Figure 4.** Kayak regulates macrophage germ band invasion through actin cytoskeleton associated proteins.
A. Schematics representing a pipeline of the macrophage FACS sorting.
B. Expression levels of the genes down-regulated in the macrophages expressing dominant negative version of Kayak. Fold enrichment is normalized
 and multiple comparisons statistical tests are performed as described in the Methods. (B') Genes with the strong expression in the macrophages.
(B'') Genes with the moderate expression in the macrophages.
C. Table describing genes down-regulated in the macrophages expressing dominant negative version of Kayak.
*Kayak ChIP seq data from the whole embryos at stage 16 is kindly provided by J. Zeitlinger.
** Closest mouse protein orthologs were found using UniProt BLAST bioinformatics resource, the top score hit is shown in the table.
D. Dia (red) immunostaining in wild type macrophages (green) and macrophages expressing dominant negative version of Kayak.
E. Quantification of Dia intensity on the macrophage-macrophage junction from the experiment shown in (D): Dia is reduced
at the junctions of the macrophages expressing dominant negative version of Kayak.
F. Dia (red) immunostaining in wild type macrophages (green) and macrophages expressing RNAis against Cher and TM4SF.
G. Quantification of Dia intensity on the macrophage-macrophages junction from the experiment shown in (H): Dia is reduced
at the junctions of the macrophages expressing RNAis against Cher and TM4SF.
H. Quantification of the macrophage numbers in germband from the embryos expressing Dia RNAis in the macrophages: macrophage number in germband is reduced.
I. Mid stage 12 wild type 2 embryo and mid stage 12 embryo expressing Dia RNAi in the macrophages.
J. Quantification of the macrophage numbers in germband from the embryos expressing dominant negative version of Kayak and either dominant active version of Dia
or a wild type version of Cher in the macrophages: macrophage numbers in germband is resscued to the wild type levels when dominant active Dia is expressed in the macrophages.
K. Mid stage 12 wild type expressing dominant negative version of Kayak and either dominant active version of Dia (top)
or a wild type version of Cher (bottom) in the macrophages.
L. Quantification of the macrophage numbers in germband from the embryos expressing Cher and TM4SF RNAis in the macrophages: macrophage number in germband is reduced.
Macrophages are labeled using either srp::3xH2AmCherry (K) or srpGal4 driving UASGFP (D, E, H) or srpGal4 driving UASmCherry.NLS (M). Histograms show mean +/- s.e.m. ***P<0.005, **P<0.01, *P<0.05.
Unpaired t-test was used for statistics of (F), (G),quantifications; one way ANOVA with Tukey post hoc were used for statistics of quantifications (I), (J), (L), (N). Number in the box corresponds to the number of analyzed embryos. In (F, G and I) number in the box corresponds to the number of analyzed macrophage-macrophage juncitons.

nucleus (Fig.5C, E). Nothing similar was observed in the *mac>kayDN* macrophage: the only

prominent actin structures were long thin protrusions forming in the cell front, while in the

back of the cell the actin was mostly diffuse (Fig.5C, E). Correspondingly, the nucleus was

slower in leaving the Delay 2 zone and in passing between the ectoderm and mesoderm.

Labeling microtubules of the macrophages with the CLIP::GFP allowed us to estimate the

aspect ratios of the first entering cell within the first 20 uM of the ectoderm mesoderm

interface (as CLIP::GFP intensity was largely similar between wild type and *mac>kayDN*

macrophages, Fig.5F, G; Sup.5D). We found that in *mac>kayDN* embryos the entering

macrophage was more elongated than the wild type counterpart (Fig.5F, H upper panel)

due to the increased maximal length of the cell body (Sup.5 B). This is, probably, a result of

the reduced speed of the cell rear but not the cell front as judged from tracking the leading vs. trailing edge of the first entering macrophage (Sup.5 C). Microtubule prortrusion length, on the other hand, was the same in both wild type and *mac>kayDN* macrophages (not shown).

Interestingly, we didn't observe such a shift of the aspect ratio in *mac>kayDN* macrophages in the pre germband zone: it remained very similar to the wild type one (Fig.5G, H bottom panel, Sup.5A). This strongly suggests that the GB is imposing some sort of resistance on the entering macrophage that impedes forward nuclear translocation. This effect becomes more severe in *mac>kayDN* macrophages in which the actin cytoskeleton is compromised. We tested this hypothesis by reducing the stiffness of the ectoderm with the expression of dominant negative Rho1 by means of the ectoderm-specific e22C-Gal4 driver (*e22C>RhoDN*). We used the Gal4-independent Q-system to drive a DN version of Kayak in the macrophages (*macQF>QUAS-kayDN)* in the same embryos*.* Indeed, we found that overexpression of the DN Rho1 in the ectoderm partially rescued the macrophage cell numbers in the germband of *macQF>QUAS-kayDN* embryos (Fig.5 I).

The results above suggest that Kayak strengthens the actin cortex of the macrophages to allow them to withstand the load of the surrounding tissues during invasive migration and to efficiently translocate their nucleus.

A

macrophage | actin

control

mac>kayDN

B

F-actin intensity at cortex, a.u.

***

69 | 54

ctrl | mac> Kay DN

C

ECTO | MESO

wild-type

5 μm | 0" | 120" | 240"

mac> kayDN

5 μm | 0" | 132" | 264"

1st cell

D

Actin protrusion length, um

***

18 | 55

ctrl | mac> Kay DN

E

ECTO

wild-type

MESO | 0" | 40" | 80"

mac> kayDN

MESO | 0" | 66" | 132"

2nd cell

mac>LifeAct, *RedStinger*

F

wild-type

mac>kayDN

Germband Entry

mac>CLIP::GFP

G

wild-type

10 μm

mac>kayDN

Pre Germband

mac>CLIP::GFP

H

FRONT

REAR

macro>CLIP::GFP

Probability density

Max L/MaxW in pre-germband

Probability density

Max L/MaxW in germband

I

control | *mac> kayDN* | *mac>kayDN ecto◇RhoDN*

# of macrophages in tail

*

*** | ***

20 | 21 | 21

ctrl | mac> kayDN | mac> kayDN; ecto◇ RhoDN

53

Figure 5. Kayak arranges actin cytoskeleton to facilitate macrophage forward trnaslocation under the load of the ectoderm of the germ band

A. F-actin/phalloidin (magenta) immunostaining in wild type macrophages (green) and macrophages expressing dominant negative version of Kayak.

B. Quantification of F-actin/phalloidin intensity on the macrophage-macrophages junction from the experiment shown in (A): F-actin is reduced
at the junctions of the macrophages expressing dominant negative version of Kayak.

C. Stills from the movies of the first wild type macrophage and the first macrophage expressing dominant negative version of Kayak entering
germband: actin is labelled in green and nucleus is labelled in red. Asterisk indicates an actin protrusion forming at the front and an arrowhead
indicates actin accumulation at the back of the macrophage.

D. Quantification of F-actin protrusion length of the first entering macrophage from the movies: macrophages expressing dominant negative version of Kayak have significantly longer protrusion.

E. Stills from the movies of the second wild type macrophage and the second macrophage expressing dominant negative version of Kayak entering germband: actin is labelled in green and nucleus is labeled in red. Asterisk indicates an actin protrusion forming at the front and an arrow
indicates actin accumulation at the back of the macrophage.

F. Stills from the movies of the first wild type macrophage and the first macrophage expressing dominant negative version of Kayak entering germband: microtubules outline macrophage shape are labelled in green. Blue arrow indicates the front and yellow arrow indicated the rear of the macrophage.

G. Stills from the movies of the first wild type macrophage and the first macrophage expressing dominant negative version of Kayak in the pre germband zone: microtubules outline macrophage shape are labelled in green. Blue arrow indicates the front and yellow arrow indicated the rear
of the macrophage.

H. Schematics of the macrophage showing how the aspects have been measured: vertical dashed line corresponds to the maximum length and the horizontal solid line corresponds to the maximum width. Histograms show the probability density distributions of the aspect ratios (maximum length to maximum width) of the first entering macrophage from experiment shown in (F) (top) and of the macrophages in the pre germband zone from experiment shown in (G) (bottom). Macrophages expresing dominant negative verison of Kayak are more elongated when enter the germband.

I. Schematics and quantification of the experiment with the rescue of macrophage germband entry defect : the number of the macrophages expressing dominant negative version of Kayak in germband was partially rescued by expressing dominant negative version of Rho in the ectoderm.

Macrophages are labeled using either srpGal4 driving UAS::CD8GFP (A) or srpGal4 driving UASLifeActGFP, UASRedStinger (C, E) or srpGal4 driving
UASCLIPGFP (F, G). Histograms show mean +/- s.e.m. ***P<0.005, **P<0.01, *P<0.05.
 Unpaired t-test was used for statistics of (B), (D) quantifications; one way ANOVA with Tukey post hoc were used for statistics of quantifications (I). In (B) number in the box corrsponds to the number of analyzed macrophage-macropge juncitons, in (D) number in the box corrsponds to the number of measurements (timepoints) , in (I) number in the box corrsponds to
 the number of analyzed embryos.

Chapter II. Dpp (BMP) pathway is involved in regulation of *Drosophila* macrophage invasive migration

In a search for possible additional interaction partners of Kayak, we found that Thickveins (Tkv), a receptor of the Dpp ligand, is likely to play a role in macrophage invasive migration into the germband. When Thickveins expression was down-regulated in the macrophages using a macrophage-specific driver (*srpHemo-Gal4* indicated as *mac>)* and

specific RNAi lines, the number of macrophages in the germband was significantly reduced (Fig. 6 A). Interestingly, previously Thickveins mRNA was found to be expressed in the head mesoderm where macrophage originate starting at stage 10, and mRNA of Dpp (Thickveins ligand) is expressed in the germ band at stage 12 (Fig. 6B) (Jackson & Hoffmann, 1994). To see if the Thickveins pathway is indeed active in the macrophages invading the germband, we stained embryos with an antibody against the phosphorylated form of the transcription factor Mad, a conventional reporter of Dpp pathway activity (Mad becomes phosphorylated upon Thickveins activation). We used a commercial antibody raised against the phosphorylated version of the closest mammalian ortholog of Mad, Smad3. We found that pMad is present in a subpopulation of macrophages at stage 10: they formed a small stripe on the ventral side of the macrophage group (Fig. 6 C). To further test the activity of Dpp pathway in the macrophages, we looked at the expression of a Dad::GFP.nls reporter (another conventional transcriptional reporter of Dpp pathway activity that acts downstream of pMad) in macrophages labeled with mCherry::H2A. Complementary to our previous finding, we detected Dad::GFP.nls signal in a subpopulation of macrophages at stage 12 (Fig. 6 D). Interestingly, they were among the first macrophages entering the germ band.

To test if Kayak and Thickveins could act in the same pathway, we performed a genetic interaction test in which we compared macrophage numbers in the germband of the wild type, kay^2/+ heterozygous, +/tkv^4 heterozygous and kay^2/tkv^4 transheterozygous embryos. We found no significant change in macrophage numbers in germ band in the single heterozygous embryos; however, there was a strong reduction in macrophage numbers in the germ band of transheterozygous embryos (Fig. 6 E). This result indicates that Thickveins and Kayak likely act it the same genetic pathway. However, as both of these genes are expressed not only in the macrophages, but also in the tissues of the germ band, it is not clear whether the reduction of the macrophage numbers is caused by macrophage-autonomous action of Kayak and Thickveins.

Altogether, these results point to a possible role of Dpp signaling pathway in a subpopulation of macrophages to regulate invasive migration into the germband. This role could be fulfilled in partnership with Kayak, for example, through interaction between Kayak and Mad (for example, via their direct binding on the promoters of the genes and cooperative activation of transcription).
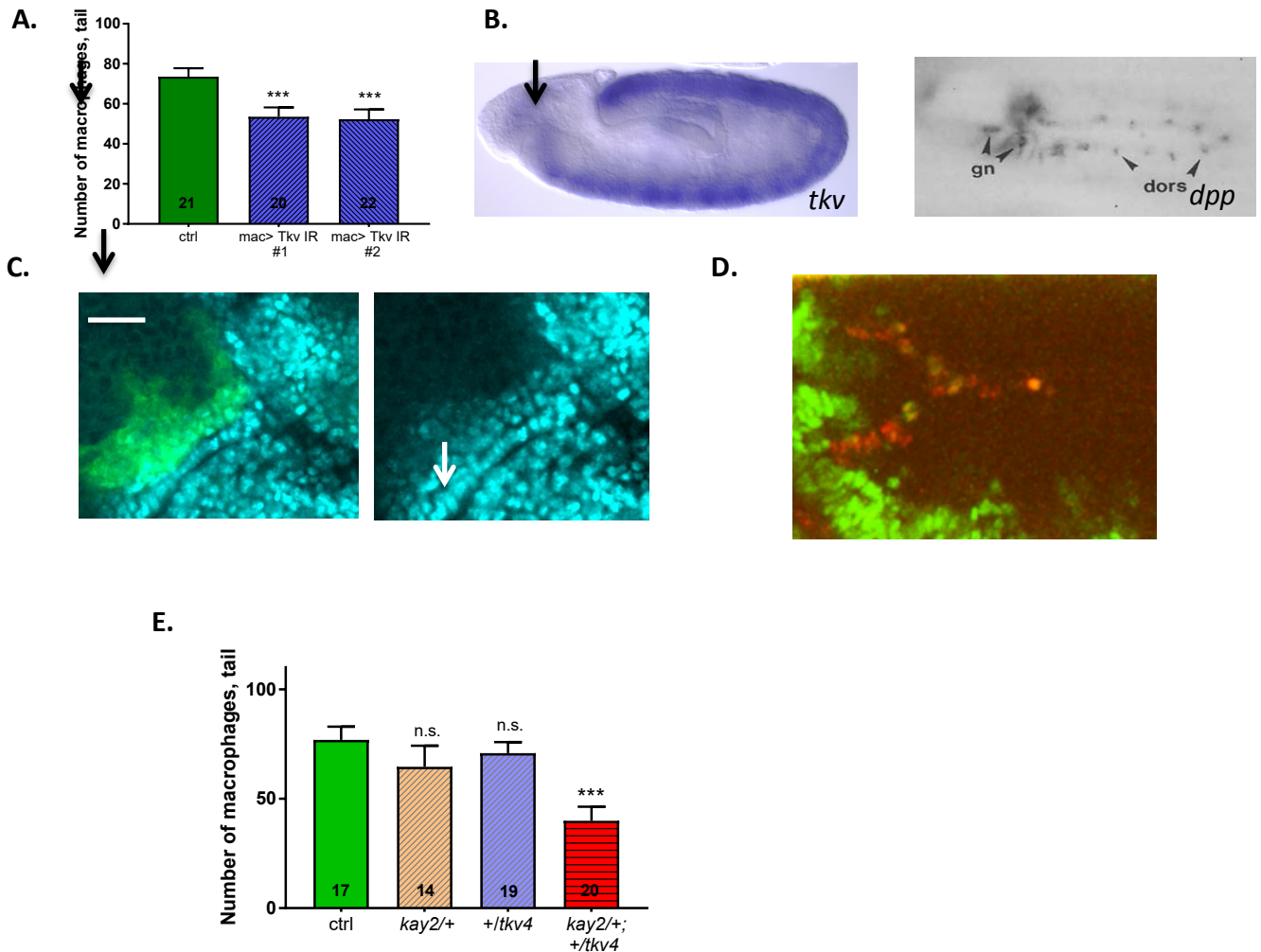
Figure 6. The Dpp pathway is active in macrophages and is important for their number in the germband at stage 12.

A. Quantification of macrophage numbers in the germband from the embryos expressing Thickveins RNAi in the macrophages: the macrophage number in the germband is significantly reduced.

B. *In situ* hybridization of embryos with *thickveins* (left, stage 10, courtesy of BDGP) and *dpp* (right, stage 11, courtesy of (Jackson & Hoffmann, 1994)) riboprobes: lateral view, arrows point to either the head mesoderm (left embryo) or tip of the germband (right embryo). Kayak expression is enriched in the macrophages before migration.

C. Immunostaining of pMad protein (blue) at stage 10: pMad is present in a subpopulation of macrophages (green); lateral view.

D. Snapshot from a movie showing Dad:.GFP.nls-positive macrophages (green, arrow) entering the germband. Macrophages are labeled in red; dorsal view.

E. Quantification of the macrophage numbers in the germband from embryos with a $kay^2/+$ genotype, a $+/tkv^4$ genotype and a combination of both. Macrophage numbers in the germband are significantly reduced when $kay^2/+$ is combined with $+/tkv^4$.

Scale bar corresponds to 50 μm in (B) and to 10 μm in (C) and (D). Macrophages are labeled using either srp-Gal4 driving UAS-GFP (C) or srp::3xH2AmCherry (D). Histograms show mean +/- s.e.m. ***$P<0.005$, **$P<0.01$, *$P<0.05$. One way ANOVA with Tukey post hoc were used for statistics. Number in the box corresponds to the number of analyzed embryos.

Chapter III. Report of the genetic screen for additional regulators of *Drosophila* macrophage invasive migration

The clockwork orange transcription factor is not involved in the regulation of macrophage invasive migration

Another hit in the screen for genes controlling macrophage germband invasion (see Chapter I) was Clockwork orange (Cwo), a Myc-type helix-loop-helix transcription factor that is involved in the regulation of the circadian rhythm of *Drosophila* and acts in this process through an interaction with Vrille (Fathallah-Shaykh, Bona, & Kadener, 2009). Cwo mRNA seems to be expressed in the macrophage anlage (Fig. 7A), and the original result obtained by Cornelia Schwayer, indicated that embryos containing a P-element insertion in Cwo upstream regulatory sequences (*CwoB9*) had increased numbers of macrophages in the germ band (Fig. 7B). This result was not reproduced in the author's own experiment (Fig. 7C). The discrepancy has, probably, arisen from the different reporters used in both experiments. Namely, C. Schwayer has used *mac>GFP* to label macrophages. However, the *CwoB9* allele already contained another UASGFP insertion. This has likely led to an overestimation of the macrophage numbers in *CwoB9* as compared to control embryos. The author, in contrast, used *mac>mCherry.nls* to label macrophages. Therefore, this last result is more reliable than the original one and suggests that Cwo is dispensable for macrophage germ band invasion.

An alternative explanation of this discrepancy is that maternal but not zygotic Cwo is important for the macrophage germ band invasion. In the experiment performed by C. Schwayer parental flies were homozygous for *CwoB9* mutation and therefore had no maternal Cwo mRNA and protein. In the experiment performed by the author parental flies were heterozygous for *CwoB9* mutation and therefore contained maternal Cwo mRNA and protein.

Screen for transporters that could regulate macrophage invasive migration
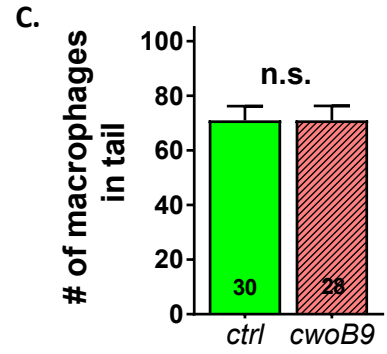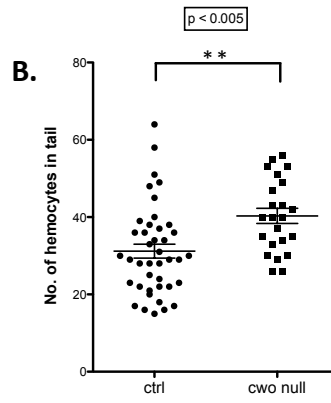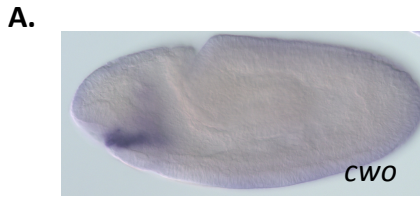
Additional hits in the screen for genes controlling macrophage germ band invasion (see Chapter I) were several transporter proteins. As transporters are largely underexplored yet very intriguing group of proteins that modulate action of their partners and could couple

cell migration machinery with the surrounding environment as well as with cell metabolism, we decided to validate if several transporters found in original screen indeed regulate macrophage germ band invasion. The transporters investigated and corresponding mutant lines were: Genderblind (Gb, a glutamate transporter), $gb^{kg07905}$; CG10413 (an amino acid permease and potassium:chloride symporter), P{EP}CG10413^{EP2164} (P_CG10413); CG5850 (an organic solute transporter), PBac{PB}CG5850^{c03122} (P_CG5850); MFS15 (a major facilitator superfamily transporter), P{EPgy2}MFS15^{EY06280} (P_MFS15). Furthermore, in the same screen Basigin (Bsg), a protein of immunoglobulin superfamily, was found to control macrophage number in germ band (mutant line P{lacW}Bsg^{k13638} (P_Bsg)). As Bsg has been shown to form complexes with monocarboxylate transporters, we thought it could be interesting to test if it is indeed involved in the macrophage invasive migration.
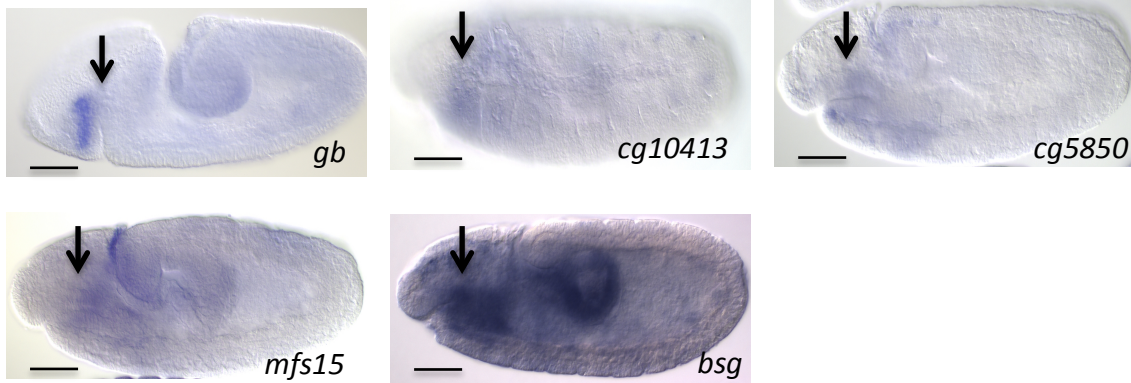
All of the genes indicated above seem to be expressed in the macrophages prior to migration (Fig. 7D). We generated fly lines containing a P-element insertions in the regulatory sequences of the genes of interest (P-element containing flies were ordered from Bloomington Stock Center) combined with *mac>* driving nuclear marker H2A::RFP in the macrophages. We compared macrophage number in germ band in control and corresponding P-element mutants (as described before). The result is shown in (Fig. 7E). Out of all genes tested only Bsg and CG10413 were confirmed to affect macrophage number in germband. CG10413, however, also affected macrophage numbers along the VNC (Fig.7F) and, therefore, is likely to be important for the general migration of macrophages. Bsg had no effect on the macrophage number along the VNC (Fig. 7F).

These results indicate that CG10413 and Bsg are important for macrophage migration. CG10413 is presumably important for general migration, while Bsg is likely to be important specifically for macrophage migration into the germband. However, it is not clear whether both of these genes are required autonomously in the macrophages.

A.

B.

p < 0.005

**

No. of hemocytes in tail

ctrl   cwo null

cwo

C.

# of macrophages in tail

n.s.

ctrl   cwoB9

30   28

D.

gb

cg10413

cg5850

mfs15

bsg

E.

# of macrophages in tail

n.s.

ctrl   gb^{kg07905}/gb^{kg07905}

12   11

F.

# of macrophages in tail

n.s.   n.s.

*   **

ctrl   P_CG10413/P_CG10413   P_MFS15/P_MFS15   P_Bsg/P_Bsg   P_CG5850/P_CG5850

31   27   28   30   24

# of macrophages along VNC

n.s.

*

ctrl   P_CG10413/P_CG10413   P_Bsg/P_Bsg

10   10   9

59
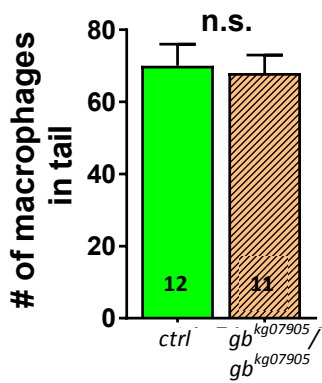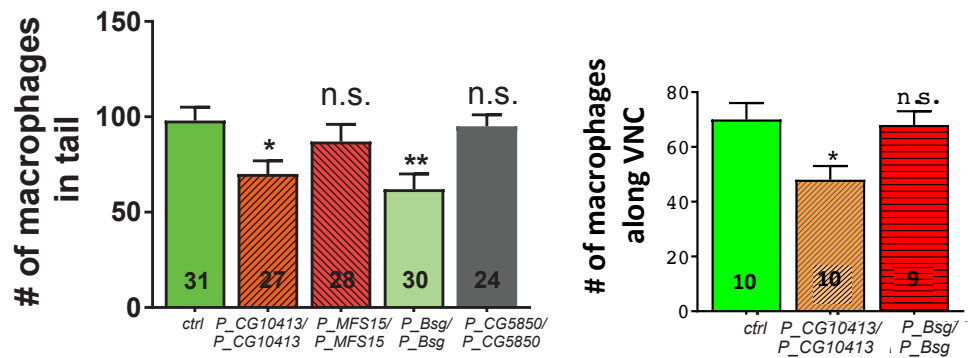
Figure 7. Report of the genetic screen for possible regulators of macrophage germ band invasion.

A. *In situ* hybridization of embryos with the *cwo* riboprobe (stage 11, courtesy of BDGP): lateral view, arrows point to macrophages.

B. Quantification of the macrophage numbers in the germband from *cwoB9* embryos: macrophage number in the germband is significantly increased (courtesy of C. Schwayer).

C. Quantification of the macrophage numbers in the germband from *cwoB9* embryos: macrophage number in the germband is not altered.

D. *In situ* hybridization of embryos with riboprobes against the mRNA of *gb, CG10413, CG5850, mfs15 and bsg* (stage 11, courtesy of BDGP): lateral view, arrows point to macrophages.

E. Quantification of the macrophage numbers in the germband from *gb, CG10413, CG5850, mfs15 and bsg* mutant embryos from the screen: macrophage numbers in the germband are significantly reduced in in P{EP}CG10413^{EP2164} and P{lacW}Bsg^{k13638} mutants.

F. Quantification of the macrophage numbers along the vnc from *CG10413 and bsg* mutant embryos from the screen: macrophage numbers are significantly reduced in P{EP}CG10413^{EP2164} and not altered P{lacW}Bsg^{k13638} mutants.

Scale bar corresponds to 50 μm. Macrophages are labeled using either srp-Gal4 driving UAS-GFP (B and E left graph), srp-Gal4 driving UAS-mCherry.NLS (C) or srp-Gal4 driving UAS-his::RFP (E, right graph, F and G). Histograms show mean +/- s.e.m. ***$P < 0.005$, **$P < 0.01$, *$P < 0.05$. Unpaired t-test was used for statistics in (B), (C), (E left graph) and (G). One way ANOVA with Tukey post hoc were used for statistics in (E right graph and F). Number in the box corresponds to the number of analyzed embryos.

Discussion

<u>Chapter I</u>

Our studies indicate a role for the *Drosophila* transcription factor Kayak in the facilitation of a particular step of embryonic macrophage migration, namely, the invasion of the germband between the ectoderm and mesoderm. In addition, we have found that its partner in the circadian clock machinery (Ling, Dubruille, & Emery, 2012) with a previously unknown role in migration, Vrille, inhibits this step.

Kayak in *Drosophila* has previously been linked to regulation of the cell shape of the epithelium during dorsal closure (Zeitlinger et al., 1997), cell fate decisions (Riesgo-Escovar & Hafen, 1997; Szüts & Bienz, 2000), and the formation of metastases by Ras[v12], *scrib-*tumors (Atkins et al., 2016; Igaki, Pagliarini, & Xu, 2006; Kulshammer & Uhlirova, 2013; Uhlirova & Bohmann, 2006)*.* (Kulshammer & Uhlirova, 2013; Uhlirova & Bohmann, 2006) have shown that the invasive tumor phenotype was caused by the metalloprotease MMP1 and filamin Cher acting downstream of the JNK pathway and Kayak. However, as live imaging is difficult in the adult fly the underlying cause of the increased metastasis rate was not clear. Our work provides evidence that during normal development Kayak is important specifically at the initial step of invading between the confining ectoderm and mesoderm of the germband, suggesting that it acts to allow efficient translocation of the macrophage body under ectodermal load. This is also evident as softening of the ectoderm partially rescues the ability of Kayak-deficient macrophages to enter the germband. Another indication that Kayak regulates the ability of macrophages to translocate into confinement is the fact that, at least in some circumstances, Kayak-deficient macrophages that enter the germband adopt a more elongated cell shape as an apparent consequence of the slower speed of their rear.

We found that Kayak up-regulates the expression of a number of genes potentially involved in actin cytoskeleton regulation, cell adhesion, cell metabolism as well as down-regulates the expression of several heat shock proteins and a transcription factor. We focused on the down-regulated actin cross-linker filamin Cher and an integral membrane protein tetraspanin TM4SF. We found that Kayak, Cher and TM4SF increase the level of the formin Dia at the macrophage cortex. Cher, TM4SF and Dia appeared all to be important for

macrophage germband invasion, while a dominant active version of Dia was capable of rescuing the germ band invasion defect of Kayak-deficient macrophages.

Complementarily, the level and dynamics of F-actin were altered in Kayak-deficient macrophages entering the germband. Live imaging revealed that a massive actin mesh forms at the rear of the first entering macrophage and some sort of actin re-arrangement occurs from the front to the rear of the second entering macrophage (this was observed in two out of three recorded movies). This rearrangement and the rear actin structure were not observed in Kayak-deficient macrophages, although the leading edge filopodia was still present in both wild type and Kayak-deficient macrophages. These results suggest that Kayak shapes the architecture and dynamics of the macrophage actin cortex. We speculate that this could be achieved through the downstream targets of Kayak, Cher and TM4SF, as well as by an indirect effect on Dia. Cher or TM4SF could facilitate the cortical localization of Dia, while Dia promotes actin polymerization there. It has been shown that filamins and tetraspanins can regulate the cortical localization of Rho GTPases (Delaguillaumie, Lagaudrière-Gesbert, Popoff, & Conjeaud, 2002; Kühn & Geyer, 2017; Rousso, Shewan, Mostov, Schejter, & Shilo, 2013; Seth, Otomo, & Rosen, 2006; Stossel et al., 2001) that could, in turn, activate Dia and stabilize its membrane localization. Interestingly, the absence of Dia was found to have no effect on general macrophage migration (Davis et al., 2015) but rather was required for macrophage contact inhibition of locomotion, a process important for normal macrophage distribution during the course of development. Thus, Dia could be specifically required when macrophages face some kind of resistance from the surrounding cells that they have to counteract. In addition, Cher cross-links actin making it elastic and dense, and hence, capable of supporting macrophage shape and of counteracting the resistance of the ectoderm. Indeed, Cher is known to be important for the structural integrity of cardiac and muscle cells for support against mechanical stress (Fujita et al., 2012).

In the future it will be important to dissect which aspect of actin organization is regulated by each of the Kayak targets. Can it be that TM4SF organizes the cortex and defines the places of Dia accumulation, while Cher simply cross-links and increases the stability, rigidity and density of the actin cortex? This could be tested by quantifying actin and Dia intensity and localization in invading macrophages expressing RNAis against TM4SF and Cher, labeled with LifeAct and expressing tagged Dia::GFP live or in fixed embryos with Dia antibody and

Phalloidin staining. The role of Dia in actin polymerization in macrophages can be addressed by live imaging of invading macrophages labeled with LifeAct and expressing RNAi against Dia and then assessing actin intensity and localization. In principle, these experiments can alternatively be carried out in fixed embryos if the macrophages entering the germband are compared in stereotyped positions using either transgenic constructs or antibody staining to label actin and its components.

There are several other aspects of actin organization in the macrophage that could be examined further to unravel the cellular mechanisms of macrophage invasive migration. It has to be emphasized that development of an *in vitro* system for *Drosophila* macrophage migration would be highly beneficial to study the cellular biology of this process as the spatiotemporal resolution of live imaging would increase and photo toxicity would decrease (see "Future directions" for more details). So far imaging invading macrophages with fine cellular details and without photo damage that deep in the embryo has proven to be difficult if not impossible. Assuming that imaging is optimized we could ask how the expression of constitutively active Dia (DiaCA), expressed in macrophages ectopically, rescues the germband invasion of *mac>kayDN* macrophages. In a recent study it was shown that endogenous Dia localizes to the cortex and filopodia of *Drosophila* macrophages (Bilancia et al., 2014). The researchers have also shown that DiaCA regulates formation of actin protrusions with a distinct morphology and dynamics. Interestingly, Dia interaction with another actin nucleator, Ena, was shown to modulate the dynamics of protrusion.

In our study, we have observed that the rear actin mesh as well as the speed of the rear are affected in *mac>kayDN* invading macrophages. However, we cannot exclude that the actin cytoskeleton in the front of the macrophage was affected as well. Therefore, DiaCA could have either rescued actin polymerization uniformly along the macrophage cortex or it could have rescued it only in the rear of the cell. This can be addressed by imaging invading macrophages (using *mac>*) expressing the F-actin marker LifeActRuby and DiaCA fused to GFP. LifeActRuby would allow imaging and quantification of the intensity and integrity of F-actin as a read out of Dia activity in the wild type, *mac>kayDN* and *mac>kayDN* macrophages expressing DiaCA. The question we would seek to answer is where exactly in the cell F-actin is disrupted in the mutant and restored in the Dia rescue, in the front or the rear? A pilot experiment can be carried out in fixed embryos (using either transgenic constructs or antibody staining to label actin and Dia) with further confirmation

by live imaging. If F-actin is indeed rescued by DiaCA selectively in the rear of the cell, it would be interesting to test whether DiaCA::GFP localization to the rear of the cell can explain that bias. It has been shown that a constitutively active Dia-like formin was localized to the rear of the polarized amoeba *Dictyostelium discoideum* and was important for efficient migration in confinement (Ramalingam et al., 2015). Another study has demonstrated an increase in the localization of endogenous mDia1 at the rear upon LPS stimulation and its importance there for the migration of mouse dendritic cells in a confined 2D channel. If DiaCA::GFP localization is indeed biased in the invading *Drosophila* macrophage, it will be interesting to answer which biochemical or physical cues prompt its polarization and how they are translated into a specific localization. Finally, it is worth testing whether the DiaCA construct on its own can facilitate macrophage invasion and, therefore, could have rescued the *mac>kayDN* invasion defect not by compensating for the reduction of endogenous Dia protein at the cortex, but rather by overriding the effects of the other missing Kayak targets. One way to test this hypothesis is to overexpress DiaCA in wild type macrophages and see if the number of macrophages in the germband exceeds the wild type number. If this scenario is observed, it could be that higher levels of active Dia further increase the elasticity of the cortex and allow macrophages to overcome the load imposed by the germband ectoderm faster. However, one might also expect that in this case macrophage number in the germband could be rather reduced as compared to the wild type situation as suggested by recent work by (Chugh et al., 2017), because overly long actin filaments (generated by an excess of Dia) would not generate sufficient tension. In one experimental setup it was demonstrated that *Drosophila* macrophages overexpressing DiaCA have a reduced velocity during the inflammatory response to wounds (Bilancia et al., 2014).

In live imaging and electron microscopy experiments one could assess the actin dynamics, intensity and distribution in wild type macrophages expressing DiaCA to explain its effect on the properties of the actin cortex. Another way to test the specificity of the macrophage invasion rescue by DiaCA is to try to rescue the macrophage invasion defect caused by mutation of a gene that has nothing to do with endogenous Dia levels.

Our data also causes us to wonder if the degree of actin cross-linking is an important parameter modulated to facilitate invasion, since the filamin Cher is a transcriptional target of Kayak and is important for the macrophage invasion. If cross linking is truly the function

provided by Cher for invasion then expressing Cher and other *Drosophila* cross-linkers (e.g. fascin) should be able to rescue the germband invasion phenotype. If only Cher is capable of rescue, this would mean that Cher plays a more specific role and it would be interesting to figure out, what. If Cher rescue works, it could be that Cher can bring another formin to the macrophage cortex in the rescue experiment and thus restores both cross-linking and actin polymerization (or it could also be that the levels of Dia that remain at the cortex of *mac>kayDN* macrophages polymerize sufficient levels of actin to rescue macrophage invasion when this actin is cross-linked by an ectopically overexpressed Cher).

Since macrophages move as a dense group of cells, several aspects of their group migration could also be tuned by Kayak. *mac>kayDN* macrophages are slowed down already in their initial germ band entry, when they move between the ectoderm and the yolk sac, and therefore accumulate more slowly within the germband. Can it be that this reduced accumulation itself contributes to the slower speed of migration on the interface of the ectoderm and mesoderm, for example, if front macrophages use rear macrophages as a stiff substrate to push themselves forward? To test this, the number of invading macrophages could be reduced by expressing RNAi against cyclins in the macrophages and then their speed could be estimated. Another aspect of macrophage group migration is that there is a leader cell that is followed by the rest of the macrophages. If this leader cell expresses *mac>kayDN* and hence is deficient in invasion, would this be sufficient to inhibit the invasion of the wild type follower macrophages? The answer is likely to be partially yes, since the first five invading macrophages had similarly reduced migration speed (and, therefore, contributed to the final reduction of the invasion speed). However, it is interesting to test to what extent the first cell contributes to invasion, particularly, due to the previous study that has suggested that specifically in the conditions of the increased stiffness of the ectoderm in the *eiger* mutant embryos the first cell is the only one that had decreased speed (Ratheesh et al., 2018). However, the situation in the wild type could be different from the one in *eiger[1]* mutant.

This can be done by means of clone generation using Cre-recombinase expressed from a heat-shock promoter and a *mac>STOP>kayDN* construct. Cre-recombinase would stochastically excise the stop-cassette from a *mac>STOP>kayDN* construct and generate Kayak-deficient macrophages that could occasionally occur in the leading position. After that the macrophage number in the germband can be quantified as a primary read out of

invasion efficiency or the speed of the invading macrophage could be measured after live imaging. Live imaging is particularly informative since follower cells can take over leader position (in case the leading cell is not performing its function) and rescue the invasion, the process that can be detected only during live imaging (or it will never occupy the leader position).

Furthermore general aspects of macrophage migration into the germband could be explored. For example, do macrophages rely on Integrin-based adhesion at the germband entry where Kayak promotes macrophage motility? If not, how do macrophages generate traction forces at germband entry? At an early stage the ECM just starts being deposited (Matsubayashi et al., 2017) and it could well be that macrophages have to rely on Integrin-independent adhesion. It is challenging to completely remove Integrin signaling specifically from the macrophages by eliminating both mRNA and maternal protein. One possibility to test the requirement for Rhea, the fly Talin, in the macrophages is to generate a CRISPR null mutant of *rhea* in the macrophages using a macrophage-specific driver to express a guide RNA against Rhea (however, no such experiments have been carried out so far in *Drosophila*). In case there is no effect on the macrophage invasion one has to exclude the possibility that maternally deposited Rhea product compensates lack of zygotic Rhea in the macrophages. To do this one could develop and use dominant negative version of Rhea that would block both zygotic and maternal protein (a dominant negative can represent the variant of wild type Rhea that would be depleted of a vinculin-binding domain and thus would reduce the ability of the cell to form stable adhesions by competing with the wild type Rhea).

It is tempting to speculate that the first macrophage entering the germband uses the dense actin mesh at the cell rear to push its nucleus between the ectoderm and mesoderm and thereby open a gap between these two tissues, while the second macrophage, at least in some cases, uses a rearward actin flow to generate a traction force (Paluch et al., 2016) and propel itself forward in the gap opened by the first macrophage. For the first entering macrophage, this could be tested by increasing the stiffness of the ectoderm (for example, by ectopic expression of dominant active Rho1) and observing and quantifying the density of the actin at the cell rear using LifeAct, quantifying the speed of the nucleus and of the cell rear at germband entry: the prediction is that under increased ectodermal load the actin mesh would intensify while the speed of the first entering macrophage would decrease. The

best functional test would be to disrupt the actin cortex at the rear of the first entering macrophage by expressing a specific regulator of the actin cortex in the rear using mosaics and to quantify the speed of its nucleus. The specific regulator of the rear actin assembly can be searched for in an RNAi screen where specific rear actin structures will be used as a read out. For the second entering macrophage, the presence of actin flow has to be confirmed by using higher time resolution imaging, potentially with light sheet microscopy, and also observing myosin dynamics. Next, a correlation of the speed of the observed rearward actin flow and forward nucleus movement can be done to test for a possible link between these two events. After that, an *in vitro* system should be used to test whether actin flow in the second macrophage generates traction forces on the walls of the confinement channel it enters. Traction forces can be measured by tracking beads embedded in the walls of the confinement channel (Paluch et al., 2016) and then have to be correlated with the rearward actin flow and forward nuclear displacement. Finally, functionality of the actin flow can be tested by genetically blocking it using myosin inhibitors and then quantifying the forward displacement of the nucleus as well as the traction forces generated by the macrophage.

Another result of our research is our identification of targets downstream of the mammalian ortholog of Kayak, Fos, that were previously unknown. Studies of the mechanisms acting in cell migration downstream of Fos have unraveled several downstream regulators (Galvagni, Orlandini, & Oliviero, 2013; Kelley, Shahab, & Weed, 2008; Lamb et al., 1997; Milde-Langosch, 2005; Ramachandran et al., 2011), however, filamins and tetraspanins have never been identified as downstream targets of Fos. In collaboration with Prof. Maria Sibilia (Medical University of Vienna) we have found that expression of the various filamins as well as the closest ortholog of TM4SF is enhanced in c-Fos induced bone cancer in the mouse (data not shown). It would be of particular interest to investigate why Fos up-regulates filamins and tetraspanins in this particular tissue and condition and if there are any circumstances of migration that these tumor cells engage in which that can be beneficial.

In addition, nothing is known about the role of NFIL3/E4BP4, a mammalian ortholog of Vrille, in cell migration and about its interaction with Fos, which are the important questions to address in the future. Additional experiments can substantiate Vrille's role in invasive migration into the germband as well as confirm the molecular players acting

downstream of Vrille. These experiments include defining which step of migration is affected when Vrille is overexpressed in macrophages (by live imaging and tracking), testing if Cher and Dia are up-regulated in the *vrille* null mutant macrophages as well as performing an epistasis test for Vrille and Kayak interactions by combining the *vrille* null mutant with dominant negative Kayak expressed in the macrophages. Of course, another more comprehensive approach is to do RNA sequencing to search for all Vrille targets and to see if there are the ones shared with Kayak.

In summary, we have identified transcription factors that together tune the invasive migration of *Drosophila* macrophages: Kayak tunes macrophage cortical proteins and Vrille inhibits them. This raises the interesting possibility that the systemic modulation of a set of proteins can allow the cell to acquire certain physical properties to adapt and migrate in a particular tissue environment. It would be interesting to investigate whether there is some kind of combinatorial codes set by different transcription factors, each of which would define a particular mode of cell migration.

Chapter II

Our results point to a role for Dpp signaling in macrophage invasive migration, and to the fact that the Dpp pathway can act together with Kayak. It was demonstrated that the Dpp pathway interacts with Kayak in gut cell fate specification during *Drosophila* embryo development (Szüts & Bienz, 2000), and both Dpp and Kayak are important for dorsal closure of *Drosophila* embryo (Zeitlinger et al., 1997). However, the Dpp pathway and Kayak have never been linked to the regulation of cell migration autonomously in the migrating cells in the fly, although in mammals the BMP pathway and Fos signaling are both linked to cancer dissemination and metastasis formation (Papageorgis, 2015).

Moreover, it is intriguing that pMad is active only in a subpopulation of the macrophages, which is also evident for early Kayak expression: Kayak and pMad seem to be present in a similar ventral stripe of macrophages at stage 10. To our best knowledge, the combined

appearance of these two factors in a subpopulation of cells of a defined lineage has not been observed before. However, an interaction between Fos and Smad (the mammalian ortholog of Mad) was described and was shown to promote cancer (Sundqvist et al., 2013). It would be extremely interesting to further investigate the relevance of Dpp signaling for *Drosophila* macrophage invasive migration (especially, if the pMad macrophage subpopulation plays a certain role in this process) and to find if downstream molecular targets are possibly shared with Kayak.

Chapter III

We performed a genetic screen in which we identified previously unknown regulators of *Drosophila* macrophage invasive migration: the gene CG10413 with a putative yet experimentally not proven function in amino acid transport and sodium::potassium symport, and Basigin, an immunoglobulin family protein that could be involved in an interaction with transporters. In the future, it would be interesting to test what exactly the functions of these two genes are in macrophage migration and if they could interact with each other.

Thus, the *Drosophila* embryo has proven itself as an excellent model system to carry out screens and to search for players and downstream mechanisms involved in invasive migration through confined tissues *in vivo.*

Future directions

There are many further directions and questions that one could follow to study macrophage migration. One of them that seems to be of particular interest and importance is to establish an *in vitro* system of macrophage migration. It would very interesting to generate a minimal tissue and extracellular matrix environment based on *in vivo* descriptions of different macrophage routes and the corresponding substrates for migration. One could modulate different parameters (such as the concentration of the matrix, stiffness of the tissues, chemoattractant positioning etc.) to try to make macrophages migrate and to find optimal conditions. Moreover, one could expose macrophages to different types of tissue compositions and observe how they adapt their mode of migration. Another advantage of an *in vitro* system would be to significantly improve imaging possibilities as there would be

no light dissipation in the external embryonic tissues. Two-color live imaging of the macrophages entering the germband is a challenging task as they migrate deep in the tissues where high laser power is required to generate images of good quality; high laser power, in turn, often leads to the phototoxicity and overheating that result in artifacts and the death of the embryo. In addition macrophages migrate in 3D and actively change their positions during invasion, to capture macrophage trajectory fully one needs to acquire multiple Z stacks per timeframe. This, in turn, reduces the spatiotemporal resolution of live imaging, but could be overcome yet again in an *in vitro* system where macrophages could move in a simple 2D microchannel, the shape of which could be modified and made more complex on demand to fit it to different tissue architectures.

Another interesting aspect of *Drosophila* embryonic macrophage migration is that they migrate as a dense group that disseminates over time, but macrophages still maintain physical contacts to each other while migrating within the germband. It is interesting to study the functional significance of these contacts, their types and the dependence of different macrophage functions (such as migration or ECM secretion) on the presence and number of these contacts as well as on the number of macrophages *per se*.
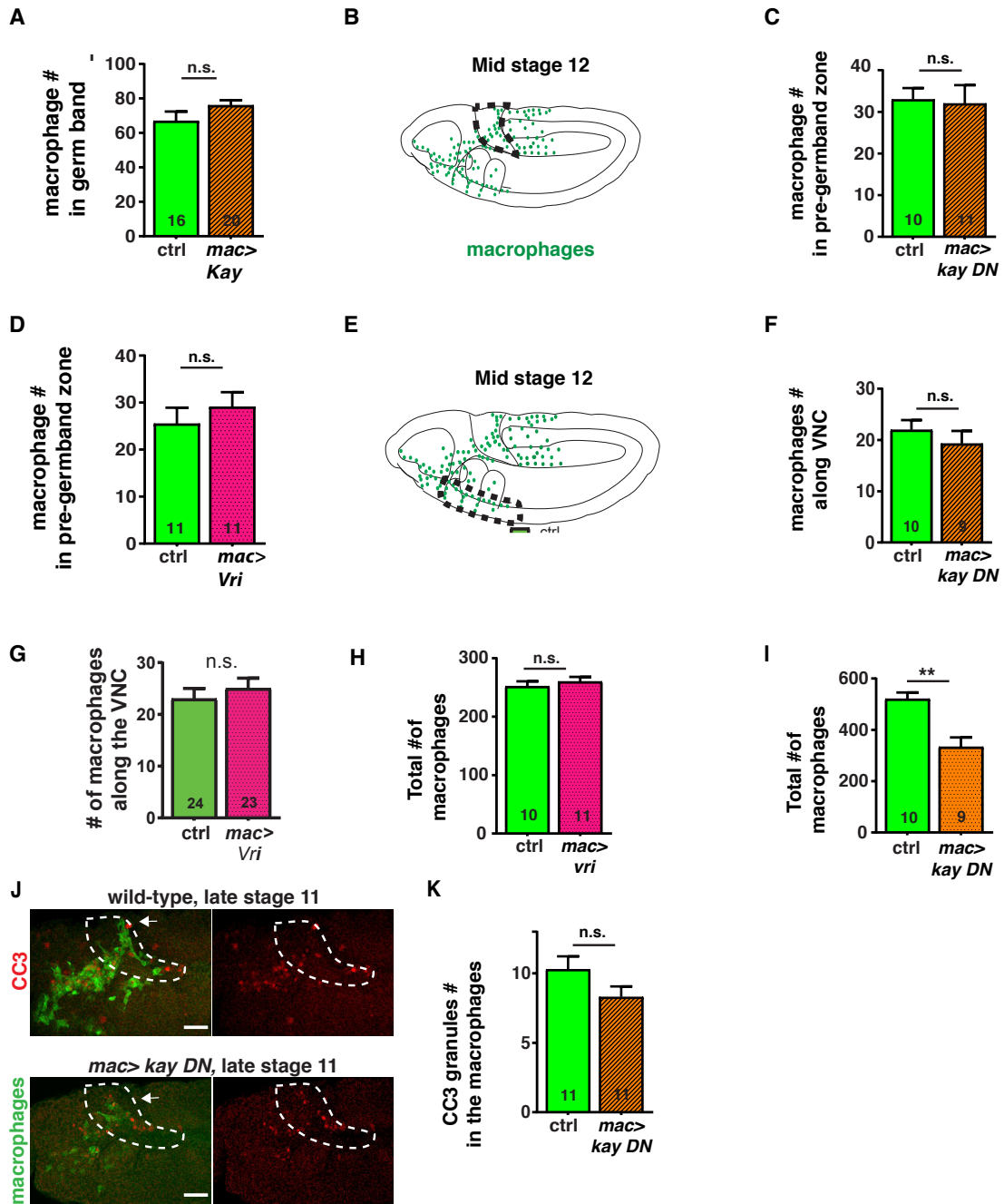
Supplementary information
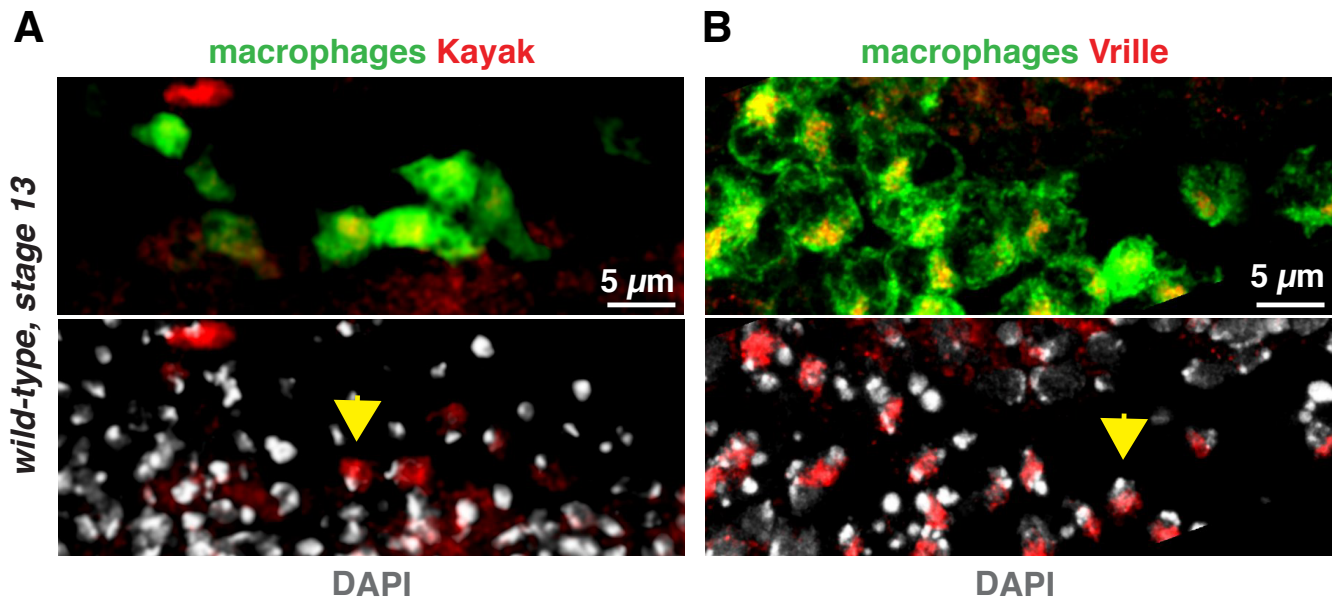
Supplementary figure 1. Kayak (Dm-Fos) and Vrille (Dm-NFIL3) transcription factors are co-expressed in migrating macrophages at stage 13.
A. Expression of Kayak protein at stage 13: Kayak is present in all macrophages.
B. Expression of Vrille protein at stage 13: Vrille is present in all macrophages.

Supplementary figure 2. Kayak facilitates and Vrille inhibits macrophage migration into the germband.

A. Quantification of the number of macrophages that overexpress wild type version of Kayak: macrophage number in germband is not altered.

B. Schematics of a lateral view of a mid stage 12 embryo with the macrophages in pre-tail zone outlined with the black dashed line.

C. Quantification of the number of macrophages that express dominant negative version of Kayak in the pre-tail zone: macrophage number is not altered.

D. Quantification of the number of macrophages that overexpress wild type version of Vrille in the pre-tail zone: macrophage number is not altered.

E. Schematics of a lateral view of a mid stage 12 embryo with the macrophages (green) along VNC route outlined with the black dashed line.

F. Quantification of the number of macrophages that express dominant negative version of Kayak in the VNC route: macrophage number is not altered.

G. Quantification of the number of macrophages that overexpress wild type version of Vrille in the VNC route: macrophage number is not altered.

H. Quantification of the total number of macrophages that overexpress wild type version of Vrille: macrophage number is not altered.

I. Quantification of the total number of macrophages that express dominant negative version of Kayak: macrophage number is not reduced.

J. Apoptotoc corpses in the late stage 11 embryos detected with the anti CC3 antibodies (red): cell death level is not altered in the macrophages (green) expressing cominant negative version of Kayak.

K. Quantification of the apoptotic corpses in the macrophages from experiment in (J).

E. Table with the quantification of the number of macrophages that express dominant negative version of Kayak in the pre-tail zone from live late stage 11 embryos.

Macrophages are labeled using either srp-Gal4 driving UAS-GFP ((c) and (k)) or srp-Gal4 driving UAS-LifeAct::GFP (f). Scale bar corresponds to 10 µm.

Histograms show mean +/- s.e.m. ***P<0.005, **P<0.01, *P<0.05. Unpaired t-test was used for statistics of all quantifications.

A.

B. wild type

C.

D.

E.
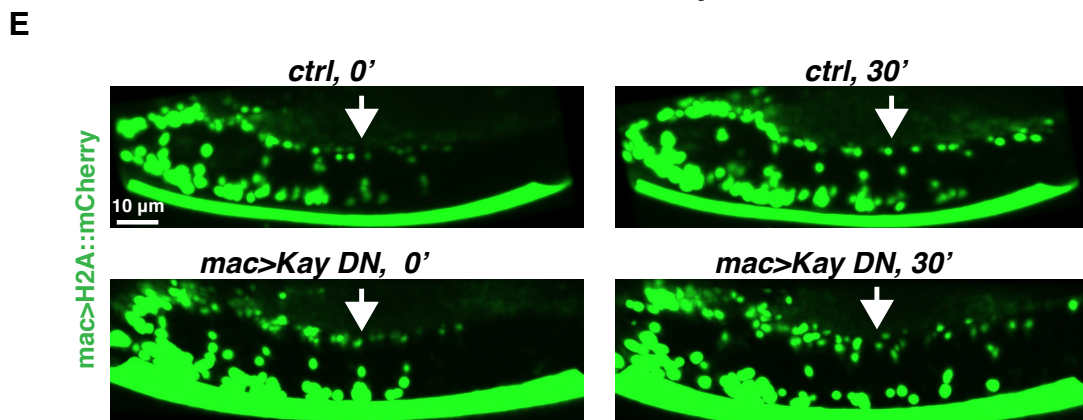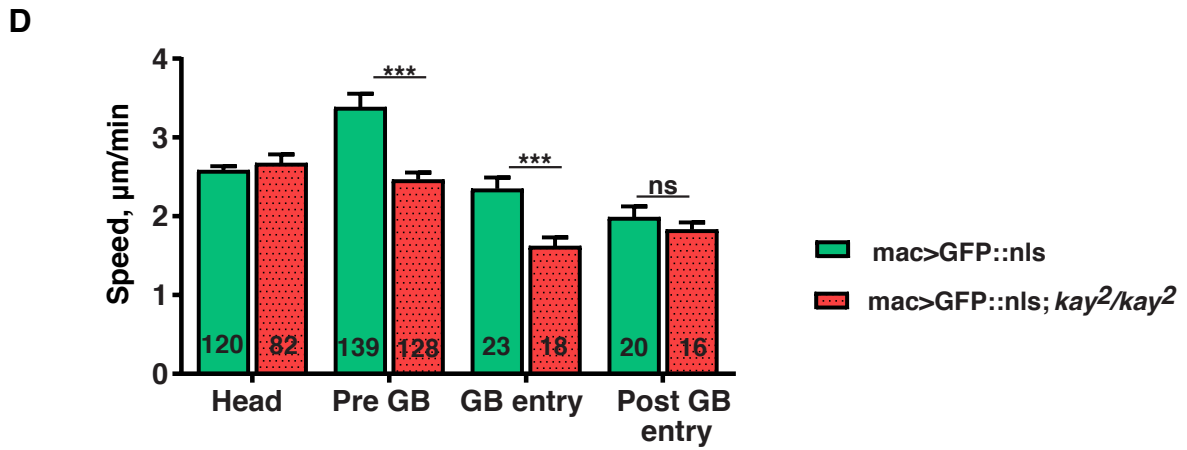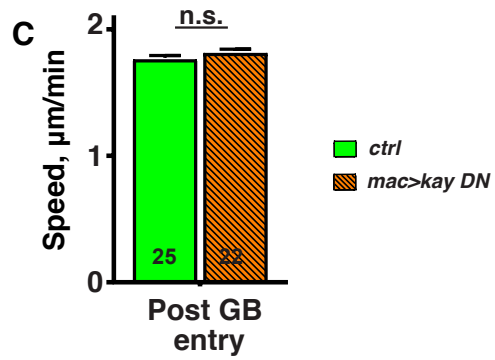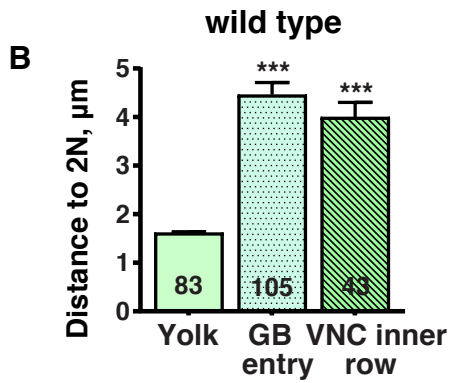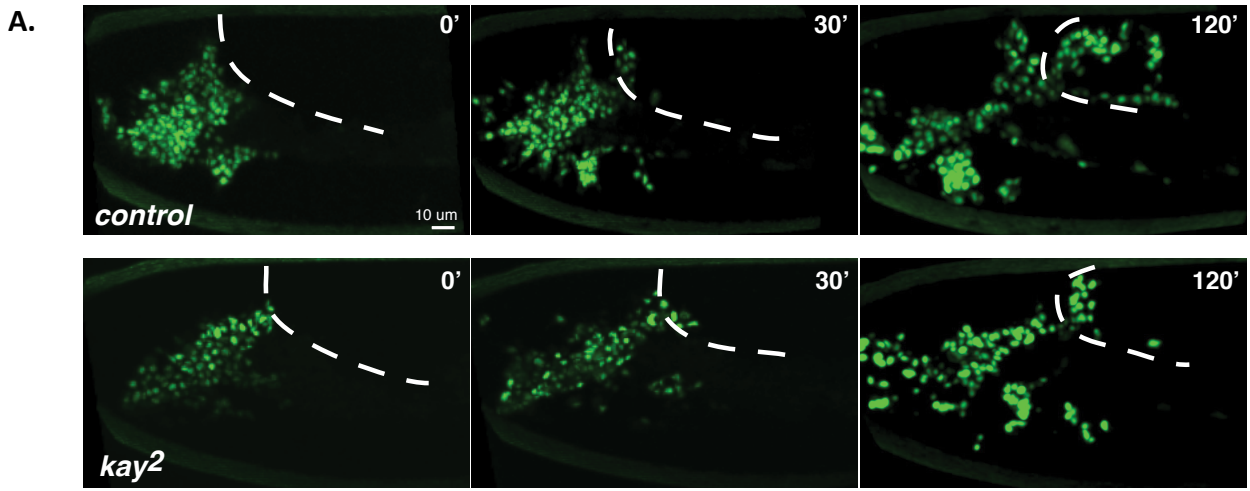
Supplementary figure 3. Kayak facilitates macrophage motility at the germband entry

A. Stills from the movies showing wild type macrophages and kay2/kay2 macrophages entering the germ band (the border of the germband is outlined with the dashed line).

B. Quantification of the distance between macrophage and its two neighbours at germband entry, pre germband and along the VNC route. Macrophages disseminate as

they move along the germband and VNC.

C. Quantification of the speed of the macrophages in the post GB entry: the speed of the macrophages expressing dominant negative version of Kayak is not altered.

D. Quantification of the speed of the macrophages in the head, pre GB entry, GB entry and post GB entry: the speed fo kay2/kay2 macrophages is significantly

reduced in the pre GB entry and at GB entry.

E. Stills from the movies showing wild type macrophages and macrophages expressing dominant negative version of Kayak moving along the VNC inner row (indicated with

an arrow).

Macrophages are labeled using either srpGal4 driving UASGFP.nls (A) or srp::3xH2AmCherry (E). Histograms show mean +/- s.e.m. ***P<0.005, **P<0.01, *P<0.05.

 Unpaired t-test was used for statistics of all quantifications. Number in the box corresponds to the number of analyzed tracks. 3-4 embryos are recorded per each genotype.

A (ctrl, *mac>kayDN*, *mac>Vri*): macrophage Diaphanous / Diaphanous

B Dia intensity at cortex, a.u. — ctrl (33), mac>Vri (34) *

C Dia uniformity at cortex, a.u. — ctrl (33), mac>Vri (33) ***

D Expression level, a.u. — ctrl, mac>Kay DN — Frl, DAAM, Dia, Capu

E Expression level, a.u. — ctrl, mac>Kay DN — Ack-like, Cip4, Cdc42, Miro, Mtl, Rac1, Rac2, Rho1, RhoU, RhoGAP16F, RhoGAP18B, RhoGAP5A, RhoGAPp190, RhoGEF4, RhoGAP93B, RhoL, RhoGAP54D, RhoGAP8F

F Expression level, a.u. — ctrl, mac>Kay DN — Act5C, Act42A

G Expression level, a.u. — ctrl, mac>Kay DN — Cher *, Jbug

H Expression level, a.u. — ctrl, mac>Kay DN — Sqh, Mlc-c, Zip

I Expression level, a.u. — ctrl, mac>Kay DN — Cad87A, Shg, Cals, a-Cat, Arm, p120ctn

J Expression level, a.u. — ctrl, mac>Kay DN — ItgaPS4, If, Mew, Mys, Rhea, Vinc, Ilk, Fak, Pax

K Expression level, a.u. — ctrl, mac>Kay DN — LanA, LanB2, LanB1, Dg, Col4a1, Vkg, Mmp2, CtsB1

L Expression level, a.u. — ctrl, mac>Kay DN — N, Ser, Pvr, Pvf3, Pvf2

M Expression level, a.u. — ctrl, mac>Kay DN — Srp, Gcm, Lz, Gcm2A

N (ctrl, *mac> Cher IR*, *mac> TM4SF IR*): macrophage Diaphanous / Diaphanous

O # of macrophages in pre GB zone — ctrl (20), mac> Dia IR1 (21) n.s., mac> Dia IR2 (21) n.s.

P # of macrophages along VNC — ctrl (18), mac> Dia IR1 (20) n.s., mac> Dia IR2 (20) n.s.

Q. Cher normalized expression — ctrl, *mac>Vrille* ***

76

R. TM4SF normalized expression — ctrl, *mac>Vrille* n.s.

Supplementary figure 4. Kayak regulates macrophage germ band invasion through actin cytoskeleton associated proteins

A. Dia (red) immunostaining in wild type macrophages (green), macrophages expressing dominant negative version of Kayak and macrophages overexpressing
Vrille.

B. Quantification of Dia intensity on the macrophage-macrophage junction from the experiment shown in (B): Dia is reduced
at the junctions of the macrophages overexpressing Vrille.

C. Quantification of Dia uniformity on the macrophage-macrophage junction from the experiment shown in (B): Dia is less uniformly distributed
at the junctions of the macrophages overexpressing Vrille.

(E-M) Comparative (mRNA) expression levels of the different groups of genes in wild type macrophages and macrophages expresing dominant negative version of Kayak:

D. Comparative expression of formin-related genes.

E. Comparative expression of Rho GTPases.

F. Comparative expression of actins.

G. Comparative expression of filamins.

H. Comparative expression of myosin chains.

I. Comparative expression of cadherin-related genes.

J. Comparative expression of integrin-related genes.

K. Comparative expression of ECM-related genes.

L. Comparative expression of PVR and Notch-related genes

M. Comparative expression of cell fate specification genes.

 N. Dia (red) immunostaining in wild type macrophages (green) and macrophages expressing RNAis agains Cher and TM4SF.

O. Quantification of the macrophage numbers in the pre GB zone from the embryos expressing Cher and TM4SF RNAis in the macrophages:
macrophage number is not altered.

P. Quantification of the macrophage numbers along VNC from the embryos expressing Cher and TM4SF RNAis in the macrophages: macrophage number is not altered.

Q. Quantification of the mRNA level of Cher in FACS sorted macrophages through qPCR: Cher mRNA level is significantly reduced in the macrophages overexpressing Vrille,

R. Quantification of the mRNA level of TM4SF in FACS sorted macrophages through qPCR: TM4SF mRNA level is not altered in the macrophages overexpressing Vrille.

Macrophages are labeled using srpGal4 driving UAS::CD8GFP. Histograms show mean +/- s.e.m. ***$P<0.005$, **$P<0.01$, *$P<0.05$; in (R) and (S) histograms show mean +/- s.d.

Unpaired t-test was used for statistics of (C), (D), (R), (S) quantifications; one way ANOVA with Tukey post hoc were used for statistics of quantifications (P), (Q). In (C and D) number in the box corresponds to the number of
analyzed macrophage-macropge juncitons, in (P and Q) number in the box corresponds to the number of embryos.
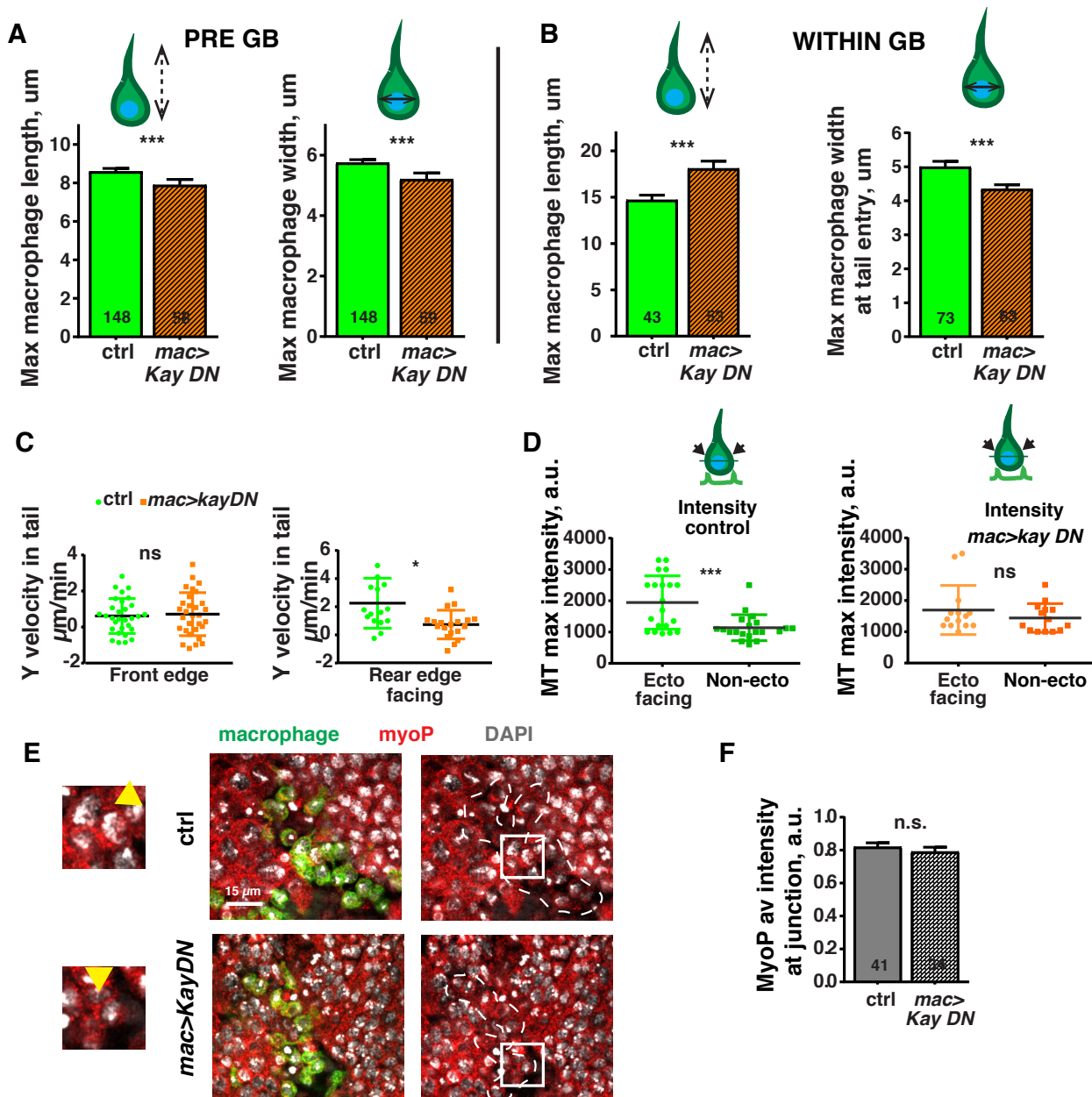
Supplementary figure 5. Kayak arranges actin cytoskeleton to facilitate macrophage forward translocation under the load of the ectoderm of the germ band.

A. Quantification of the maximum length and maximum width of the macrophage in the pre GB zone: macrophages expressing dominant negative

version of Kayak are shorter and thinner than the wild type macrophages.

B. Quantification of the maximum length and maximum width of the first macrophage entering the GB: the rear of the macrophage expressing dominant negative

version of Kayak are longer and thinner than the wild type macrophages.

C. Quantification of the speed of the front and the rear of the first macrophage entering the GB: the rear of the macrophage expressing dominant negative

version of Kayak moves significantly slower.

D. Quantification of the microtubule intensity of ectoderm and non-ectoderm facing side of the first macrophage entering the GB: microtubule intensity of

the ectoderm facing side of the macrophage expressing dominant negative version of Kayak is reduced.

E. MyoP (red) immunostaining in wild type macrophages (green) and macrophages expressing dominant negative version of Kayak.

F. Quantification of myoP intensity on the macrophage cortex from the experiment shown in (G): myoP level is not altered

in the macrophages expressing dominant negative version of Kayak.

Macrophages are labeled using srpGal4 driving UAS::CD8GFP (G). Histograms show mean +/- s.e.m. ***P<0.005, **P<0.01, *P<0.05.
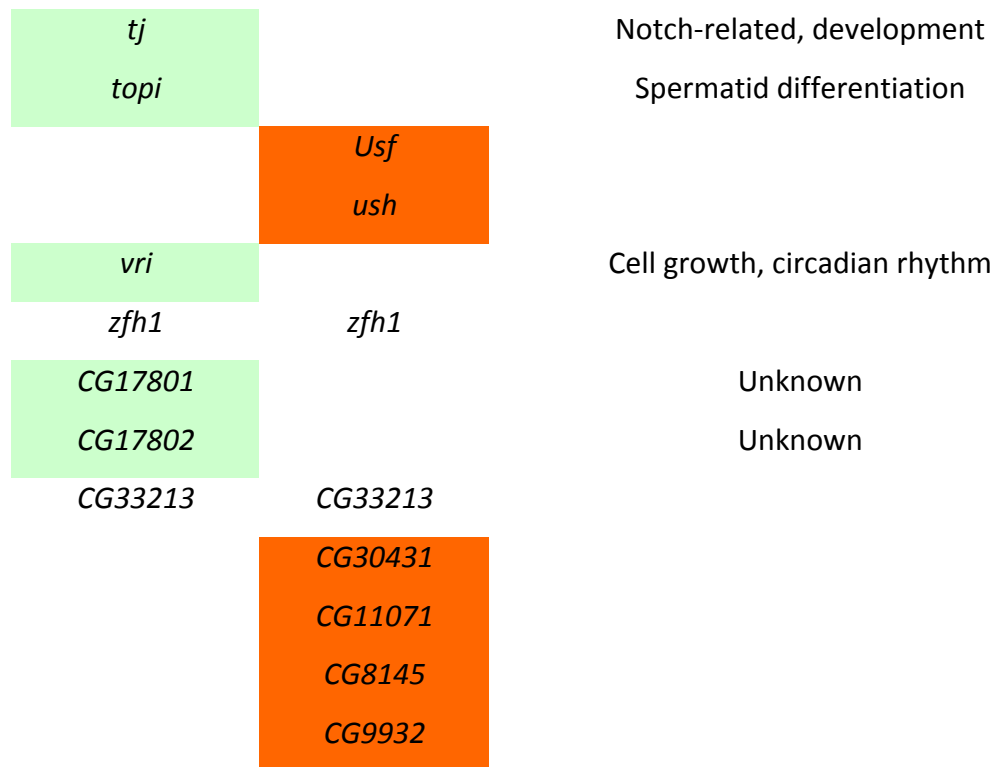
 Unpaired t-test was used for statistics of quantifications. In (B and H) number in the box corresponds to the number of

analyzed macrophage-macrophage junctions, in (C and D) number in the box corresponds to the number of measurements (timepoints).

Table S1. Comparison of transcription factors mRNA expression in the macrophages at stages 11-12 and 13-16 (based on (Hammonds et al., 2013))**.**

Macrophages acquire different TFs profiles at different stages of embryo development. TFs expressed in the macrophages only at stages 11-12 are highlighted in green; TFs expressed in the macrophages only at stages 13-16 are highlighted in orange; TFs expressed in macrophages throughout stages 11-16 are not highlighted. Function is annotated only to TFs expressed in the macrophages at stages 11-12.

Stages 11-12	Stages 13-16	Function
brk		Dpp-related, development
Bteb2	Bteb2	
c15	c15	
croc		Early embryo patterning
	Dif	
	dm	
foxo	foxo	
gcm	gcm	
	gcm2	
ham		Neuronal cell fate
kay		Cell fate determination, circadian rhythm
kn		Early embryo patterning
lz	lz	
Mad	Mad	
MafS		Transcription
MTF1	MTF-1	
odd	odd	
	Pdp1	
	pros	
	Rel	
six4		Development
slp1	slp1	
srp	srp	
svp	svp	

tj   Notch-related, development

topi   Spermatid differentiation

                Usf

                ush

vri   Cell growth, circadian rhythm

zfh1   zfh1

CG17801   Unknown

CG17802   Unknown

CG33213   CG33213

                CG30431

                CG11071

                CG8145

                CG9932

Table S2. List of the antibodies used in this study.

Antibody	Source animal	Type of fixation	Dilution	Provided by
Anti-Diaphanous	Rabbit	Hand devitellinization	1:200	S. Wasserman (UCSD, USA)
Phalloidin 633	-	Hand devitellinization	1:200	Invitrogen (A22284)
Anti-Sqh1P	Guinea pig	4% paraformaldehyde and methanol devitellinization	1:200	R. Ward (KU, USA)
Anti-Kayak	Rabbit	Hand devitellinization	1:50	J. Zeitlinger (Stowers Institute, USA)
Anti-Vrille	Guinea pig	4% formaldehyde and ethanol devitellinization	1:50	J. Blau (NYU, USA).
Anti-GFP	Chicken	4% formaldehyde and methanol devitellinization	1:500	Abcam (ab13970)
Anti-mCherry	Goat	4% formaldehyde and methanol devitellinization	1:200	Invitrogen (M11217)
Anti-Cleaved Caspase (CC3)	Mouse	4% formaldehyde and methanol devitellinization	1:200	R&D Systems (Asp175)
Anti-Smad3 (phospho S423 + S425)	Rabbit	4% formaldehyde and methanol devitellinization	1:200	Abcam

Table S3. Macrophage expression of several genes is regulated by Kayak at the stage of the germ band invasion.

Sequencing of total mRNA from the wild type and Kayak-deficient macrophages sorted from the embryos at early stage 12 (start of the germ band invasion). 3 independent replicates of each genotype were compared. Genes with down-regulated expression are highlighted in red, genes with up-regulated expression are highlighted in green.

* Kayak ChIP seq data from the whole embryos at stage 16 is kindly provided by J. Zeitlinger.

** Closest mouse protein orthologs were found using UniProt BLAST bioinformatics resource, the top score hit is shown in the table.

*** Possible bZIP domain was detected using Prosite bioinformatics resource.

	Expression in the wt macrophages	Expression in *kayDN* macrophages	Adj. p-value	Kayak ChIP target*	Possible cellular function	Mouse ortholog, % identity **
Dhc36C	8.49	0.01	0.02	yes	Cargo transport	Dynein, axonemal, heavy chain 7C, 56.8 %
CG14204	8.09	0	0.03	no	Acyl-CoA metabolism	O-acyltransferrase like protein, 26.3 %
CG42402	3.64	0	0.04	yes	Homophilic adhesion	Protein eva-1 homolog C, 34.6%
CR43767	21.87	0	0.045	no	Endopeptidase downregulation	no orhtolog
TM4SF	12.62	0.97	0.03	no	Cell membrane organisation	Tetraspanin-6, 23.7%
CG42260	9.25	1.05	0.001	no	Ion transport	Cyclic nucleotide-gated olfactory channel, 50.3%
cher	3.73	0.64	0.045	yes	Actin crosslinking	Filamin A, 52.9%
GstT4	166.71	38.23	0.02	no	Detoxification (glutathione transfer)	Gluthathione S-transferrase theta-3, 38.8%
Xrp1	83.93	21.54	0.001	yes	Possible bZIP***	Epiglycanin, 22%
Tspo	138.33	43.93	0.045	yes	Mitochondrial transport	Translocator protein, 46%
CG31337	235.25	86.41	0.045	yes	Proteolysis	no orholog
Hsp70Ab	4.00	36.14	0.0007	no	Unknown	Heat shock 70 kDa protein 1B, 72.2%
CG13321	2.06	15.05	0.03	no	Unknown	Tensin-2, 34.1%
Hsp68	24.75	171.06	0.02	no	Unfolded protein binding	Heat shock 70 kDa protein 1B, 72.2%
Hsp70Aa	3.70	19.71	0.03	no	Unknown	Heat shock 70 kDa protein 1A, 76.3%
CG1673	27.91	144.93	0.0002	no	Transamination of branched-chain-amino-acids	Branched-chain-amino-acid aminotransferase, 53.9%
CG6574	5.17	25.85	0.046	no	Transport of folate	Thiamine transporter 1, 37.3%
l(1)G0469	48.37	211.47	0.01	no	Unknown	SKI/DACH domain-containing protein 1, 44.8%
sug	39.01	151.93	0.03	no	Transcription	Zinc finger protein GLIS2, 57.4%

					Unknown	Heat shock 70 kDa protein 1A, 76.6%
Hsp70Bc	33.22	100.99	0.03	no		

References

Alerting, E. (1990). The Drosophila Fos-related AP-1 protein is a developmentally regulated transcription factor, 822–834. https://doi.org/10.1101/gad.4.5.822

Aliee, M., Röper, J. C., Landsberg, K. P., Pentzold, C., Widmann, T. J., Jülicher, F., & Dahmann, C. (2012). Physical mechanisms shaping the Drosophila dorsoventral compartment boundary. *Current Biology*, *22*(11), 967–976. https://doi.org/10.1016/j.cub.2012.03.070

Anders, S., Pyl, P. T., & Huber, W. (2015). HTSeq-A Python framework to work with high-throughput sequencing data. *Bioinformatics*, *31*(2), 166–169. https://doi.org/10.1093/bioinformatics/btu638

Atkins, M., Potier, D., Romanelli, L., Jacobs, J., Mach, J., Hamaratoglu, F., … Halder, G. (2016). An Ectopic Network of Transcription Factors Regulated by Hippo Signaling Drives Growth and Invasion of a Malignant Tumor Model. *Current Biology*, *26*(16), 2101–2113. https://doi.org/10.1016/j.cub.2016.06.035

Bergert, M., Erzberger, A., Desai, R. A., Aspalter, I. M., Oates, A. C., Charras, G., … Paluch, E. K. (2015). Force transmission during adhesion-independent migration. *Nature Cell Biology*, *17*(4), 524–529. https://doi.org/10.1038/ncb3134

Bilancia, C. G., Winkelman, J. D., Tsygankov, D., Nowotarski, S. H., Sees, J. A., Comber, K., … Peifer, M. (2014). Article Enabled Negatively Regulates Diaphanous-Driven Actin Dynamics In Vitro and In Vivo. *Developmental Cell*, *28*(4), 394–408. https://doi.org/10.1016/j.devcel.2014.01.015

Bruckner, K., Kockel, L., Duchek, P., Luque, C. M., Rorth, P., & Perrimon, N. (2004). The PDGF/VEGF receptor controls blood cell survival in Drosophila. *Developmental Cell*, *7*(1), 73–84. Retrieved from http://eutils.ncbi.nlm.nih.gov/entrez/eutils/elink.fcgi?dbfrom=pubmed&id=15239955&retmode=ref&cmd=prlinks

Brückner, K., Kockel, L., Duchek, P., Luque, C. M., Rørth, P., & Perrimon, N. (2004). The PDGF/VEGF receptor controls blood cell survival in Drosophila. *Developmental Cell*, *7*(1), 73–84. https://doi.org/10.1016/j.devcel.2004.06.007

Brummel, T. J., Twombly, V., Marques, G., Wrana, J. L., Newfeld, S. J., Attisano, L., …

Gelbartt, W. Y. (1994). Characterization and Relationship of Dpp Receptors Encoded by the saxophone and thick veins Genes in Drosophila, *78*.

Bunt, S., Hooley, C., Hu, N., Scahill, C., Weavers, H., & Skaer, H. (2010). Hemocyte-secreted type IV collagen enhances BMP signaling to guide renal tubule morphogenesis in Drosophila. *Developmental Cell*, *19*(2), 296–306. https://doi.org/10.1016/j.devcel.2010.07.019

Casano, A. M., Albert, M., & Peri, F. (2016). Developmental Apoptosis Mediates Entry and Positioning of Microglia in the Zebrafish Brain. *Cell Reports*, *16*(4), 897–906. https://doi.org/10.1016/j.celrep.2016.06.033

Chinenov, Y., & Kerppola, T. K. (2001). Close encounters of many kinds : Fos-Jun interactions that mediate transcription regulatory speci ® city, 2438–2452.

Cho, N. K., Keyes, L., Johnson, E., Heller, J., Ryner, L., Karim, F., & Krasnow, M. A. (2002). Developmental control of blood cell migration by the Drosophila VEGF pathway. *Cell*, *108*(6), 865–876. Retrieved from http://eutils.ncbi.nlm.nih.gov/entrez/eutils/elink.fcgi?dbfrom=pubmed&id=1195 5438&retmode=ref&cmd=prlinks

Chugh, P., Clark, A. G., Smith, M. B., Cassani, D. A. D., Dierkes, K., Ragab, A., … Paluch, E. K. (2017). Actin cortex architecture regulates cell surface tension. *Nature Cell Biology*, *19*(6), 689–697. https://doi.org/10.1038/ncb3525

Collinet, C., Rauzi, M., Lenne, P., & Lecuit, T. (2015). Local and tissue-scale forces drive oriented junction growth during tissue extension, *17*(10). https://doi.org/10.1038/ncb3226

Craig, E. M., Dey, S., & Mogilner, A. (2011). The emergence of sarcomeric, graded-polarity and spindle-like patterns in bundles of short cytoskeletal polymers and two opposite molecular motors. *Journal of Physics Condensed Matter*, *23*(37). https://doi.org/10.1088/0953-8984/23/37/374102

Curran, T., Peters, G., Van Beveren, C., Teich, N. M., & Verma, I. M. (1982). FBJ murine osteosarcoma virus: identification and molecular cloning of biologically active proviral DNA. *Journal of Virology*, *44*(2), 674–682. Retrieved from http://www.pubmedcentral.nih.gov/articlerender.fcgi?artid=256311&tool=pmcentrez &rendertype=abstract

Dahmann, C., Oates, A. C., & Brand, M. (2011). Boundary formation and maintenance in

tissue development. *Nature Reviews Genetics*, *12*(1), 43–55. https://doi.org/10.1038/nrg2902

Danuser, G., Allard, J., & Mogilner, A. (2013). Mathematical Modeling of Eukaryotic Cell Migration: Insights Beyond Experiments. *Annual Review of Cell and Developmental Biology*, *29*(1), 501–528. https://doi.org/10.1146/annurev-cellbio-101512-122308

Davidson, P. M., Sliz, J., Isermann, P., Denais, C., & Lammerding, J. (2015). Design of a microfluidic device to quantify dynamic intra-nuclear deformation during cell migration through confining environments. *Integrative Biology (United Kingdom)*, *7*(12), 1534–1546. https://doi.org/10.1039/c5ib00200a

Davis, J. R., Luchici, A., Miodownik, M., Stramer, B. M., Davis, J. R., Luchici, A., … Stramer, B. M. (2015). Inter-Cellular Forces Orchestrate Contact Inhibition of Locomotion Article Inter-Cellular Forces Orchestrate Contact Inhibition of Locomotion. *Cell*, *161*(2), 361–373. https://doi.org/10.1016/j.cell.2015.02.015

Delaguillaumie, A., Lagaudrière-Gesbert, C., Popoff, M. R., & Conjeaud, H. (2002). Rho GTPases link cytoskeletal rearrangements and activation processes induced via the tetraspanin CD82 in T lymphocytes. *Journal of Cell Science*, *115*(Pt 2), 433–443. Retrieved from http://www.ncbi.nlm.nih.gov/pubmed/11839793

Dietzl, G., Chen, D., Schnorrer, F., Su, K., Barinova, Y., Fellner, M., … Dickson, B. J. (2007). ARTICLES A genome-wide transgenic RNAi library for conditional gene inactivation in Drosophila, *448*(July). https://doi.org/10.1038/nature05954

Dobin, A., Davis, C. A., Schlesinger, F., Drenkow, J., Zaleski, C., Jha, S., … Gingeras, T. R. (2013). STAR: Ultrafast universal RNA-seq aligner. *Bioinformatics*, *29*(1), 15–21. https://doi.org/10.1093/bioinformatics/bts635

Ellenberger, T. E., Brandl, C. J., Struhl, K., & Harrison, S. C. (1992). The GCN4 Basic Region Leucine Zipper Binds DNA as a Dimer of Uninterrupted Helices : Crystal Structure of the Protein-DNA Complex, *71*, 1223–1237.

Eresh, S., Riese, J., Jackson, D. B., Bohmann, D., & Bienz, M. (1997). A CREB-binding site as a target for decapentaplegic signalling during Drosophila endoderm induction. *EMBO Journal*, *16*(8), 2014–2022. https://doi.org/10.1093/emboj/16.8.2014

Fagotto, F. (2014). The cellular basis of tissue separation. *Development*, *141*(17), 3303–3318. https://doi.org/10.1242/dev.090332

Fathallah-Shaykh, H. M., Bona, J. L., & Kadener, S. (2009). Mathematical model of the

Drosophila circadian clock: Loop regulation and transcriptional integration. *Biophysical Journal*, *97*(9), 2399–2408. https://doi.org/10.1016/j.bpj.2009.08.018

Friedl, P., & Bröcker, E. B. (2000). The biology of cell locomotion within three-dimensional extracellular matrix. *Cellular and Molecular Life Sciences*, *57*(1), 41–64. https://doi.org/10.1007/s000180050498

Friedl, P., Locker, J., Sahai, E., & Segall, J. E. (2012). Classifying collective cancer cell invasion. *Nature Cell Biology*, *14*(8), 777–783. https://doi.org/10.1038/ncb2548

Friedrich, B. M., Fischer-Friedrich, E., Gov, N. S., & Safran, S. A. (2012). Sarcomeric pattern formation by actin cluster coalescence. *PLoS Computational Biology*, *8*(6). https://doi.org/10.1371/journal.pcbi.1002544

Fujita, M., Mitsuhashi, H., Isogai, S., Nakata, T., Kawakami, A., Nonaka, I., … Kudo, A. (2012). Filamin C plays an essential role in the maintenance of the structural integrity of cardiac and skeletal muscles , revealed by the medaka mutant zacro. *Developmental Biology*, *361*(1), 79–89. https://doi.org/10.1016/j.ydbio.2011.10.008

Galvagni, F., Orlandini, M., & Oliviero, S. (2013). Role of the AP-1 transcription factor FOSL1 in endothelial cells adhesion and migration. *Cell Adhesion & Migration*, *7*(5), 408–411. https://doi.org/10.4161/cam.25894

Gao, F. B., Brenman, J. E., Jan, L. Y., & Jan, Y. N. (1999). Genes regulating dendritic outgrowth, branching, and routing in Drosophila. *Genes and Development*, *13*(19), 2549–2561. https://doi.org/10.1101/gad.13.19.2549

Garvie, C. W., & Wolberger, C. (2001). Recognition of Specific DNA Sequences Review, *8*, 937–946.

Gerhardt, H., Golding, M., Fruttiger, M., Ruhrberg, C., Lundkvist, A., Abramsson, A., … Betsholtz, C. (2003). VEGF guides angiogenic sprouting utilizing endothelial tip cell filopodia. *Journal of Cell Biology*, *161*(6), 1163–1177. https://doi.org/10.1083/jcb.200302047

Ghabrial, A. S., & Krasnow, M. A. (2006). Social interactions among epithelial cells during tracheal branching morphogenesis. *Nature*, *441*(7094), 746–749. https://doi.org/10.1038/nature04829

Hagedorn, E. J., & Sherwood, D. R. (2011). Cell invasion through basement membrane: The anchor cell breaches the barrier. *Current Opinion in Cell Biology*, *23*(5), 589–596. https://doi.org/10.1016/j.ceb.2011.05.002

Hammonds, A. S., Bristow, C. C. a, Fisher, W. W., Weiszmann, R., Wu, S., Hartenstein, V., … Celniker, S. E. (2013). Spatial expression of transcription factors in Drosophila embryonic organ development. *Genome Biology*, *14*(12), R140. https://doi.org/10.1186/gb-2013-14-12-r140

Hawkins, R. J., Poincloux, R., Bénichou, O., Piel, M., Chavrier, P., & Voituriez, R. (2011). Spontaneous contractility-mediated cortical flow generates cell migration in three-dimensional environments. *Biophysical Journal*, *101*(5), 1041–1045. https://doi.org/10.1016/j.bpj.2011.07.038

Holz, A. (2003). The two origins of hemocytes in Drosophila. *Development*, *130*(20), 4955–4962. https://doi.org/10.1242/dev.00702

Igaki, T., Pagliarini, R. A., & Xu, T. (2006). Loss of Cell Polarity Drives Tumor Growth and Invasion through JNK Activation in Drosophila. *Current Biology*, *16*(11), 1139–1146. https://doi.org/10.1016/j.cub.2006.04.042

Jackson, P. D., & Hoffmann, F. M. (1994). Embryonic expression patterns of the drosophila decapentaplegic gene: Separate regulatory elements control blastoderm expression and lateral ectodermal expression. *Developmental Dynamics*, *199*(1), 28–44. https://doi.org/10.1002/aja.1001990104

Jacobelli, J., Friedman, R. S., Conti, M. A., Lennon-Dumenil, A. M., Piel, M., Sorensen, C. M., … Krummel, M. F. (2010). Confinement-optimized three-dimensional T cell amoeboid motility is modulated via myosin IIA-regulated adhesions. *Nature Immunology*, *11*(10), 953–961. https://doi.org/10.1038/ni.1936

John, M., Leppik, R., Busch, S. J., Granger-schnarr, M., & Schnarr, M. (1996). DNA binding of Jun and Fos bZip domains : homodimers and heterodimers induce a DNA conformational change in solution, *24*(22), 4487–4494.

Kelley, L. C., Shahab, S., & Weed, S. A. (2008). Actin cytoskeletal mediators of motility and invasion amplified and overexpressed in head and neck cancer. *Clinical and Experimental Metastasis*, *25*(4), 289–304. https://doi.org/10.1007/s10585-008-9154-6

Krens, S. F. G., Veldhuis, J. H., Barone, V., Čapek, D., Maître, J.-L., Brodland, G. W., & Heisenberg, C.-P. (2017). Interstitial fluid osmolarity modulates the action of differential tissue surface tension in progenitor cell segregation during gastrulation. *Development*, *144*(10), 1798–1806. https://doi.org/10.1242/dev.144964

Krieg, M., Arboleda-Estudillo, Y., Puech, P. H., Käfer, J., Graner, F., Müller, D. J., &

Heisenberg, C. P. (2008). Tensile forces govern germ-layer organization in zebrafish. *Nature Cell Biology*, *10*(4), 429–436. https://doi.org/10.1038/ncb1705

Krieger, J. W. (2015a). Evidence for Homodimerization of the c-Fos Transcription Factor in Live Cells Revealed by Fluorescence Microscopy and Computer, *35*(21), 3785–3799. https://doi.org/10.1128/MCB.00346-15.Address

Krieger, J. W. (2015b). Evidence for Homodimerization of the c-Fos Transcription Factor in Live Cells Revealed by Fluorescence Microscopy and Computer, *35*(21), 3785–3798. https://doi.org/10.1128/MCB.00346-15.Address

Kühn, S., & Geyer, M. (2017). Formins as effector proteins of Rho GTPases Formins as effector proteins of Rho GTPases, *1248*(August). https://doi.org/10.4161/sgtp.29513

Kulshammer, E., & Uhlirova, M. (2013). The actin cross-linker Filamin/Cheerio mediates tumor malignancy downstream of JNK signaling. *Journal of Cell Science*, *126*(4), 927–938. https://doi.org/10.1242/jcs.114462

Labrousse, A. M., Zappaterra, M. D., Rube, D. A., Bliek, V. Der, Cell, M., Sesaki, H., … Horwitz, A. R. (2003). Cell Migration Integrating Signals from front to back, *302*(December), 1704–1710. https://doi.org/10.1126/science.1092053

Lamb, R. F., Ozanne, B. W., Roy, C., McGarry, L., Stipp, C., Mangeat, P., & Jay, D. G. (1997). Essential functions of ezrin in maintenance of cell shape and lamellipodial extension in normal and transformed fibroblasts. *Current Biology*, *7*(9), 682–688. https://doi.org/10.1016/S0960-9822(06)00295-8

Lämmermann, T., Afonso, P. V., Angermann, B. R., Wang, J. M., Kastenmüller, W., Parent, C. A., & Germain, R. N. (2013). Neutrophil swarms require LTB4 and integrins at sites of cell death in vivo. *Nature*, *498*(7454), 371–375. https://doi.org/10.1038/nature12175

Lämmermann, T., Bader, B. L., Monkley, S. J., Worbs, T., Wedlich-Söldner, R., Hirsch, K., … Sixt, M. (2008). Rapid leukocyte migration by integrin-independent flowing and squeezing. *Nature*, *453*(7191), 51–55. https://doi.org/10.1038/nature06887

Lebestky, T., Chang, T., Hartenstein, V., & Banerjee, U. (2000). Specification of Drosophila Hematopoietic Lineage by Conserved Transcription Factors. *Science*, *288*(5463), 146 LP-149. Retrieved from http://science.sciencemag.org/content/288/5463/146.abstract

Lecuit, T., & Lenne, P. F. (2007). Cell surface mechanics and the control of cell shape, tissue patterns and morphogenesis. *Nature Reviews Molecular Cell Biology*, *8*(8), 633–644.

https://doi.org/10.1038/nrm2222

Lemaitre, B., & Hoffmann, J. (2007). The Host Defense of *Drosophila melanogaster*. *Annual Review of Immunology*, *25*(1), 697–743. https://doi.org/10.1146/annurev.immunol.25.022106.141615

Ling, J., Dubruille, R., & Emery, P. (2012). KAYAK- Modulates Circadian Transcriptional Feedback Loops in Drosophila Pacemaker Neurons. *Journal of Neuroscience*, *32*(47), 16959–16970. https://doi.org/10.1523/JNEUROSCI.1888-12.2012

Liu, Y. J., Le Berre, M., Lautenschlaeger, F., Maiuri, P., Callan-Jones, A., Heuzé, M., … Piel, M. (2015). Confinement and low adhesion induce fast amoeboid migration of slow mesenchymal cells. *Cell*, *160*(4), 659–672. https://doi.org/10.1016/j.cell.2015.01.007

Luster, A. D., Alon, R., & von Andrian, U. H. (2005). Immune cell migration in inflammation: Present and future therapeutic targets. *Nature Immunology*, *6*(12), 1182–1190. https://doi.org/10.1038/ni1275

Maitre, J.-L., & Heisenberg, C.-P. (2011). The role of adhesion energy in controlling cell-cell contacts. *Current Opinion in Cell Biology*, *23*(5), 508–514. https://doi.org/10.1016/j.ceb.2011.07.004

Malawista, S. E., De Chevance, A. B., & Boxer, L. A. (2000). Random locomotion and chemotaxis of human blood polymorphonuclear leukocytes from a patient with Leukocyte Adhesion Deficiency-1: Normal displacement in close quarters via chimneying. *Cell Motility and the Cytoskeleton*, *46*(3), 183–189. https://doi.org/10.1002/1097-0169(200007)46:3<183::AID-CM3>3.0.CO;2-2

Mandeville, J. T. H., Lawson, M. A., & Maxfield, F. R. (1997). Dynamic imaging of neutrophil migration in three dimensions: Mechanical interactions between cells and matrix. *Journal of Leukocyte Biology*, *61*(2), 188–200. https://doi.org/10.1002/jlb.61.2.188

Matsubayashi, Y., Louani, A., Dragu, A., Sánchez-Sánchez, B. J., Serna-Morales, E., Yolland, L., … Stramer, B. M. (2017). A Moving Source of Matrix Components Is Essential for De Novo Basement Membrane Formation. *Current Biology*, *27*(22), 3526–3534.e4. https://doi.org/10.1016/j.cub.2017.10.001

McDonald, J. a., Pinheiro, E. M., & Montell, D. J. (2003). PVF1, a PDGF/VEGF homolog, is sufficient to guide border cells and interacts genetically with Taiman. *Development (Cambridge, England)*, *130*(15), 3469–3478. https://doi.org/10.1242/dev.00574

Milde-Langosch, K. (2005). The Fos family of transcription factors and their role in

tumourigenesis. *European Journal of Cancer*, *41*(16), 2449–2461. https://doi.org/10.1016/j.ejca.2005.08.008

Miller, M. (2009). *Curr Protein Pept Sci*., *10*(3), 244–269.

Montell, D. J., Yoon, W. H., & Starz-Gaiano, M. (2012). Group choreography: Mechanisms orchestrating the collective movement of border cells. *Nature Reviews Molecular Cell Biology*, *13*(10), 631–645. https://doi.org/10.1038/nrm3433

Munoz, M. A., Biro, M., & Weninger, W. (2014). T cell migration in intact lymph nodes in vivo. *Current Opinion in Cell Biology*, *30*(1), 17–24. https://doi.org/10.1016/j.ceb.2014.05.002

Nakabeppu, Y., Ryder, K., & Nathans, D. (1988). DNA Binding Activities of Three Murine Jun Proteins : Stimulation by Fos, *55*, 907–915.

Naumanen, P., Lappalainen, P., & Hotulainen, P. (2008). Mechanisms of actin stress fibre assembly. *Journal of Microscopy*, *231*(3), 446–454. https://doi.org/10.1111/j.1365-2818.2008.02057.x

Ninomiya, H., David, R., Damm, E. W., Fagotto, F., Niessen, C. M., & Winklbauer, R. (2012). Cadherin-dependent differential cell adhesion in Xenopus causes cell sorting in vitro but not in the embryo. *Journal of Cell Science*, *125*(8), 1877–1883. https://doi.org/10.1242/jcs.095315

Nüsslein-volhard, C., & Wieschaus, E. (1980). Mutations affecting segment number and polarity in drosophila. *Nature*, *287*(5785), 795–801. https://doi.org/10.1038/287795a0

Paluch, E. K., Aspalter, I. M., & Sixt, M. (2016). Focal Adhesion–Independent Cell Migration. *Annual Review of Cell and Developmental Biology*, *32*(1), 469–490. https://doi.org/10.1146/annurev-cellbio-111315-125341

Papageorgis, P. (2015). TGF ? Signaling in Tumor Initiation , Epithelial-to-Mesenchymal Transition , and Metastasis, *2015*. https://doi.org/10.1155/2015/587193

Parisi, F., Stefanatos, R. K., Strathdee, K., Yu, Y., & Vidal, M. (2014). Transformed epithelia trigger non-tissue-autonomous tumor suppressor response by adipocytes via activation of toll and eiger/TNF signaling. *Cell Reports*, *6*(5), 855–867. https://doi.org/10.1016/j.celrep.2014.01.039

Parsons, B., & Foley, E. (2013). The Drosophila platelet-derived growth factor and vascular endothelial growth factor-receptor related (Pvr) protein ligands Pvf2 and Pvf3 control

hemocyte viability and invasive migration. *The Journal of Biological Chemistry*, *288*(28), 20173–20183. https://doi.org/10.1074/jbc.M113.483818

Pastor-Pareja, J. C., Wu, M., & Xu, T. (2008). An innate immune response of blood cells to tumors and tissue damage in Drosophila. *Disease Models and Mechanisms*, *1*(2–3), 144–154. https://doi.org/10.1242/dmm.000950

Porte, D., Oertel-buchheit, P., John, M., Granger-schnarr, M., & Schnarr, M. (1997). DNA binding and transactivation properties of Fos variants with homodimerization capacity, *25*(15), 3026–3033.

Porte, D., Oertel-buchheit, P., Schnarr, M., Val, L., & Met, P. (1995). Fos Leucine Zipper Variants with Increased Association Capacity *, *270*(39), 22721–22730.

Ramachandran, A., Gong, E. M., Pelton, K., Ranpura, S. A., Mulone, M., Seth, A., … Adam, R. M. (2011). FosB regulates stretch-induced expression of extracellular matrix proteins in smooth muscle. *American Journal of Pathology*, *179*(6), 2977–2989. https://doi.org/10.1016/j.ajpath.2011.08.034

Ramalingam, N., Franke, C., Jaschinski, E., Winterhoff, M., Lu, Y., Brühmann, S., … Faix, J. (2015). A resilient formin-derived cortical actin meshwork in the rear drives actomyosin-based motility in 2D confinement. *Nature Communications*, *6*. https://doi.org/10.1038/ncomms9496

Ratheesh, A., Belyaeva, V., & Siekhaus, D. E. (2015). Drosophila immune cell migration and adhesion during embryonic development and larval immune responses. *Current Opinion in Cell Biology*, *36*, 71–79. https://doi.org/10.1016/j.ceb.2015.07.003

Ratheesh, A., Biebl, J., Vesela, J., Smutny, M., Papusheva, E., Krens, S. F. G., … Siekhaus, D. E. (2018). Drosophila TNF Modulates Tissue Tension in the Embryo to Facilitate Macrophage Invasive Migration. *Developmental Cell*, *45*(3), 331–346.e7. https://doi.org/10.1016/j.devcel.2018.04.002

Ratheesh, A., Gomez, G. A., Priya, R., Verma, S., Kovacs, E. M., Jiang, K., … Yap, A. S. (2012). Centralspindlin and α-catenin regulate Rho signalling at the epithelial zonula adherens. *Nature Cell Biology*, *14*(8), 818–828. https://doi.org/10.1038/ncb2532

Razzell, W., Wood, W., & Martin, P. (2014). Recapitulation of morphogenetic cell shape changes enables wound re-epithelialisation, 1814–1820. https://doi.org/10.1242/dev.107045

Riesgo-Escovar, J. R., & Hafen, E. (1997). Common and distinct roles of DFos and DJun

during Drosophila development. *Science*, *278*(5338), 669–672. https://doi.org/10.1126/science.278.5338.669

Rousso, T., Shewan, A. M., Mostov, K. E., Schejter, E. D., & Shilo, B. (2013). Apical targeting of the formin Diaphanous in Drosophila tubular epithelia, 1–19. https://doi.org/10.7554/eLife.00666

Ruprecht, V., Wieser, S., Callan-Jones, A., Smutny, M., Morita, H., Sako, K., … Heisenberg, C. P. (2015). Cortical contractility triggers a stochastic switch to fast amoeboid cell motility. *Cell*, *160*(4), 673–685. https://doi.org/10.1016/j.cell.2015.01.008

Sears, H. C. (2003). Macrophage-mediated corpse engulfment is required for normal Drosophila CNS morphogenesis. *Development*, *130*(15), 3557–3565. https://doi.org/10.1242/dev.00586

Seeger, M., Tear, G., Ferres-Marco, D., & Goodman, C. S. (1993). Mutations affecting growth cone guidance in drosophila: Genes necessary for guidance toward or away from the midline. *Neuron*, *10*(3), 409–426. https://doi.org/10.1016/0896-6273(93)90330-T

Seth, A., Otomo, C., & Rosen, M. K. (2006). Autoinhibition regulates cellular localization and actin assembly activity of the diaphanous-related formins FRL α and mDia1, *174*(5), 701–713. https://doi.org/10.1083/jcb.200605006

Shaw, T. J., & Martin, P. (2016). Wound repair: A showcase for cell plasticity and migration. *Current Opinion in Cell Biology*, *42*, 29–37. https://doi.org/10.1016/j.ceb.2016.04.001

Siekhaus, D., Haesemeyer, M., Moffitt, O., & Lehmann, R. (2010). RhoL controls invasion and Rap1 localization during immune cell transmigration in Drosophila. *Nature Cell Biology*, *12*(6), 605–610. https://doi.org/10.1038/ncb2063

Smutny, M., Ákos, Z., Grigolon, S., Shamipour, S., Ruprecht, V., Čapek, D., … Heisenberg, C. P. (2017). Friction forces position the neural anlage. *Nature Cell Biology*, *19*(4), 306–317. https://doi.org/10.1038/ncb3492

St Johnston, D. (2002). The art and design of genetic screens: Drosophila melanogaster. *Nature Reviews. Genetics*, *3*(3), 176–188. Retrieved from http://eutils.ncbi.nlm.nih.gov/entrez/eutils/elink.fcgi?dbfrom=pubmed&id=11972155&retmode=ref&cmd=prlinks

Steinberg, M. S., & Gilbert, S. F. (2004). Townes and Holtfreter (1955): Directed movements and selective adhesion of embryonic amphibian cells. *Journal of Experimental Zoology Part A: Comparative Experimental Biology*, *301*(9), 701–706.

https://doi.org/10.1002/jez.a.114

Stossel, T. P., Condeelis, J., Cooley, L., Hartwig, J. H., Schleicher, M., & Shapiro, S. S. (2001). FILAMINS AS INTEGRATORS OF CELL MECHANICS AND SIGNALLING, *2*(February), 138–145.

Sun, J., & Hemler, M. E. (2001). Regulation of MMP-1 and MMP-2 production through CD147/extracellular matrix metalloproteinase inducer interactions. *Cancer Research*, *61*(5), 2276–2281. Retrieved from http://eutils.ncbi.nlm.nih.gov/entrez/eutils/elink.fcgi?dbfrom=pubmed&id=11280798&retmode=ref&cmd=prlinks

Sundqvist, A., Zieba, A., Vasilaki, E., Herrera Hidalgo, C., Söderberg, O., Koinuma, D., … Van Dam, H. (2013). Specific interactions between Smad proteins and AP-1 components determine TGFβ-induced breast cancer cell invasion. *Oncogene*, *32*(31), 3606–3615. https://doi.org/10.1038/onc.2012.370

Supatto, W., McMahon, A., Fraser, S. E., & Stathopoulos, A. (2009). Quantitative imaging of collective cell migration during Drosophila gastrulation: Multiphoton microscopy and computational analysis. *Nature Protocols*, *4*(10), 1397–1412. https://doi.org/10.1038/nprot.2009.130

Szüts, D., & Bienz, M. (2000). An autoregulatory function of Dfos during Drosophila endoderm induction. *Mechanisms of Development*, *98*(1–2), 71–76. https://doi.org/10.1016/S0925-4773(00)00455-X

Toyjanova, J., Flores-Cortez, E., Reichner, J. S., & Franck, C. (2015). Matrix confinement plays a pivotal role in regulating neutrophil-generated tractions, speed, and integrin utilization. *Journal of Biological Chemistry*, *290*(6), 3752–3763. https://doi.org/10.1074/jbc.M114.619643

Tozluoğlu, M., Tournier, A. L., Jenkins, R. P., Hooper, S., Bates, P. A., & Sahai, E. (2013). Matrix geometry determines optimal cancer cell migration strategy and modulates response to interventions. *Nature Cell Biology*, *15*(7), 751–762. https://doi.org/10.1038/ncb2775

Uhlirova, M., & Bohmann, D. (2006). JNK- and Fos-regulated Mmp1 expression cooperates with Ras to induce invasive tumors in Drosophila. *EMBO Journal*, *25*(22), 5294–5304. https://doi.org/10.1038/sj.emboj.7601401

Vinson, C. R., & Boyd, S. M. (1993). Dimerization specificity of the leucine zipper-containing

bZIP motif on DNA binding : prediction and rational design, 1047–1058.

Wacker, S., Grimm, K., Joos, T., & Winklbauer, R. (2000). Development and control of tissue separation at gastrulation in Xenopus. *Developmental Biology*, *224*(2), 428–439. https://doi.org/10.1006/dbio.2000.9794

Weng, M., & Wieschaus, E. (2017). Polarity protein Par3 / Bazooka follows myosin-dependent junction repositioning. *Developmental Biology*, *422*(2), 125–134. https://doi.org/10.1016/j.ydbio.2017.01.001

Wilson, C. A., Tsuchida, M. A., Allen, G. M., Barnhart, E. L., Applegate, K. T., Yam, P. T., … Theriot, J. A. (2010). Myosin II contributes to cell-scale actin network treadmilling through network disassembly. *Nature*, *465*(7296), 373–377. https://doi.org/10.1038/nature08994

Wilson, K., Lewalle, A., Fritzsche, M., Thorogate, R., Duke, T., & Charras, G. (2013). Mechanisms of leading edge protrusion in interstitial migration. *Nature Communications*, *4*(May), 1–12. https://doi.org/10.1038/ncomms3896

Wood, W., Faria, C., & Jacinto, A. (2006). Distinct mechanisms regulate hemocyte chemotaxis during development and wound healing in Drosophila melanogaster. *The Journal of Cell Biology*, *173*(3), 405–416. https://doi.org/10.1083/jcb.200508161

Wood, W., & Jacinto, A. (2007). Drosophila melanogaster embryonic haemocytes: masters of multitasking. *Nature Reviews. Molecular Cell Biology*, *8*(7), 542–551. https://doi.org/10.1038/nrm2202

Zeitlinger, J., Kockel, L., Peverali, F. A., Jackson, D. B., Mlodzik, M., & Bohmann, D. (1997). Defective dorsal closure and loss of epidermal decapentaplegic expression in Drosophila fos mutants. *EMBO Journal*, *16*(24), 7393–7401. https://doi.org/10.1093/emboj/16.24.7393

Zhou, L., Hashimi, H., Schwartz, L. M., & Nambu, J. R. (1995). Programmed cell death in the Drosophila central nervous system midline. *Current Biology*, *5*(7), 784–790. https://doi.org/10.1016/S0960-9822(95)00155-2

Zumdieck, A., Kruse, K., Bringmann, H., Hyman, A. A., & Jülicher, F. (2007). Stress generation and filamnet turnover during actin ring constriction. *PLoS ONE*, *2*(8). https://doi.org/10.1371/journal.pone.0000696